| I.A.D Innovative Aerospace Design | Final Report | Ref.: MAE 4351-001-2017<br>Date: 17. Apr. 2026<br>Page: 1 of 97 Pages<br>Status: Completed |
|---|---|---|

| Designing a Light Twin-Engine GA Aircraft | | | | |
|---|---|---|---|---|
| **Signatures:** | | | | |
| | **Name:** | **Signature:** | **Dept.:** | **Date:** |
| **Author:** | Jonathan Carrera<br>Abram Suarez<br>Travis Webb<br>Nazmus Sakib<br>Boot Nguyen<br>Michael Gibson | | MAE | 4/17/2026 |
| **Seen:** | Dr. Smith | | MAE | |

**Summary:**

**The following report summarizes this team's efforts in designing a general aviation aircraft in the conventional configuration delineated in previous report, and the integration of new technologies onto this configuration. The procedures delineated in Jan Roskam's Airplane Design series were mainly utilized along with other well-known authors for reference. The *conceptual* sizing of the aircraft was determined early in the design process. Quantities such as aircraft geometry, performance parameters, etc. are *preliminary* design milestones that followed. *Preliminary Design – Level I* (PD I) was completed during the first semester and is summarized here. *Preliminary Design – Level II* (PD II) was completed during this final semester were refining/and slight modifications occurs. A Cad model of the Tecnam P2006T was generated to run *Computational Fluid Dynamics* (CFD) to calibrate and update a synthesis code in order to implement new technology onto this configuration. The main purpose of this semester's efforts was to implement a hybrid electric-propulsive systems and evaluate feasibility, trade-offs and the risk associated. It was concluded that with the energy density in batteries currently manufactured an extremely significant amount of payload is sacrificed. It is currently not feasible to implement this technology on this desired aircraft configuration.**

| Distribution: | | |
|---|---|---|
| **Institution:** | **Dept.:** | **Name:** |
| The University of Texas at Arlington | MAE | Dr. Smith |

## Work Disclosure Statement

The work we performed to document the results presented in this report was performed by us, or it is otherwise acknowledged.

Date: 4/17/2026

Signature:

# Contents

## List of Figures

PART I



PART II

## List of Tables

PART I



PART II

## Nomenclature

$a$ = Speed of sound
$a_0$ = Section lift curve slope of a 2D wing
$a_t$ = 3D lift curve slope of a horizontal tail
$a_w$ = 3D lift curve slope of a wing
a,b,c,d = Regression line constants
$AR$ = Aspect ratio
$ARH$ = Aspect Ratio of Horizontal Tail
$ARV$ = Aspect Ratio of Vertical Tail
$ARw$ = Aspect Ratio of Main Wing
$b$ = Wing Span [ft]
$bht$ = Wing Span of Horizontal Tail
$bvt$ = Wing Span of Vertical Tail
$bhp$ = Brake Horsepower
$c_p$ = Specific fuel consumption, [lbs./hp/hr.]
$C$ = Main Wing Chord
$C_D$ = Drag Coefficient
$C_D$ = Drag Coefficient
$C_{D0l}$ = Zero-Lift Drag Coefficient
$C_{Do}$ = Zero lift drag coefficient
$C_{Do}$ = Zero lift drag coefficient
$cg$ = Center of Gravity
$CGR$ = Climb gradient, [rad]
$CGRP$ = Climb gradient parameter, [rad]
$C_L$ = Lift Coefficient
$C_{Lmax}$ = Coefficient of Lift clean
$C_{LmaxL}$ = Coefficient of Lift at Landing
$C_{Lmaxr}$ = Coefficient of Lift at the root of the wing
$C_{Lmaxt}$ = Coefficient of Lift at Tip of Wing
$C_{LmaxTO}$ = Coefficient of Lift at Takeoff
$C_{l\beta}$ = Dihedral effect
$C_P$ = Power Coefficient
$C_Q$ = Torque Coefficient
$C_T$ = Thrust Coefficient
$C_{n\beta_f}$ = Change in aerodynamic yawing moment coefficient with sideslip angle of the fuselage
$C_{n\beta_v}$ = Change in aerodynamic yawing moment coefficient with sideslip angle of the vertical tail
$C_{n\beta_w}$ = Change in aerodynamic yawing moment coefficient with sideslip angle of the wing
$C_{n\delta_r}$ = Change in yawing moment with respect to rudder deflection
$C_{y\beta_v}$ = Change in the aerodynamic side force coefficient with respect to sideslip angle
$C_{L\alpha}$ = Change in lift coefficient with respect to angle of attack
$C_{n\beta}$ = Aerodynamic yawing moment coefficient change with sideslip angle
$(dC_N/d\alpha)_{N_{P_{Tc=0}}}$ = Change in normal force coefficient with respect to the angle of attack
$\left(\frac{dC_m}{dC_L}\right)_P$ = Change in pitching moment coefficient with respect to the lift coefficient for the propeller
$\left(\frac{dC_m}{dC_L}\right)_{fus}$ = Change in pitching moment coefficient with respect to the lift coefficient for the fuselage

$\left(\frac{dC_m}{dC_L}\right)_{wing}$ = Change in pitching moment coefficient with respect to the lift coefficient for the wing
$\frac{dC_m}{dC_L}$ = Total change in pitching moment coefficient with respect to the the lift coefficient
$\frac{dT_c}{dC_L}$ = Change in thrust coefficient with respect to the lift coefficient
$D$ = Diameter [ft]
$D$ = Drag, [lbs.]
$D_p$ = Propeller diameter, [ft.]
$E$ = Endurance, [hours]
$f$ = Equivalent parasite area, [ft$^2$]
$F$ = Weight sensitivity parameter, [lbs.]
$FAR$ = Federal Air Regulation
$h$ = Altitude, [ft]
$h$ = Altitude, [ft.]
HP = Horsepower
$I_p$ = Power index, [(hp/ft$^{2)1/3}$]
$J$ = Advance Ratio
$K_N$ = Empirically determined factor
$K_{R1}$ = Reynold's number correlation factor
$K_f$ = Fuselage stability coefficient
$l_p$ = Distance to the center of the propeller from the center of the fuselage
$L_f$ = Length of the fuselage
$L$ = Lift, [lbs.]
$L, ht$ = Length of Aerodynamic Center of Horizontal Tail
$L, vt$ = Length of Aerodynamic Center for the Vertical Tail
$L/D$ = Lift-to-drag ratio
$L/D$ = Lift-to-drag ratio
$M$ = Mach Number
$M_{ff}$ = Mission Fuel Fraction, [end weight/ begin weight]
$MGC$ = Mean Geometric Chord
$n$ = Propeller Ω [rps]
$N$ = Number of propellers
$N$ = Number of engines
$N_{t_{crit}}$ = Critical one engine out yawing moment
$N_0$ = Stick fixed neutral point
$N_{0wind}$ = Neutral point for propeller windmilling
$N_D$ = Drag induced yawing moment
$\Delta N_0$ = Forward shift of the neutral point due to critical powered flight
$nm$ = Nautical mile, [6,076 ft.]
P = Power [HP/550 ft-pound per sec]
$P$ = Power, [hp]
$q$ = Dynamic Pressure [psf]
$\bar{q}_{mc}$ = Dynamic pressure [psf]
$Q$ = Torque [lb-ft]
$R$ = Range, [nm]
$RC$ = Rate of climb, [fpm, fps]
$RCP$ = Rate of climb parameter, [hp/lbs.]
$s$ = Distance (used in takeoff and landing Equations)
$S_{wet}$ = Wetted Area
$S$ = Wing Area [ft$^2$]

$Sh$ = Historical Horizontal Tail Area
$ShT$ = Area of Horizontal Tail
$S_P$ = Propeller disk area
$S_c$ = Canard tail surface area
$Svh$ = Historical Vertical Tail Area
$SvT$ = Vertical Tail Area
$Sw$ = Wing Area
$Swh$ = Historical Wing Area
T = Thrust [lb]
t/c = Thickness ratio in relation of the chord
$thp$ = Total Horsepower
$TOP_{23}$ = FAR 23 Take-off parameter
$TSFC$ = Thrust Specific Fuel Consumption [lbm/hr/lb]
$V$ = True air speed
$\bar{V}$ = Tail volume coefficient
$V_{mc}$ = Velocity at minimum control
$V_{cr}$ = Cruise velocity, [mph, fps, kts.]
$V_{cr}$ = Cruise velocity, [mph, fps, kts.]
$Vht$ = Volume Coefficient of Horizontal Tail
$Vvt$ = Volume Coefficient of Vertical Tail
$W$ = Weight [lb]
$W_{CREW}$ = Weight of the crew, [lbs.]
$W_E$ = Empty weight, [lbs.]
$W_F$ = Fuel weight, [lbs.]
$W_{FEQ}$ = Fixed equipment weight, [lbs.]
$W_{Fres}$ = Reserved fuel quantity, [lbs.]
$W_{Fused}$ = Actual fuel used, [lbs.]
$W_{ME}$ = Manufactures empty weight, [lbs.]
$W_{OE}$ = Operating empty weight, [lbs.]
$W_{PL}$ = Weight of payload, [lbs.]
$W_{tfo}$ = Trapped fuel and oil in engine, [lbs.]
$W_{TO}$ = Takeoff weight, [lbs.]
$W_{UL}$ = Useful load, [lbs.]
$W$ = Total Weight of Aircraft
$Xh$ = Chord of Horizontal Tail
$Xv$ = Chord of Vertical Tail
$w_f$ = Fuselage width
$y_t$ = Lateral thrust moment arm
$z_f$ = Vertical height of the fuselage at the root chord
$z_v$ = The z-axis distance from the *cg* to the vertical tail aerodynamic center

$\pi$ = 3.1415
$\rho$ = Air density, [slugs/ft$^3$]
$\sigma$ = Density ratio
$\mu_G$ = Ground friction
$\eta_p$ = Propeller efficiency
$\delta_{\epsilon 0}$ = Elevator deflection required at zero lift
$\delta_{\epsilon max}$ = Maximum elevator deflection
$\delta_r$ = Rudder deflection
$\eta_t$ = Horizontal tail efficiency
$\Delta$ = Angle of sweep, Change in-.
$\alpha_0$ = Zero lift Angle of Attack [rad]
$\beta$ = Pitch Angle
$\theta$ = Angle of Attack [rad]
$\rho$ = Density [slug/ft$^3$]
$\sigma$ = Solidity
$\Phi$ = Induced Angle [rad]
$d\beta/d\alpha$ = Change in sideslip with respect to angle of attack
$d\varepsilon/d\alpha$ = Change in downwash with respect to angle of attack
$\beta$ = Mach number correction

$Cl$ = Coefficient of Lift
$q$ = Dynamic Pressure
$S$ = Surface Area
$Yavg$ = Wing Displacement
$L$ = Lift
$d$ = Distance
$\tau$ = Shear Stress
$\tau avg$ = Average Shear Stress
$I_{xx}$ = Moment Of Inertia
$H$ = Height of the Web
$b$ = Thickness of the Web
$h$ = Hight of the Caps
$\sigma_{bending}$ = Bending Stress
$M$ = Moment
$Cm$ = Coefficient of Moment
$c$ = Chord Distance
$T$ = Torque
$G$ = Modulus of Rigidity
$J$ = von Mises yield criterion
$\theta$ = Angle of Twist
$A$ = Airfoil Area
$t$ = Skin Thickness
$S_1$ = Parameter of Skin 1 or 2

## Introduction

The following report summarizes the procedures delineated in Jan Roskam's Airplane Design series. These procedures were implemented to design an aircraft of the desired type. A summary of the conceptual sizing of a Light-Economical-General-Aviation-Trainer -Twin Aircraft will be shown in the first portion of this report along with FAR-23 (Federal Aviation Regulations) in order to ensure a safe and reliable product that is built to federal standards. A refinement of preliminary performance parameters was made. Initially, assumptions were made about the aircraft based on empirical data from similar aircraft. Weights were estimated based on empirical data and mission conditions. The effects other variables have on the takeoff weight such as payload weight and empty weight were calculated (known as Sensitivity Gradients). A graph shows trends between the stall speed sizing, takeoff sizing, landing field sizing, FAR requirements, and cruise speed as power loading and wing loading vary with each other to determine the defining criteria between all the given conditions. Historical data was utilized to size the empennage, locate the center of gravity, and find the placement of the undercarriage. Other parameters were analyzed and established such as drag polars, propeller and engine specifications, refined weights and balance, first pass at static stability and performance parameters to ensure these meet our configuration and FA regulations (this will conclude the summary portion of the *Preliminary Design – Level I* portion). During the Preliminary Design – Level II further refinements were made and a synthesis code created to automate the design process with geometric inputs such as aspect ratio, tapper ratio, wing area, aircraft length, girth, etc. A Cad model of the Tecnam P2006T was generated to run Computational Fluid Dynamics (CFD) to calibrate and update a synthesis code in order to implement new technology onto this configuration. A hybrid electric-propulsive system was incorporated and its feasibility, trade-offs and risks associated were determined.

# I. Conceptual Design

## Sizing Procedure Overview

Conceptual parameters were determined in the following order. Due to the complexity of such task it is important to being with a parameter that will latter help yield other important parameters, hence the order of flow. The reader is encouraged to refer to previous reports for added detail[1].

1) Specifications
2) Takeoff Weight, $W_{TO}$
3) Sensitivity Gradients
4) Wing Loading, Power Loading, Drag Polars, (W/S, P/W, $C_l^{3/2}/C_d$)
5) Cruise Speed

All of these parameters were matched together to present constrains to determine the best approach to continue preliminary design.

## Specifications

Specifications the aircraft must meet are seen in **Table 1-1**. These requirements are crucial for the first iteration preliminary sizing.

**Table 1-1 Design Requirements**

| Light Economical Twin Aircraft | | |
|---|---|---|
| **Requirement** | **Value** | **Unit** |
| **Seating Capacity** | 4 | Persons |
| **Useful load** | 950 | lb. |
| **Baggage Allowance** | 176 | lb. |
| **Baggage Volume** | 23 | $Ft^3$ |
| **Cabin Interior Width** | 48 | in. |
| **Cabin Height** | 36 | in. |
| **Maximum dry tank range** | 725 | nm. |
| **$V_{SL0}$** <= | 48 | knots. |
| **$V_{MC}$** < | $V_S$ | |
| **Service Ceiling** >= | 15,000 | ft. |
| **$V_{CR}$ @ 75% Power** >= | 140 | knots. |
| **Single Engine ROC @ SLS** | 250 | fpm |

The specifications for this aircraft fall under the light-twin-engine aircraft type. The Beech Duchess, as seen in **Fig. 1-1**, is an adequate model to obtain reasonable initial parameters. As mentioned above, most initial parameters are derived of selected based on historical data. It is important to make sure that the data that is collected corresponds to the specified family of aircraft. Assumptions will be made through out this document, it is important for the reader to be sure to understand these assumptions.

**Figure 1 - 1 Beech Douches**

## Preliminary Weight Calculations

Finding the takeoff weight of the aircraft, $W_{TO}$, is essential to determining other preceding parameters. The reader is encouraged to refer back to previous reports for added detail[1]. Summarized here is the overview

on finding a first pass of the takeoff weight of the aircraft. First, different weight parameters were found utilizing common weight definitions. Breguet's range equation of propeller-driven aircraft along with historical statistical data was utilized to obtain fuel mission fractions. The *Mission Fuel Fraction, $M_{ff}$*, is then obtained through the product of these fuel mission fractions, yielding the ratio of landing weight to takeoff weight as seen in equation (2).

**Fig. 1-2** shows a schematic of a generic mission (not to scale, not accurate). Roskam suggests a value for each one of these phases as seen in Table 1-2.

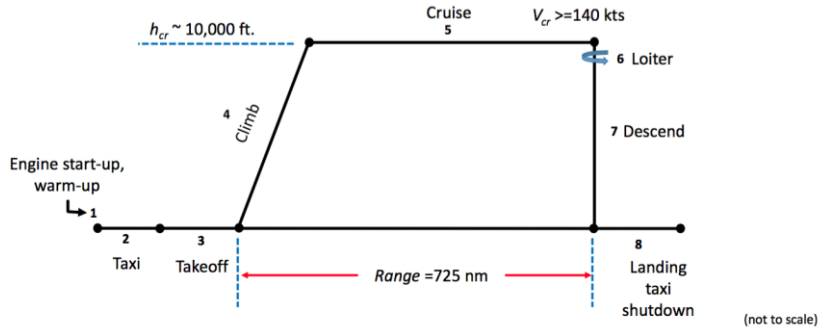


**Figure 1 - 2 Mission Definition**

This fuel fraction can be estimated from the Breguet's range Eqn., which is represented as follows for propeller-driven aircraft.

$$R_{cr} = 375\left(\frac{\eta_p}{C_p}\right)_{cr}\left(\frac{L}{D}\right)_{cr}\ln\left(\frac{W_4}{W_5}\right) \quad (1)$$

Were $R_{cr}$ is in statute miles. **Eqn. (1)** makes use of the Lift-to-Drag Ratio and the ratio between propeller efficiency and specific fuel consumption. These values are selected from historical data provided by Roskam.

These values are based on experience and/or judgment. Roskam encourages the reader to allow these values to be modified when common sense calls for it. We have chosen the Lift-to-Drag coefficient, *L/D* to be 11, the propeller efficiency, $\eta_p$ to be 82% and the specific fuel consumption, $c_p$ to be 0.5.

**Table 1- 2 Initial Assumptions**

| | Value | Unit |
|---|---|---|
| **Average weight per person** | 175 | lb. |
| **Average weight per baggage** | 30 | lb. |
| **Fuel weight** | 6 | lb/gal |
| **Lift-to-Drag coefficient, L/D** | 11 | - |
| **Propeller efficiency, $\eta_p$** | .82 | - |
| **Specific fuel consumption** | 0.5 | - |

Substituting these values and the desired range value of 725 nm into **Eqn. (1)** and solving for the cruise fuel fraction, $W_5/W_4$ yield a value of 0.884.

This case yields a *Mission Fuel Fraction* of about 85%.

$$M_{ff} = \left(\frac{W_1}{W_{TO}}\right)\prod_{i=1}^{i=7}\left(\frac{W_{i+1}}{W_i}\right) \quad (2)$$

In other words, the aircraft will be about 15 % lighters when it lands then when it took off. This is only one component of the many needed to successfully determine a reasonable takeoff weight.

The next immediate objective is to calculate an empty weight, $W_E$ based on empirical mission data along with a tentative empty weight, $W_{Etent}$. This procedure is delineated on previous report[1]. The take-off weight obtained was that of 2740 lbs.

## Sensitivity Gradients

It is important to reiterate the fact that the results obtained in the fuel-fraction method depend on the values selected from the historical data, especially those in the Breguet range and endurance Equations (Equation (2)). Several variables affect our takeoff weight.

1. Payload Weight, $W_{PL}$
2. Empty Weight, $W_E$
3. Range, R
4. Endurance, E
5. Lift-to-drag ratio, L/D
6. Specific fuel consumption, $c_p$
7. Propeller efficiency, $\eta_p$

The effect of these variables on the resultant takeoff weight, $W_{TO}$, must be determined to identify the one with a greater influence in order to allocate efforts effectively to ensure that mission requirements can be achieved. Roskam provided the following Equations; the derivation of parameters will not be presented in this report. If the reader is interested in the derivation of these, it is encouraged to reference *Airplane Design Volume 1* by Roskam[2] or previous report for more detail[1]. Table 1-3 lists these results.

**Table 1- 3 Calculated Sensitivity Gradients**

| Partial Derivatives (SENSITIVITY GRADIENTS) | | | | | | |
|---|---|---|---|---|---|---|
| | ***Airplane Growth*** | ***[lb/lb]*** | ***[lb/lb/hp/hr]*** | ***[lbs.]*** | ***[lbs.]*** | |
| *d(Wto)/R* | *d(Wto)/dy* | *d(Wto)/d($W_{PL}$)* | *d(Wto)/d(cp)* | *d(Wto)/d(L/D)* | *d(Wto)/d(eta_prop)* | *d(Wto)/d(E)* |
| *1.60* | *4.05* | *4.05* | *2321.3* | *-105.51* | *-1415.42* | *1.82* |

Nominal values for the sensitivity of takeoff weight range from 4 to 6 lb./nm but because our aircraft is made out of composite and evaluation at max range, the derivative is smaller than normal. As seen in Table 1-3, it is apparent that the specific fuel consumption has the greatest influence on the takeoff weight and range has the least amount of influence on the takeoff weight. The power plant characteristics are of most importance. This conclusion will become evident as the report progresses.

## Sizing

There are additional performance criteria that need to be met such as stall speed, takeoff field distance, landing field distance, cruise speed / maximum speed, rate of climb when all engines are operating, rate of climb when one engine is inoperative, time-to-climb, maneuvering etc. Determining these values is done by strategically using common variables between them to make a plotted graph that will show which sizing criteria is most critical and the limits when choosing the dimensions of the wing. These are the common variables:

1) Main Wing Area, S
2) Thrust at takeoff, $T_{TO}$
3) Power at takeoff, $P_{TO}$
4) Maximum required lift coefficient, $C_{Lmax}$, with a clean configuration (flaps up)
5) Maximum required lift coefficient at takeoff, $C_{L,max,TO}$
6) Maximum required lift coefficient at landing, $C_{L,max,L}$
7) Wing Loading (W/S)
8) Thrust Loading (T/S)
9) Power Loading (W/P)

It is desirable to find a combination of the highest possible wing loading and the lowest possible thrust (or Power) that resides within the requirements. This will generally result in the lowest weight, therefore the lowest cost. It is important to also make sure to meet FAR Part 23 requirements on stall/cruise speeds for aircrafts of the same type. According to FAR Part 23 for aircraft with a takeoff weight, less than 6,000 lbs. must have a stall speed of no more than 61 kts, unless certain climb gradient criteria are met. The following are only results; refer to previous report for details[1].

1. *STALL SPEED SIZING*
   The limit has been set at a wing loading (W/S) of 15.6 psf. Dividing the determined takeoff weight by this wing loading will yield a wing area of 175.6 $ft^2$.
2. *TAKEOFF DISTANCE REQUIREMENTS*
   The power needed for takeoff turns out to be 200 hp.
3. *LANDING DISTANCE REQUIREMENTS*
   For this light twin landing filed length of 2,500 ft. defined at a 5,000 ft. altitude on a standard day where the density is equal to 0.002049 slugs/$ft^3$ yields a landing stall velocity ($V_{SL}$) of 69.8kts and an approach velocity of 90.7kts.
4. *CLIMBING REQUIREMENTS*
   A wetted area of about 630 $ft^2$ was determined. An aspect ratio (AR) of 7 has been assumed in our calculations. **Table A5** in the appendix provides some first estimates for $\Delta C_{Do}$ and 'e' for different configurations.
   **Table 1- 4** shows the values calculated for the drag polar ($C_L^{3/2}/C_D$)

**Table 1- 42 Coefficients of Drag and Drag Polar Results**

| Configuration | $C_D$ | $C_{Do}$ | $1/\pi$ ARe | e | $C_L$ | $C_L^{3/2}/C_D$ |
|---|---|---|---|---|---|---|
| *CLEAN* | 0.133 | 0.0251 | 0.05478 | 0.83 | 1.4 | 12.50 |
| *TAKE-OFF* | 0.143 | 0.0351 | 0.05478 | 0.83 | 1.4 | 11.62 |
| *LANDING* | 0.287 | 0.0851 | 0.06223 | 0.73 | 1.8 | 8.42 |
| *LANDING (f&g)* | 0.312 | 0.1101 | 0.06230 | 0.73 | 1.8 | 7.74 |

Calculating the drag polar is crucial due to the fact that when $C_L^{3/2}/C_D$ is maximum the power required is the least, making the specific power the greatest. At the velocity where this occurs is when the specific power is the greatest and respectively when the highest rate of climb can be achieved. These values will be used to calculate the FAR requirements discussed later in this report.

5. *CRUISE SPEED REQUIREMENTS*
   The power index[3] (*Ip*) is introduced in this equation

$$\left(\frac{W}{P}\right) = \frac{1}{\sigma(I_P)^3}\left(\frac{W}{S}\right) \tag{3}$$

Were $I_p$ was found to be 0.88 and a value of 0.7983 for σ was used. **Eqn. (3)** then becomes a proportionality equation were the wing loading is proportional to the power loading by a factor of 1.8382. This relationship is depicted in **Fig. 1-5**.

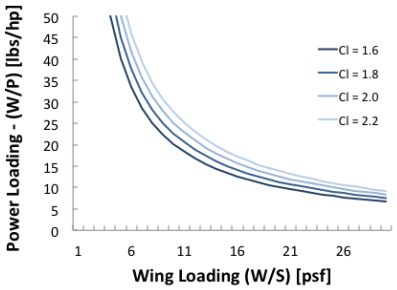


**Figure 1 - 3 Allowable Wing Loading to Meet a Landing Distance Requirements**

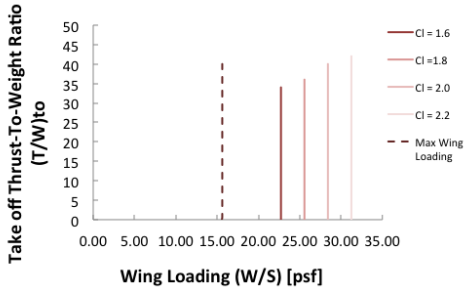


**Figure 1 - 4 Effect of the Takeoff Wing Loading and Maximum Landing Lift Coefficient on the Takeoff Power Loading**

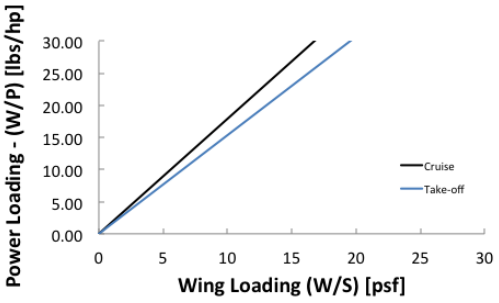


**Figure 1 - 5 Allowable Values of Wing Loading and Thrust-to-Wing Ratio to Meet a Given Cruise Speed**

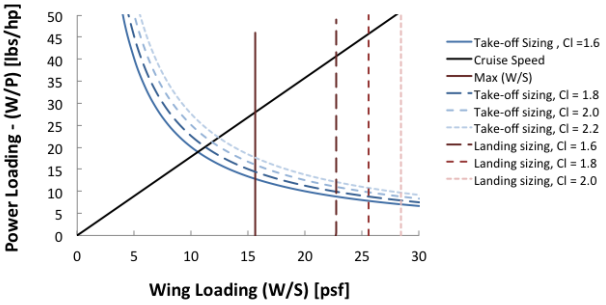


**Figure 1 - 6 Matching Sizing Requirements**

## FAR 23

The Federal Aviation Requirements (FAR) 23 delineates specific requirements that must be met in order to comply with Federal Regulations. These are taken into account when designing the aircraft. As seen in the following figures, note that any design point below and to the left of the trend lines meets such requirements, any design point above or to the right of these trend lines does not meet the requirements. For more details on these, refer to previous report[1].

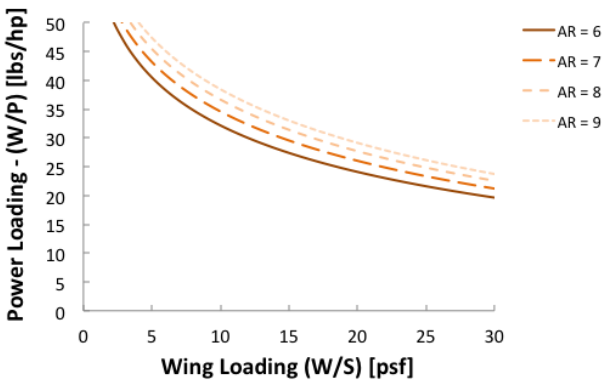


**Figure 1 - 75 FAR 23.65 Rate of Climb (AEO)**

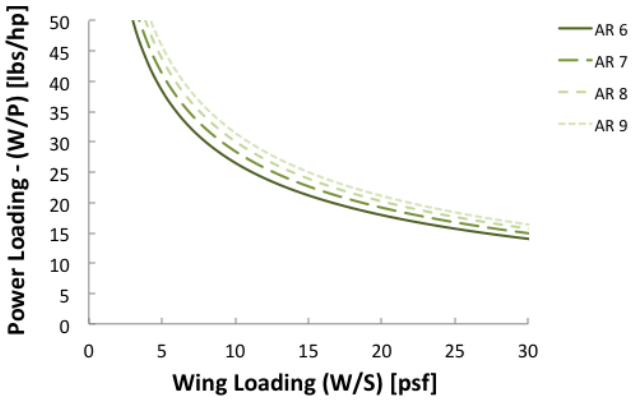


**Figure 1 - 84 FAR 23.65 Climb Gradient (AEO)**

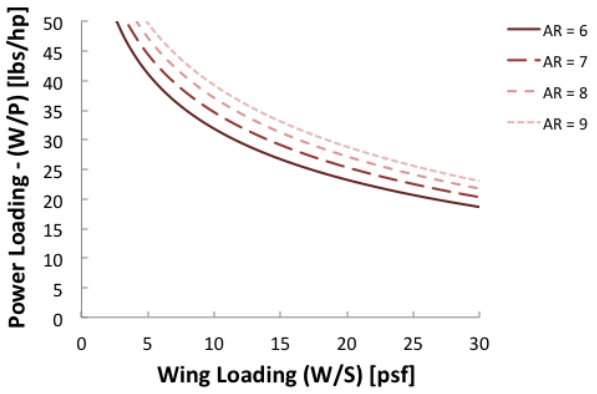


**Figure 1 - 97 FAR 23.67 Rate of Climb (OEI)**

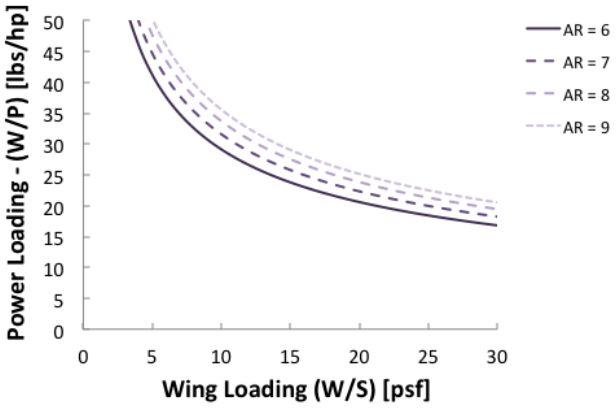


**Figure 1 - 106 FAR 23.67 Rate of Climb (OEI)**

The variation with aspect ratios is shown. **Figures 7-10. Figure 1-11** is a superposition of each FAA Requirement at an aspect ratio of 7, since this has been the aspect ratio selected.

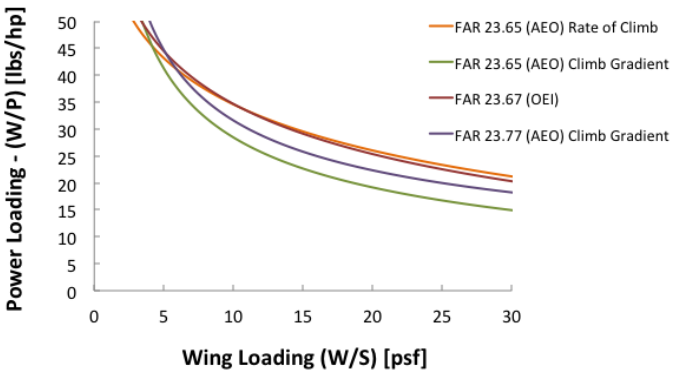


**Figure 1 - 11 Matching FAR 23 Requirements**

**Fig. 1-12** shows that bellow a wing loading of 4 FAR 23.65's rate of climb requirement dictates the limit, and for wing loadings grader and equal to 5 are dictated by FAR 23.65's climb gradient. Remember all of these were determined for a coefficient of lift, $C_L$ of 1.6.

It is desired to match all of these results and select a design point with the highest power loading (W/P) and highest wing loading (W/S). Higher power loading will yield the smallest engine that will meet these requirements. Higher wing loading will yield the less drag created on the wing and therefore lead to better fuel efficiencies.

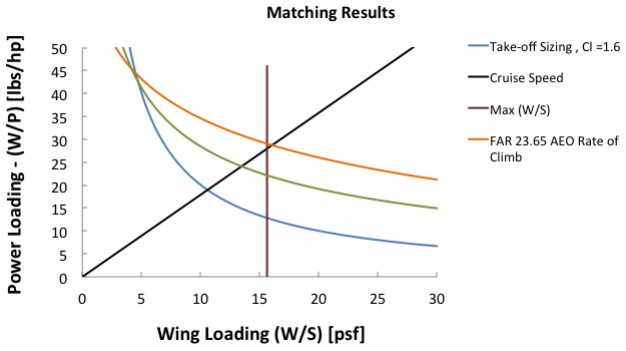


**Figure 1 - 128 Matching FAR 23 and Sizing Requirements**

It is important to note that our design point must be on or left of the Max (W/S) vertical line and under the lower most function. In this case being the takeoff-sizing requirement at a $C_L$ of 1.6. This will ensure that every single one of the limiting requirements is met. In this case, the optimal design point is at a wing loading of 15.6 $lbs./ft^2$ and at a power loading of 14 $lb./HP$.

In conclusion, for the desired range to be achieved, even though the aircraft can hold four passengers with luggage, it can only be achieved when there are three passengers and luggage. In regards to the sensitivity, the payload weight will change at a greater factor per lb. change than the empty weight, both changing at a greater pace than the range. Yet, the specific fuel consumption will have the greatest effect on the takeoff weight. Finally in regards to the power loading and wing loading sizing, the factors that determine this are the cruise speed and the landing sizing and maybe FAR 23.77 given the right changes within the other criteria. With all this info, a data could be obtained given a new set of design criteria.

## II. Preliminary Design - Level I

Preliminary design can take off after obtaining the wing loading and power loading. This team focused on sizing the empennage and control surfaces based on historical statistical data and tail volume coefficients. The cabin dimensions were delineated utilizing ergonomics based on the 5th to 9th percentile data. This defined the shape of the nose and most of the fuselage. Since this aircraft is not ascending past $10{,}000ft$ the cabin needs not to be pressurized, hence the non-circular cross-section of the fuselage. Main wing dimensions were based on mean geometric chord historical data. A pros-cons-configuration study was made that lead the team to decide a high-wing with a conventional tail configuration. A weight component analysis was completed based on historical data that allowed for calculation of the center of gravity. Once the center of gravity was calculated, a study on under garage sizing and placement was made in which the team chose a tricycle configuration based on pros-cons and historical data. The main gears were then integrated in to these weight calculations based on a $15\,degree$ pitching criteria and the tip over angle criteria. The center of gravity and gear placement were iterated until conversion. Given an initial starting point with the power loading previously determined it was understood that two $100HP$ engines would have to be employed. An analysis on different engines was made. The Rotax 912S was chosen based on its low weight, low cost and fuel consumption. Position of the engines was mainly determined by the diameter of the propellers and the 6in clearance the propellers must have with the fuselage and its center of gravity with respect to the quarter chord of the wing. Center of gravity calculations and gear placement were iterated once the power plant was incorporated. Fuel calculations were made based on the specific fuel consumption and the range and a fuel tank designed.

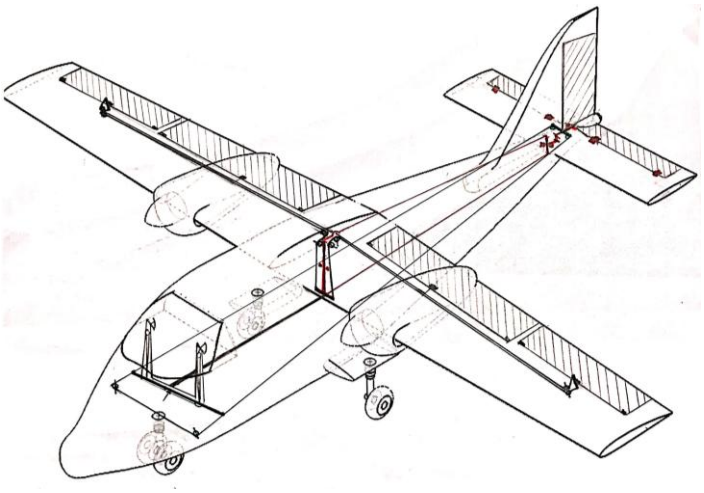

**Figure 2 - 21 Combined Layout of the Control System**

A flight envelope was determined. A variable pitch rate exploration was made via propeller blade analysis. It was concluded that a supercharger (an exterior add-on compressor connected directly to the engine and powered by the engine) was needed to increase power without increasing RPM. It is important to note this may not meet FA regulations. In order to meet longitudinal stability horizontal tail areas was iterated in order to insure a 10% static margin and *c.g.* and gear placement iterated as a result. Distinct control systems layouts were researched and a reversible flight control system was chosen. Drag calculations and drag polar was calculated utilizing drag component method. Wingspan loading was determined. Performance on the mission profile stages was determined to ensure requirements were met. A solid works model was created and used to depict the control system lay out as seen in **Figure 2 – 2** and a conceptual interior structure layout as seen in **Figure 2 - 3**.

A synthesis code was created which allowed the atomization of most of the design process by inputting geometric values. This code was used to construct a carpet plot for our aircraft and determine our most desirable geometry and necessary engine horsepower. A carpet plot was the way to see which geometries could be used for the aircraft that would allow it to complete its required mission. For the construction of a carpet plot the aircraft was evaluated at each segment of the mission profile for different geometries and wing loadings. The main segments of the mission that were evaluated were climb, cruise, and decent because those segments made up the most of the total mission range and also used the most amount of fuel. At each of these segments the fuel consumed was calculated to get the total amount of fuel need to use in order to complete the mission. For each point on the carpet plot a taper ratio and aspect ratio were picked to be use for calculations as almost all characteristics of the aircraft changed with the geometry of the wing and was checked to see if it was possible to complete the mission. For every geometry evaluated, the fuel necessary was found and from that the lowest possible take off was obtained by combining the weight of the airplane from that geometry and the weight of the total fuel required to fly the mission. It was important to determine the geometric combination that would yield the lowest takeoff weight since this was related to the lowest cost. While creating the carpet plots it was made sure that the geometry met basic mission requirements such as minimum stall speed and minimum cruise speed. After initial calculations and performance checks it was determined that it was not possible to meet cruise speed requirement of 140 knots no matter what geometry was used as long as the Rotax engine with a maximum of 100 hp was used. Because of this the supercharged version of this engine was used, which had a maximum horsepower of 132 hp. With the use of this engine, the cruise speed requirement was met for almost every geometric variable considered and the new constraint of the carpet plot was that of the minimum stall velocity. With this in mind the carpet plots were constructed for different wing loadings to see which geometric parameters were most desirable for this mission. The final product of the carpet plots for several wing loadings and varying taper and aspect ratios are shown in **Fig. 2-4**.

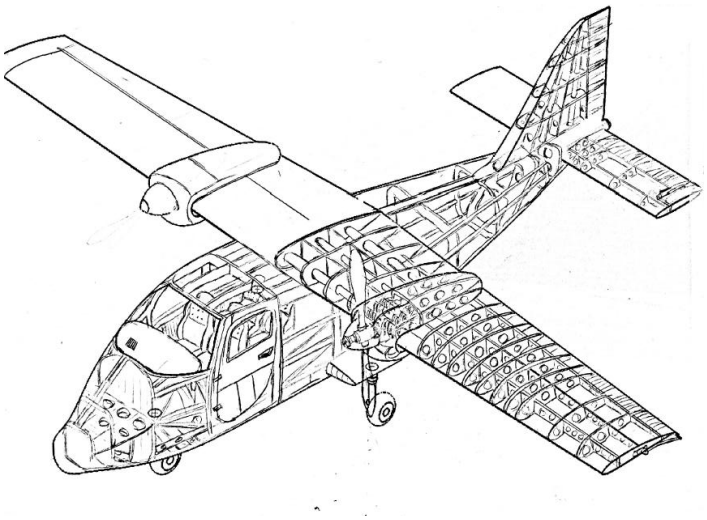

**Figure 2 - 33 Conceptual Interior Structure of Aircraft**

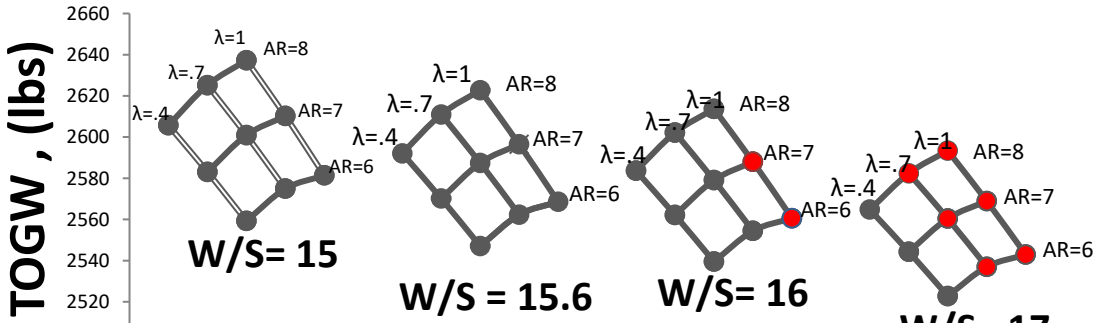


**Figure 2 - 42 Carpet Plots of Aircraft for Varying Wing Loadings**

The carpet plots above showed what type of geometries was possible for several wing loadings. The points that were marked in red were the geometries for which the aircraft did not meet the minimum stall speed requirement but could still complete the mission otherwise. The structure of the aircraft was taken into consideration when picking the final geometry, which affected the center of gravity. The point chosen was for a wing loading of 15.6, a taper ratio of .67 and an aspect ratio of 7. This point was not optimal, so it was not the very best geometry in terms of weight; however, all the requirements were met by a decent margin.

### Final Design Performance

Once final geometry was obtained, the performance analysis was repeated from the preliminary design and was made sure that this final design met all the requirements that were needed. In going through these calculations new values were obtained for things such as the required takeoff distance and the service ceiling. The calculated values for all mission requirements are shown in **Table 2 - 1**.

**Table 2 - 1 – Calculated values corresponding to mission requirements for final design.**

| | | | | |
|---|---|---|---|---|
| TakeOff Distance | | | | |
| 1380.691 | ft. | ≤ | 1500 | ft. |
| Cruise Speed | | | | |
| 146.4685 | kts | ≥ | 140 | knots |
| Dry tank Range | | | | |
| 893.7308 | nm | ≥ | 725 | nm |
| Landing Stall | | | | |
| 46.43625 | kts | ≤ | 48 | knots |
| ROC OEI | | | | |
| 263.7242 | fpm | ≥ | 250 | ft/min |
| Service ceiling | | | | |
| ≈23000 | ft. | ≥ | 15000 | ft. |

From the above table, all the mission requirements were met by the final design and it was determined that the aircraft designed performed well in all areas of the mission. Next, the center of gravity envelope (potato plot) was created to ensure the aircraft *c.g.* maintained well within that range. However, this was not possible and a solution was proposed, increasing the horizontal tail area. Due to time limitations, the proposal was not carried out. This concluded Level-1 of the preliminary design process. For further detail on each one of the processes listed in this section reference previous report[1].

## III. Preliminary Design – Level 2

Spring semester was focused mainly on conducting a level 2 preliminary design, calibrating the synthesis code created former semester, research hybrid electrical-propulsive engine technology, and implement that technology on the aircraft. In order to calibrate our synthesis code a CAD model of the Tecnam P2006T was created in order

to run CFD and obtain a $Cd_o$. This portion of the report takes the reader through that process and the details learned through the same.

## Lofting & Refining the Design

The first task of I.A.D (Innovative Aerospace Design) was to use a lofting software to recreate a three-dimensional representation of the Tecnam P2006T. It was decided to use the Tecnam P2006T because of its conventional configuration and its similar mission statement. The first step taken to loft a replication of the Tecnam P2006T was to acquire its dimensions by having a front, top, and bottom sketch representation. This was acquired by researching Tecnam's website and can be seen in **Figure 1**. The software used to create the three-dimensional representation of the aircraft was SolidWorks.

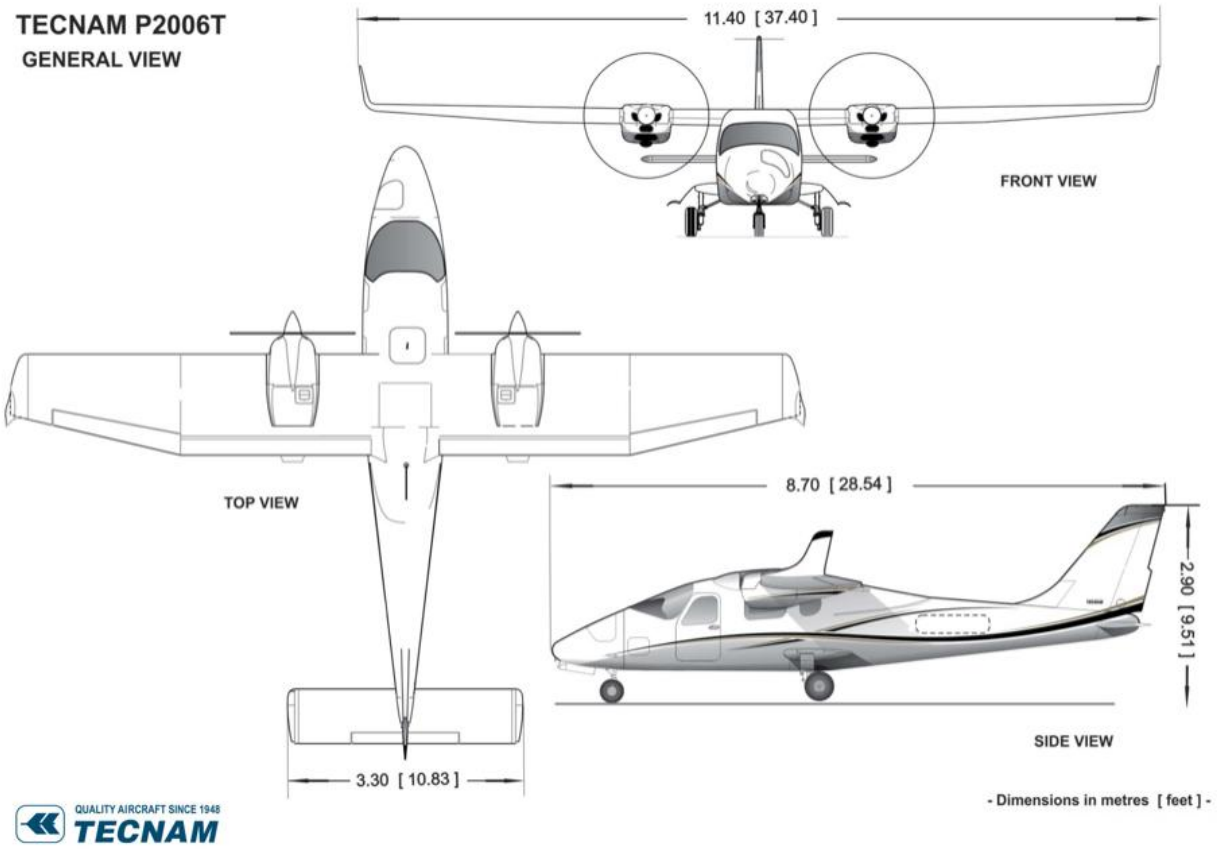


**Figure 1. Tecnam P2006T General View.**

To create the 3D aircraft in SolidWorks individual parts where first created with the dimensions given and the airfoil obtain from the Tecnam manual which is the NACA 63A. The main wing was created using the top view of the Tecnam's scale drawing. By using splines and tracing the top view into SolidWorks I.A.D was able to create the Tecnam's tapered main wing and can be seen in **Figure 2**. This model was scaled and was used as an accurate representation for the aircraft.

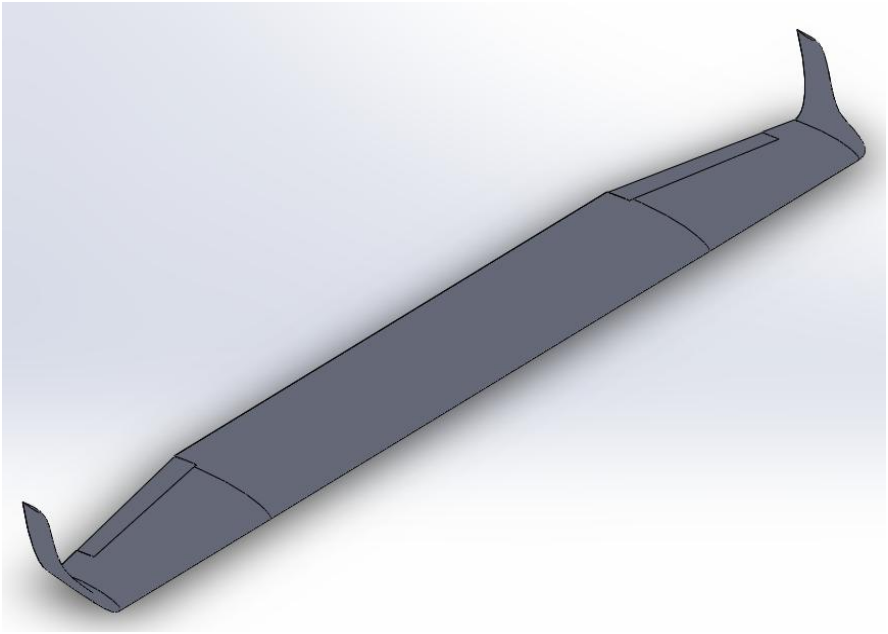

**Figure 2. Tecnam P2006T Main Wing 3D Model.**

The process was continued by creating three-dimensional versions of the fuselage, horizontal wing, vertical wing, gear slots, and nacelles in SolidWorks and can be seen in **Figure 1A-5A** in the appendix. These individual components where than put together in an assembly through SolidWorks and can be seen in **Figure 3** below. The three-dimensional model was required mainly to obtain CFD (Computational Fluid Dynamics) calculations for the aircraft and was given to the Aerodynamic Lead Engineer. After a few attempts to mesh the assembly model in the CFD software it was concluded that the assembly was not capable of meshing because of geometric conflictions. The details of why the assembly three-dimensional model was not able to mesh will be given by the Aerodynamic Lead Engineer. Although the Tecnam P2006T assembly model was ultimately not use for CFD calculation the individual components where used to acquired different deflection angles CFD data for the flaps, ailerons, rudder, and elevator of 0, 2, and 4 degrees of deflection and will be further explained by the Aerodynamic Lead.

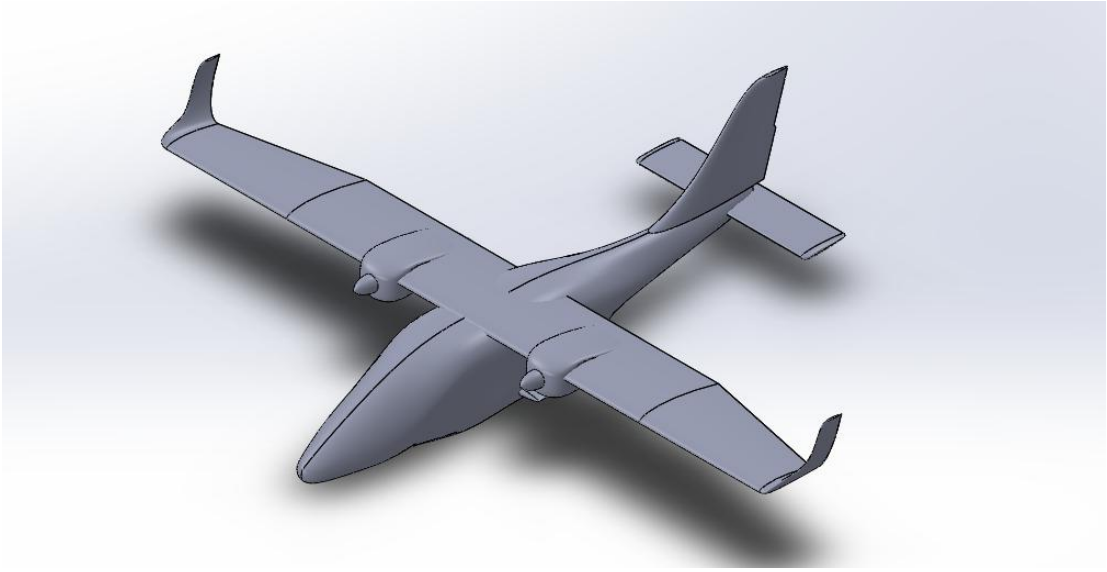

**Figure 3. Tecnam P2006T Assembly 3D Model.**

Since the assembly model created was not able to mesh and used to acquire the CFD data a new model was needed to be created as a single part. This meant that solid materials overlapping affected the meshing so lofting the outside layer and body of the aircraft into a single part would fix the geometric problem. Lofting the whole aircraft into a single part was a bit more complicated to developed. The first step of lofting the Tecnam P2006T was to insert the three scale views into SolidWorks and align them together to create the most accurate representation of the aircraft. The form in which the aircraft was lofted can be seen in **Figure 4** where all views are align to create a lofting method that would display the Tecnam P2006T as accurately.

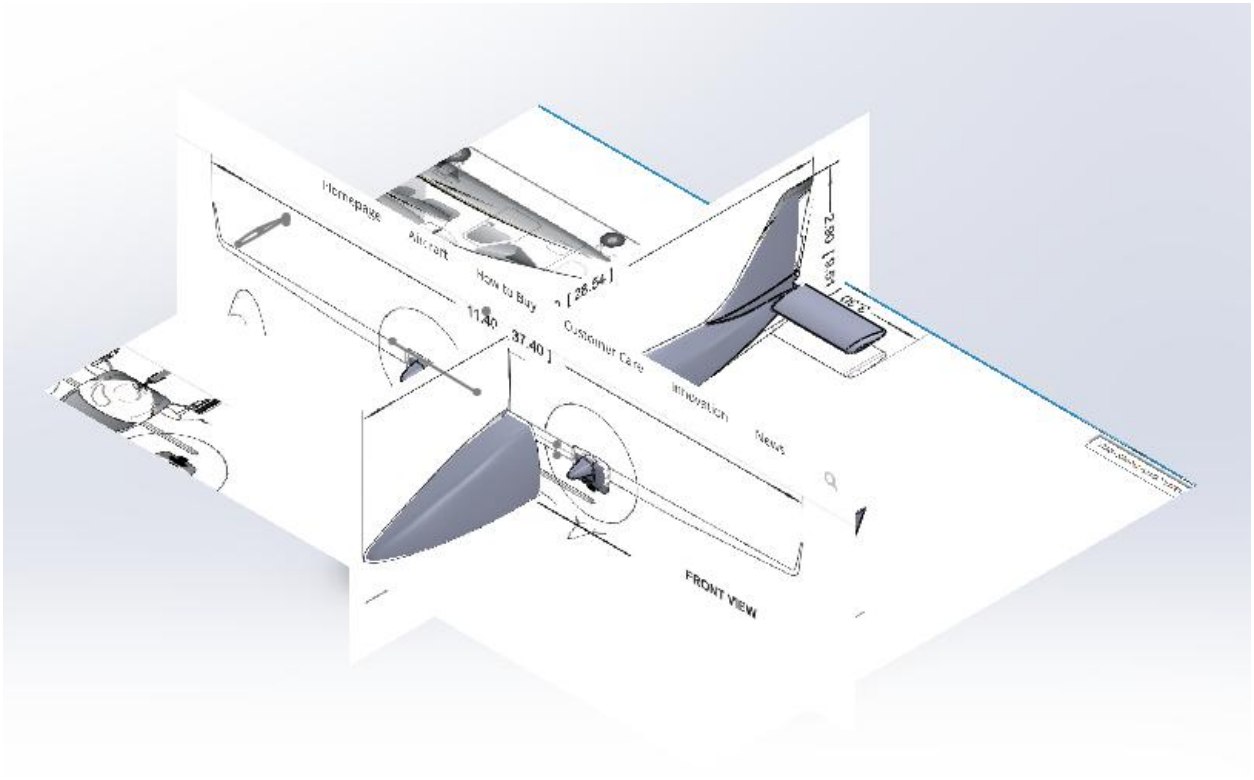


**Figure 4. Lofting Method Used to Create the Three-Dimensional Model.**

The first part that was lofted of the aircraft was the fuselage using the top ant front view to create a lofting profile from nose to tail. Furthermore, after completing the fuselage the main wing was created using the top view and reference geometry planes through the y-axis. The horizontal tail was also created by suing the top view and airfoil as seen in **Figure 4**. The vertical tail was created with the side view and airfoil with a vertical loft. After, creating the main parts of the aircraft the nacelles and gear slots where created using reference planes and the displayed views. Since the fuselage and the main wing was already created the nacelles and gear slots where easily added and placed with respect to the scale drawings. The final lofted representation of the Tecnam P2006T can be seen in **Figure 5**. This model was then transfer to the Aerodynamic Lead Engineer for further analysis using CFD software's and will be further explained in detail by the Aerodynamic Engineer.

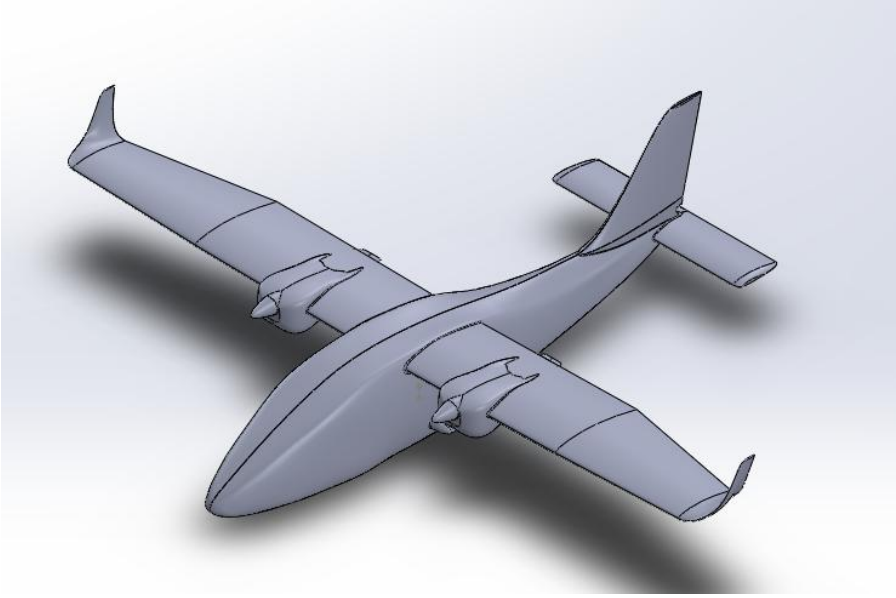

**Figure 5. Final Loft Model of the Tecnam P2006T.**

## Structural Design of Spars, Ribs, and Skin of the Aircraft.

The next step in structural design was to illustrate the capability of sizing the spars, ribs, and skin of the aircraft using the CDF data acquired from the three-dimensional model. To display the capability of designing the spars only one spar was needed to be design of the aircraft. It was decided to size the main wing's spar of the aircraft using the CFD data. The first step was analyzing how the forces acted upon the aircraft. From Structure Statics, it was known that spar was subjected to upward bending loads due to lift force. Also, downward bending loads while stationary on the ground dude to the weight of the structure. Drag loads also influenced the wing's structure due to airspeed and inertia. Rolling inertia loads and chord wise twisting loads due to aerodynamic effects where not considered. The spar cups are known to be subjected to bending loads while the web of the spar is subjected to shear load witch help in figuring out how to size them. To verify the CFD data it was known that the lift of the aircraft had to equal the weight of the aircraft and that the load throughout the wing should be in an elliptical fashion as shown in **Figure 6**.

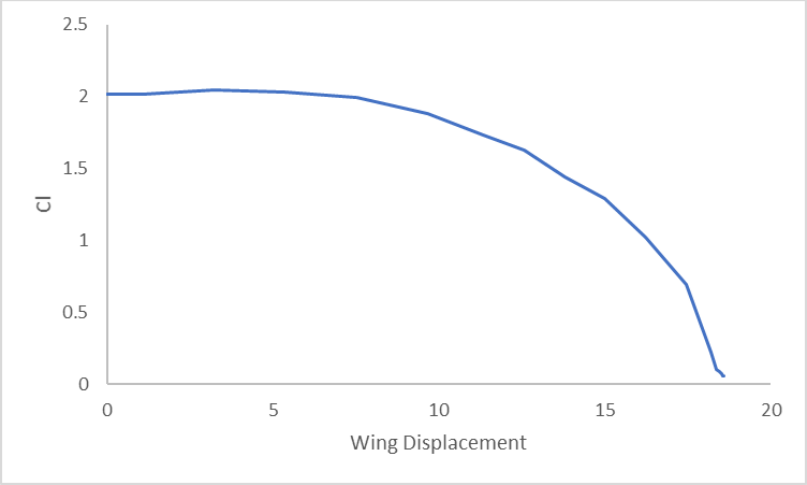


**Figure 6. Wing Loading of the Tecnam's Main Wing.**

Once the wing loading was confirmed to be an elliptical loading it was concluded that the CFD data was giving reasonable data. What was needed to size the spar of the aircraft was only the coefficient of lift raw data. The first step was to multiply the raw coefficient of lift with the ultimate loading factor to get the actual coefficient of lift. After this lift was needed to be calculated to see if the total lift of the wing equaled the weight.

$$\text{Lift} = Cl*q*S \tag{1}$$

CFD data gave the coefficient of lift throughout the chord of the wing from 0 to 4.56533 ft. To calculate the total lift produced by the entire wing numerical integration was needed to be applied to calculate the area under the Lift curve. This was determined by using trapezoidal integration by determining the effective area of each trapezoid under the curve.

$$S = (Chord_2-Chord_1)*(Yavg_2-Yavg_1)/2 \tag{2}$$

Using this **Equation 2** to calculate the effective area the lift of the aircraft throughout the wing was calculated by using **Equation 1**. Once the lift was known throughout the wing than the total lift was calculated and gave a total lift of 1295.4075. This did not equal the weight of the aircraft but we knew the loading of the wing was elliptical so a scale factor of 2.00709 was implemented of the coefficient of lift data to acquire the right wing loading to obtain a lift of 2600, which is the weight of the aircraft. Once the coefficient of lift was optimized the correct lift was determined using the same process as before with **Equations 1** and **2**.

Once the lift was lift was calculated than a material for the spar was needed to be chosen to acquire its properties and calculate the correct loads that can be applied to the material. Aluminum 6061 was chosen to design the main wing spar with properties of,

Shear Strength = 30,000 psi
Ultimate Strength = 45, 000 psi
Young's Modulus = 10,000 ksi

Knowing the shear strength and Ultimate strength the allowable shear and stress was calculated, since the factor of safety for aircraft is commonly used as 1.4 dividing this by the maximum load of the material before getting into the elastic region gives a limit needed to maintain the material from deformation.

Allowed Shar = shear strength / 1.4 = 21,429 psi

Allowed Stress = Ultimate strength / 1.4 = 32,143 psi

Once the material was known shear load throughout the aircraft was calculated by summing the lift of the aircraft throughout the wing giving the shear at each location of the wing. Furthermore, the moment was also calculated by using the lift force throughout the wing times an increment of distance to acquire the specific moment throughout the wing.

$$\text{Moment} = \text{Force} * \text{Distance} = L*D \tag{3}$$

The specific moment gave a moment at a certain distance of the aircraft main wing but to obtain the moment force applied at each position of the wing than the moments where added from tip of the wing to the fuselage respectively. For example, the tip is only subjected to the moment at the tip, but the end of the wing is subjected to all the moments on the wing.

To calculate the dimensions of the spar of the main wing than an I-beam equation was taken to divide its components into the caps and the web since both are subjected to several types of loads. The Caps are mainly subjected to bending loads while the web is mainly subjected to shear load. This is the assumption made to calculate and design the main wing spar. The first step taken was calculating the web height throughout the wing and this was possible since the geometry of the wing was known. Once the height was known the web thickness was needed to be calculated and this was possible by taking the shear loading and dividing it by the allowed shear stress times the height of the web and multiplied by 1.5 which gave an average of the actual web thickness as seen in **Equation 4**.

$$\text{Web Thickness} \approx \tau / (\tau avg * \text{Web height}) * 1.5 \tag{4}$$

After calculating the web height and thickness there was still too many unknowns to calculate the I-beam dimensions as seen in **Figure 7** and **Equation 5**. The height of the web was calculated and the thickness of the web but the length of both caps and height was still unknown. For an I-beam, there is a common structural rule that the base length of the cap should be 10 time the height. Using this common rule another unknown was taken out of the equation leaving the height of the caps as the only unknowns. The caps where calculated separately since they weren't going to be design as equal entities. The main Wing is subjected to stronger compression loadings than tension loading and since the top cap is mainly subjected to compression and the bottom cap in tension sizing them differently would save material and decrease the weight.

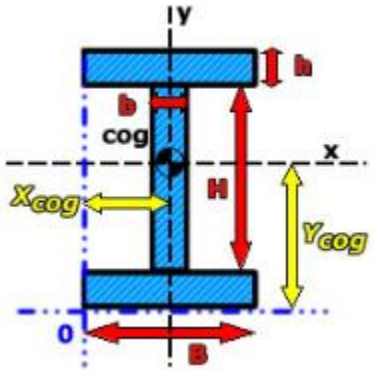


**Figure 7. I-beam representation**.

$$I_{xx} = H^3b/12 + 2[h^3B/12 + hB(H+h)^2/4] \quad (5)$$

Using the bending stress equation, the moment of inertia was calculated throughout the wing since the moment, allowable stress and height of the beam was known and can be seen in **Equation 6**. Knowing the moment of inertia applied throughout the main wing the height of the upper cap could be determined. The method of determining the height of the cap was to use Goal Seek in Excel to obtain a difference of 0 from **Equation 5** and **6** with the input being the height of the cap.

$$\sigma_{bending} = M*H/I \quad (6)$$

This process was repeated to obtain the bottom cap height with the only difference in the coefficient of lift being multiplied by the negative ultimate loading factor. The positive loading factor was used for the top cap while the negative loading factor was used to calculate the bottom cap. The web height, web thickness, top cap height, and bottom cap height can be seen in **Table 1** throughout the wing.

**Table 1. Main Wing's Spar Dimensions**

| Yavg | Web Hight, in | Web Thickness, in | top Falange, in | Bottom Falange, in |
|---|---|---|---|---|
| 0 | 7.68 | 0.067539062 | 0.648597735 | 0.423678111 |
| 1.07295 | 7.68 | 0.062761009 | 0.646942015 | 0.422567017 |
| 3.22155 | 7.68 | 0.057982955 | 0.645277839 | 0.421452541 |
| 5.37016 | 7.68 | 0.0482734 | 0.631539794 | 0.412258525 |
| 7.51876 | 7.68 | 0.038660792 | 0.60319238 | 0.393315356 |
| 9.66736 | 7.68 | 0.029215121 | 0.558185543 | 0.363317892 |
| 11.34605 | 7.684044676 | 0.020997299 | 0.501359159 | 0.325808601 |
| 12.56727 | 7.242931606 | 0.015218152 | 0.445668356 | 0.289223754 |
| 13.78843 | 6.871414648 | 0.011338659 | 0.396914217 | 0.257277895 |
| 15.00952 | 6.499917465 | 0.007850374 | 0.340621378 | 0.220407412 |
| 16.23052 | 6.12844462 | 0.004656554 | 0.271197685 | 0.175011748 |
| 17.45141 | 5.757002197 | 0.002096236 | 0.188519376 | 0.121181176 |
| 18.18027 | 5.460420507 | 0.000325656 | 0.077676598 | 0.049606825 |
| 18.36224 | 5.321871718 | 3.36438E-05 | 0.025545386 | 0.016405061 |
| 18.44333 | 5.281856958 | 1.12943E-05 | 0.015011207 | 0.009589959 |
| 18.51147 | 5.259157183 | 5.66715E-06 | 0.015011207 | 0.008751315 |
| 18.55771 | 5.241758535 | 2.38242E-06 | 0.015011207 | 0.005987692 |
| 18.58085 | 5.231204958 | 6.62289E-07 | 0.015011207 | 0.003660582 |

The next step in structural design was to size the skin of the wing. It was known that the skin of the wing was subjected to twisting and CFD data gave the coefficient of moment throughout the wing. Using the coefficient of moment, the Moment was calculated using **Equation 7** as seen below.

$$Moment = Cm*q*S*c \quad (7)$$

After calculating the moment, the torque equations where needed to be used to calculate the thickness of the skin using **Equations 8** and **9**. In both equations the only unknowns where the thickness of the skin. The Modulus of Rigidity, G = 4 E 6 psi for aluminum 6061, $\theta = 0.0055$ rad/in and this was chosen so that the entire wing of the aircraft equaled 1 degree of twist allowed. The main spar of the wing was known using Roskam to be at 15 to 30

percent of the chord and was decided to be placed 25 % of the chord. Since every element was known and the thicknesses of the spar was known the only left unknown was the thickness of the skin.

$$T = G*J*\theta \tag{8}$$

$$T = 2*A_1*t_1*\tau + 2*A_2*t_2*\tau \tag{9}$$

Using the airfoil of the Tecnam the areas and parameters where able to be obtain at the fuselage to be,

$A_1$= 66.23 $in^2$
$A_2$=190.29 $in^2$
$S_1$=26.92 in
$S_2$=76.6 in
$S_{12}$=7.68 in

Using the chord the areas and parameters of where calculated throughout the wing. The unknowns and the knowns can be seen in **Figure 8**. Once the geometry was known the von Mises yield criterion was finally able to be calculated and can be seen in **Equation 10**. This was also calculated throughout the entire wing and since only the skin thicknesses where left as unknowns both torque equations where able to be solve simultaneously using Goal Seek in Excel. The values of the skin thickness can be seen in **Table 2**.

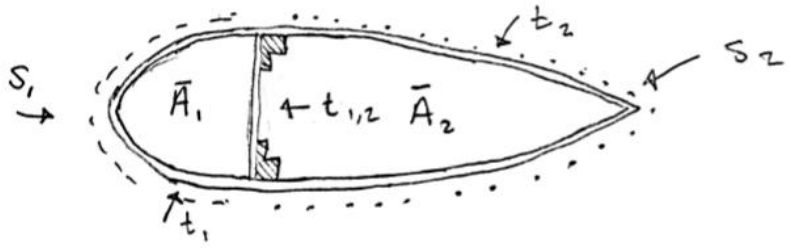


**Figure 8. Wing Thickness Air Foil Model.**

$$J = 4*A^2/(\int ds/t) = 4*A_1^2/(S_1/t_1+S_{12}/t_{12}) + 4*A_2^2/(S_2/t_2+S_{12}/t_{12}) \tag{10}$$

**Table 2. Main Wing Skin Thickness Throughout the Wing.**

| Yavg | t1 | t2 |
|---|---|---|
| 0 | 0.101684 | -0.02082 |
| 1.07295 | -0.0657 | 0.037435 |
| 3.22155 | -0.06625 | 0.039984 |
| 5.37016 | -0.05865 | 0.03705 |
| 7.51876 | 0.100406 | -0.01514 |
| 9.66736 | 0.085355 | -0.01183 |
| 11.34605 | -0.03113 | 0.023607 |
| 12.56727 | 0.043829 | -0.00609 |
| 13.78843 | -0.00816 | 0.003922 |
| 15.00952 | -0.01102 | 0.008283 |
| 16.23052 | -0.00909 | 0.01233 |
| 17.45141 | 0.034718 | 0.000753 |
| 18.18027 | 0.005276 | 0.000217 |
| 18.36224 | 0.015075 | 0.000153 |
| 18.44333 | 0.024889 | 0.0001 |
| 18.51147 | 0.025679 | 0.0001 |
| 18.55771 | 0.016749 | 0.004 |
| 18.58085 | 0.023185 | 0.00543 |

After calculating the skin thickness the ribs were also needed to be size, but in this case the ribs are just supporting material for the skin of the wing and was not needed to be size. Instead only the amount of ribs required for the wing was needed to be obtain. Looking at the Tecnam P2006T manual it was concluded that the aircraft needed to have 19 ribs displaced for each side of the entire wing with a total of 38 ribs throughout. The displacement of the ribs can be seen In **Figure 9**.

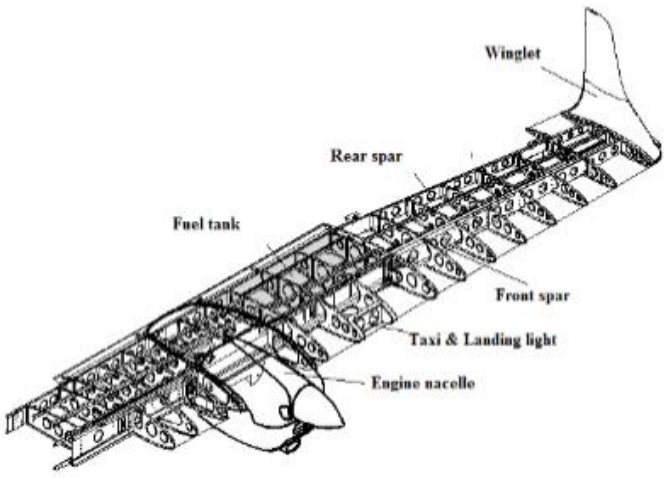


**Figure 9. Tecnam P2006T Wing Structure.**

One of the most important aspect of any aircraft design is the amount of drag it creates. This is because drag is a force that opposes the movement of an object. Lowering drag will lower the amount of power and energy needed to drive the aircraft forward. An accurate estimation of this is essential for the success and optimum of the aircraft. One of the way to calculate the drag of an aircraft is by using Computational Fluid Dynamics (CFD). CFD is a mechanic that uses numerical analysis and data structure to simulate how an aircraft would react in certain conditions. This simulation is not as accurate as a wind tunnel testing, but provides serviceable data at a very low to no expense. The TecnamP2006t was modeled and used in the CFD test. The results from this was used to calibrate a synthesis code. There are many programs out there that are capable of running this test, but each have their own complications and problems.

The first program that was used to run the CFD was Simflow. Simflow is a cutting edge, user friendly program that is more than capable of running CFD. The first step that was done in this program was establishing the mesh of the aircraft. Because the TecnamP2006T was modeled to be full size, it required a massive amount of mesh points. This, however, prove to be a problem because Simflow student edition was only capable of handling 100,000 mesh points. A solution to this could have been upgrading Simflow to the pro-version, but that would of cost 500$, which was out of our budget, so that was not possible. The other solution to this was to make the mesh size larger. This was done and can be seen in Fig. 1-1. This came with the issue that the mesh on the TecnamP2006T is not very smooth and jaggedly at the edges. This will create extra drag that otherwise would not have been there.

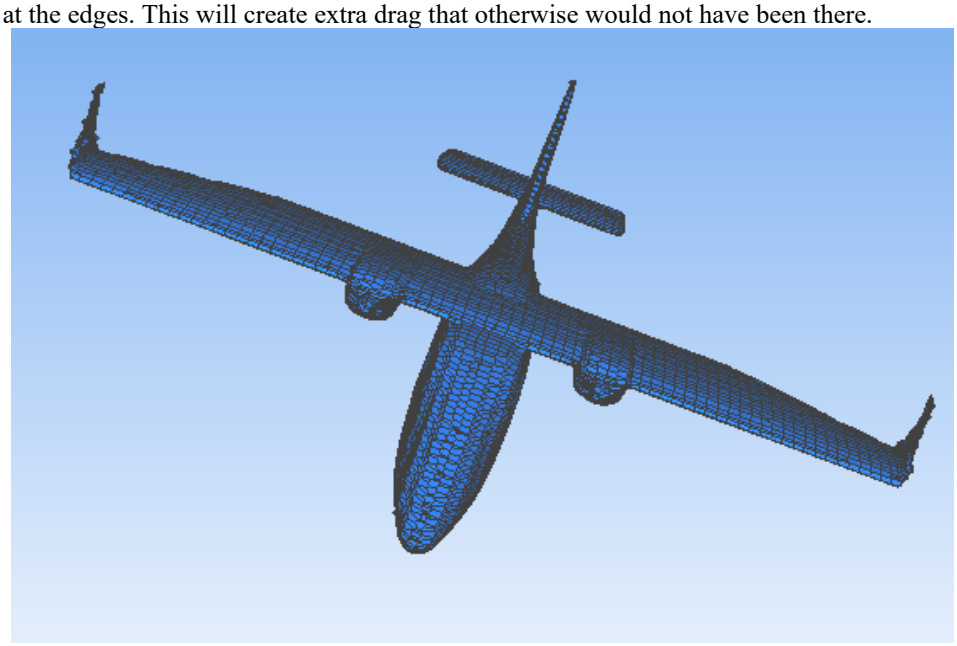

**Figure 1-1. SimFlow's Mesh for TecnamP2006T**

The second step in running the CFD was to establish the boundary. This was done by creating an enclosed space surrounding the aircraft. The enclosed box can be seen in Figure 1-2. The enclosed box may seem solid, but it is actually hollowed with the aircraft inside. The front was selected as an inlet with a velocity of 140 knots to simulate the TecnamP2006T speed at cruised, while the back was set as the open outlet. The other four walls of the enclosed box is set as solid walls. The simulation was run, but there was another problem that prevented this. SimFlow student edition did not support and provided the solutions that we needed. Once again, the only solution to this was to buy the pro-version, but that was beyond the budget. Another program was then chosen to carry out the task.

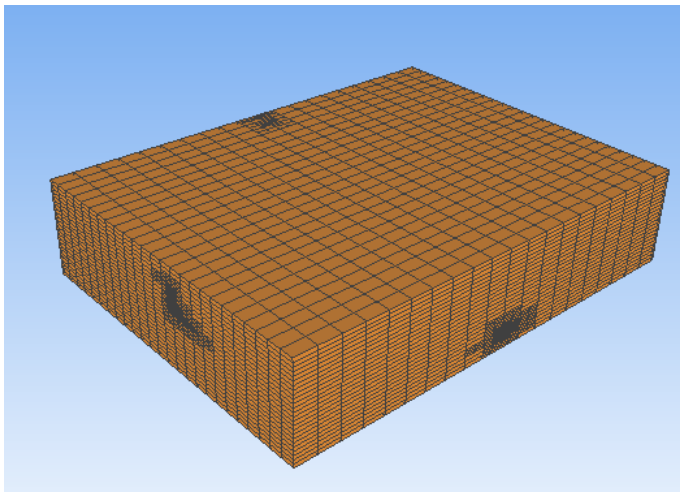

**Figure 2-2. SimFlow's Boundary for TecnamP2006T**

The second program chosen to run the CFD was ANSYS Fluent. ANSYS Fluent worked very similar to that of SimFlow. The aircraft model was imported to the program, and an enclosed box was created surrounding the aircraft as seen in Fig. 2-3. This will be where the controlled environment will be located. A mesh was then generated for the aircraft and the enclosed box. This, however, produced a solid enclosed box as seen in Fig. 2-4. Fig 2-5 shows how the meshes of the interior of the enclosed box with the aircraft by using wireframe view. This mesh is very refine and should provide a very accurate results when the CFD is computed. Airspeed of 140 knots was inputted at the inlet to simulate the cruise speed that the TecnamP2006T would be traveling at during cruise speed. There was a problem that occurred when the CFD was run. This time, the program was not the issue, but the computer itself. The computers that were used to run the CFD did not have high enough spec and drive required for the task. This then forced us to move onto a new program because there wasn't a reasonable solution to this problem.

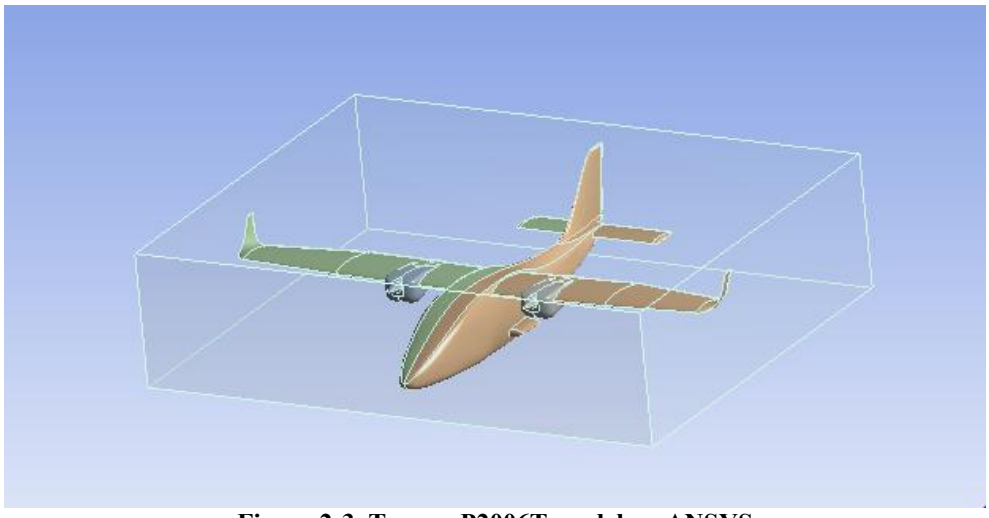

**Figure 2-3. TecnamP2006T model on ANSYS**

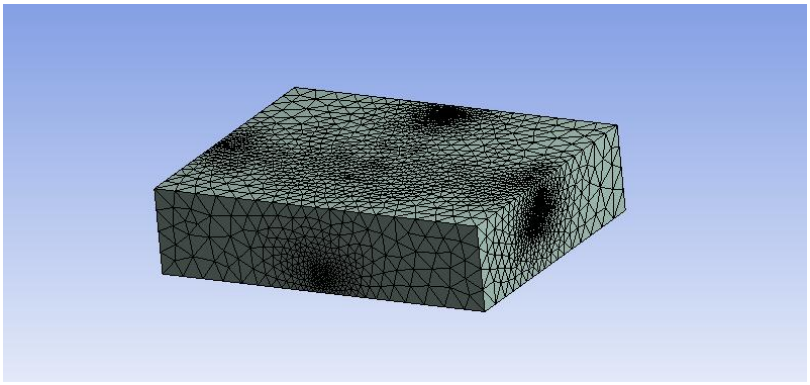

**Figure 2-4. TecnamP2006T Enclosed Mesh**

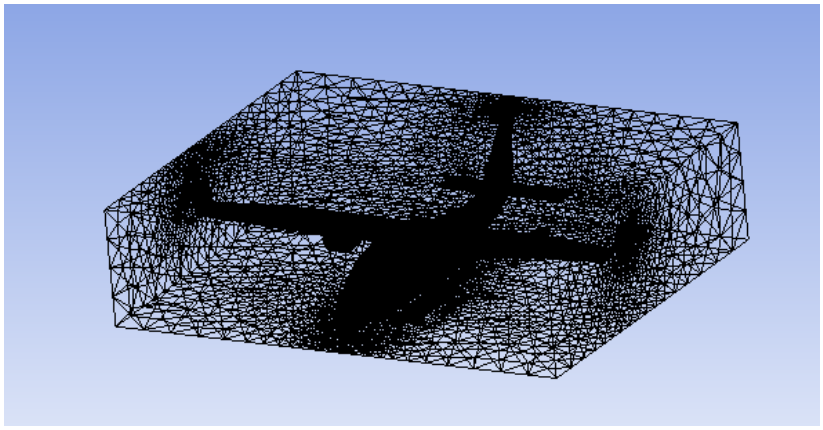

**Figure 2-5. Wireframe View of TecnamP2006T Enclosed Mesh**

The third program chosen to run the CFD was SolidWorks Airflow Simulation. SolidWorks has a built in feature to simulate flows and calculations using the model that was create rather than making a mesh out of the model. The following conditions were set for the simulation:

- Mission Phase Considered: Cruise
- Aircraft configuration: Clean
- Freestream velocity: 140 knots or 236.3 ft/s
- Altitude: 7500 ft
- Temperature: 32.273 Fahrenheit
- Pressure: 1602.23 lbs/ft$^2$

Once the simulation was ran, a contour of the pressure distribution of the TecnamP2006T can be seen in Fig.2-6. It can be seen that the pressure on the lower portion of the aircraft's wing is greater than the upper portion. This is because the air under the aircraft is slower but has higher pressure, while the air on the upper surface of the aircraft has faster air but lower pressure. The difference in this pressure generates lift that allows the aircraft to fly. The difference in the speed of the air stream can also be seen in Fig. 2-7. The air speed on the upper surface of the wing is greater than the air speed on the lower surface of the wing.

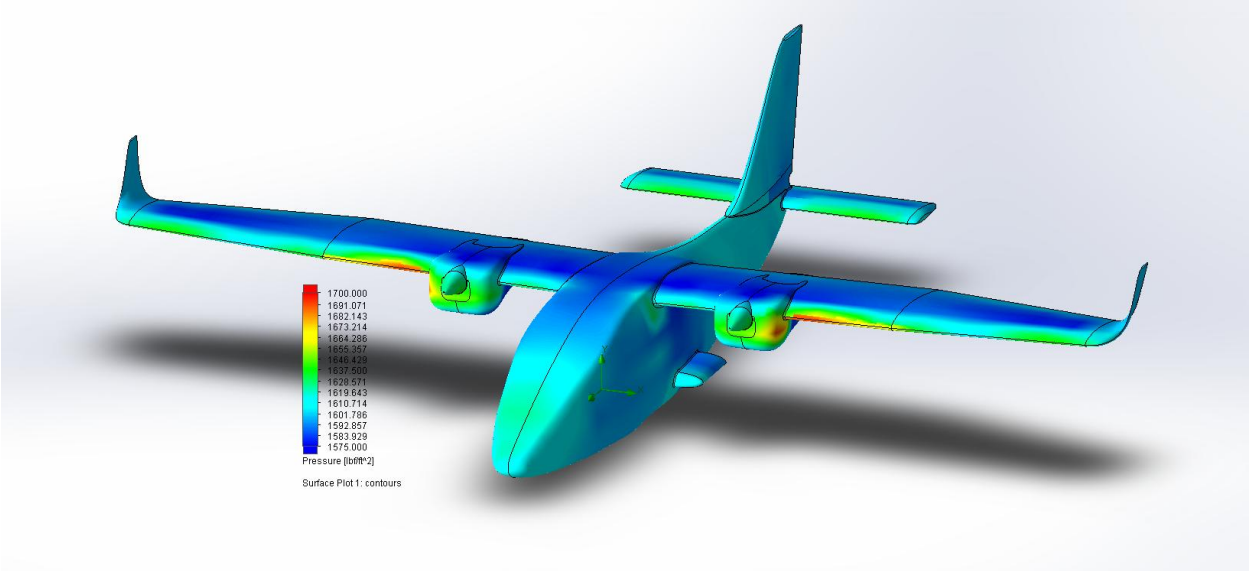


**Figure 2-6. Pressure Distribution**

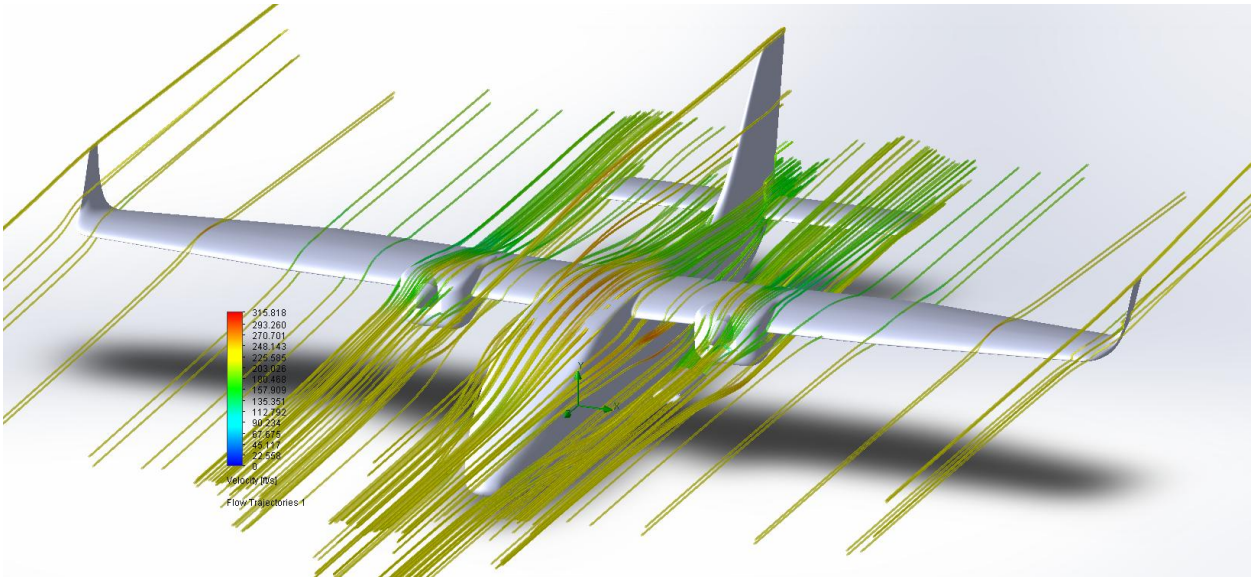


**Figure 2-7. Velocity Streamlines**

On top of seeing the pressure and velocity streamlines distribution, the CFD from SolidWorks also provides forces acting on different directions of the aircraft. Table 1-1 provides results from the CFD test. The drag force was found to be 1225.58 lbf along the Z-direction. The coefficient of drag was then found by using Equation 1-1. The density is .001897512 slugs/ft$^3$ at the altitude of 7500 ft. The reference area in this case is the wetted area of the aircraft which was found to be 919.22 ft$^2$. The velocity is the speed at cruise which is 236.3 ft/s. Plugging these values into Equation (1-1) yield a $C_{Do}$ of .0252.

$$C_D = \frac{D}{\rho A V^2/2} \qquad (1\text{-}1)$$

The lift can also be found by looking at the force in the Y-direction. This value was found to be 1328.58 lbf. This value is very absurd because the aircraft weighs approximately 2630 lbs, so at cruise, the lift should be equal to this

weight to keep the aircraft in place. This is also approximately half of what the value should be. The force in the X-direction is close to zero because there shouldn't be any forces coming from the side of the plane when the airstream is only going from the front of the plane to the back. The torque represents the moment that is created on the aircraft. The torque acting on the X-axis is largest because that is the tilting force pushing the aircraft up and back. Overall, the data accuracy ranges from case to case, but the drag force found seems very accurate to the $C_{Do}$ of the TecnamP2006T. Wanting to test the accuracy of this drag and the need for the stability derivatives, another CFD program was used.

**Table 1-1. SolidWorks CFD Results**

| Goal Name | Unit | Value | Averaged Value | Minimum Value | Maximum Value |
|---|---|---|---|---|---|
| GG Av Dynamic Pressure 1 | [lbf/ft^2] | 52.24812534 | 52.24398993 | 52.23820857 | 52.24812534 |
| GG Force 1 | [lbf] | 1807.72026 | 1801.585418 | 1782.652866 | 1811.996252 |
| GG Force (X) 1 | [lbf] | -25.64695656 | -17.79317413 | -27.33768392 | -4.783129944 |
| GG Force (Y) 1 | [lbf] | 1328.585293 | 1316.241804 | 1294.317752 | 1331.867318 |
| GG Force (Z) 1 | [lbf] | -1225.583898 | -1229.946346 | -1235.18543 | -1225.54459 |
| GG Torque (X) 1 | [lbf*ft] | 4604.902015 | 4527.302504 | 4434.402998 | 4604.902015 |
| GG Torque (Y) 1 | [lbf*ft] | 336.5044078 | 263.0664749 | 191.1546109 | 340.4551435 |
| GG Torque (Z) 1 | [lbf*ft] | 235.4577989 | 80.2066055 | -102.9244938 | 235.4577989 |

The fourth and last program that was used to run the CFD was Open VSP. This program didn't allow for the import of the SolidWork model, so a custom model of TecnamP2006T was created using the software provided by Open VSP as seen in Fig. 2-8. This model isn't as accurate as the SolidWorks model, so there might was a slight difference in the data obtained. The CFD was ran at cruise condition at different angle of attack. For the drag of the aircraft, the data at 0 degree angle of attack was examine as seen in Table 1-2. For data of the aircraft at different angle of attack, see appendix for detail. The overall coefficient of drag of the aircraft was found to be .0254 which is very close to the coefficient of drag found through using SolidWorks. This prove that the TecnamP2006T coefficient of drag is approximately .0254. Using this value, the synthesis code can be calibrated. CFD was ran again for each component of the aircraft in order to determine how much drag each component contributes. The values of the flat plate drag for the TecnamP2006T can be found in Table 1-3 given to be equal to approximately 4.0496, which gives a $C_{Do}$ value of .0254. The synthesis code was then calibrated to match these values as closely as possible.



**Figure 2-8. TecnamP2006T Model from Open VSP**

**Table 1-2. TecnamP2006T CFD Results at 0 Degree Angle of Attack**

| Iter | Mach | AoA | Beta | CL | CDo | CDi | CDtot | CS | L/D | E | CFx | CFy | CFz | CMx | CMy | CMz | T/QS |
|---|---|---|---|---|---|---|---|---|---|---|---|---|---|---|---|---|---|
| 1 | 0.21 | 0.00000 | 0.00000 | 0.09960 | 0.02542 | 0.00316 | 0.02858 | 0 | 3.48503 | 0.11339 | 0.00316 | 0 | 0.0996 | 0 | 0.29617 | 0 | 0 |
| 2 | 0.21 | 0.00000 | 0.00000 | 0.09958 | 0.02542 | 0.00316 | 0.02858 | 0 | 3.48447 | 0.1134 | 0.00316 | 0 | 0.09958 | 0 | 0.29617 | 0 | 0 |
| 3 | 0.21 | 0.00000 | 0.00000 | 0.09957 | 0.02542 | 0.00316 | 0.02858 | 0 | 3.48415 | 0.11338 | 0.00316 | 0 | 0.09957 | 0 | 0.2962 | 0 | 0 |
| 4 | 0.21 | 0.00000 | 0.00000 | 0.09961 | 0.02542 | 0.00316 | 0.02858 | 0 | 3.48561 | 0.11348 | 0.00316 | 0 | 0.09961 | 0 | 0.29619 | 0 | 0 |
| 5 | 0.21 | 0.00000 | 0.00000 | 0.09961 | 0.02542 | 0.00316 | 0.02858 | 0 | 3.48556 | 0.11349 | 0.00316 | 0 | 0.09961 | 0 | 0.29619 | 0 | 0 |

**Table 1-3. Flat Plate Drag of TecnamP2006T**

| | $\Delta f_e$ |
|---|---|
| Fuselage | 1.200534596 |
| Wings | 1.349381346 |
| Horizontal Tail | 0.273932017 |
| Vertical Tail | 0.16038474 |
| Nacelles | 0.384318719 |
| Protuberances | 0.341148018 |
| Trim | 0.3 |
| Momentum | 0.04 |
| Total | 4.049699437 |

## Tecnam p2006t Propulsion Synthesis

Since the geometry of the final aircraft has been determined the previous synthesis code can be calibrated with the new data. Since it has been determined that a constant speed prop is being used the angle of attack of the propeller blades will vary with speed to maintain a constant rpm and optimal efficiency as shown with the following figures.

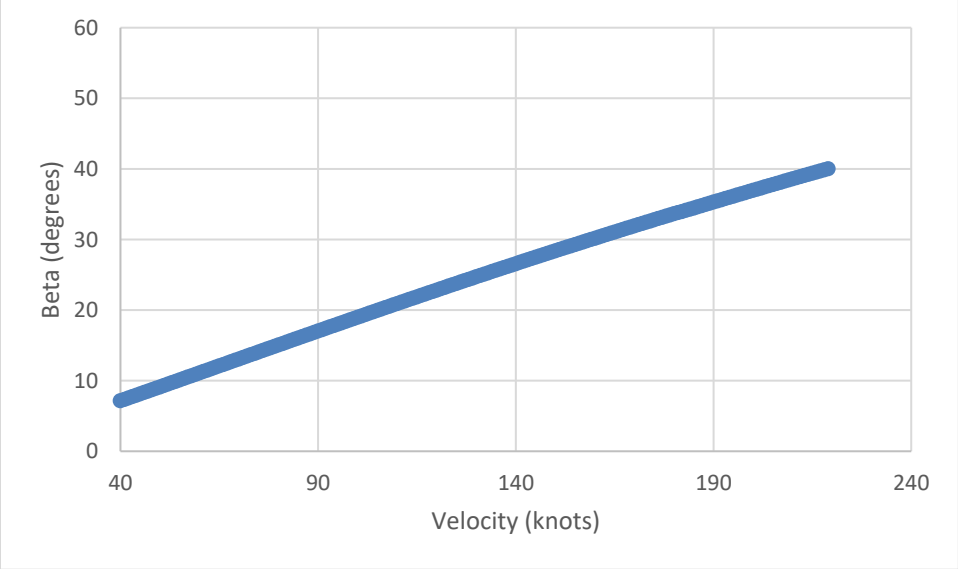


**Figure PROPTRQ - 1 Change In Propeller Angle With Aircraft Speed**

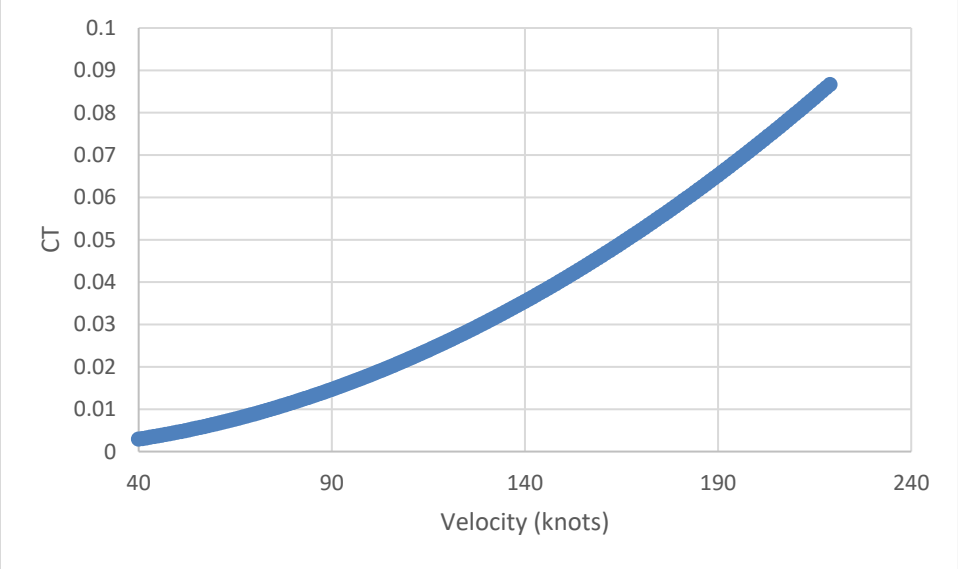


**Figure PROPTRQ - 2 Coefficient of Thrust at Cruise**

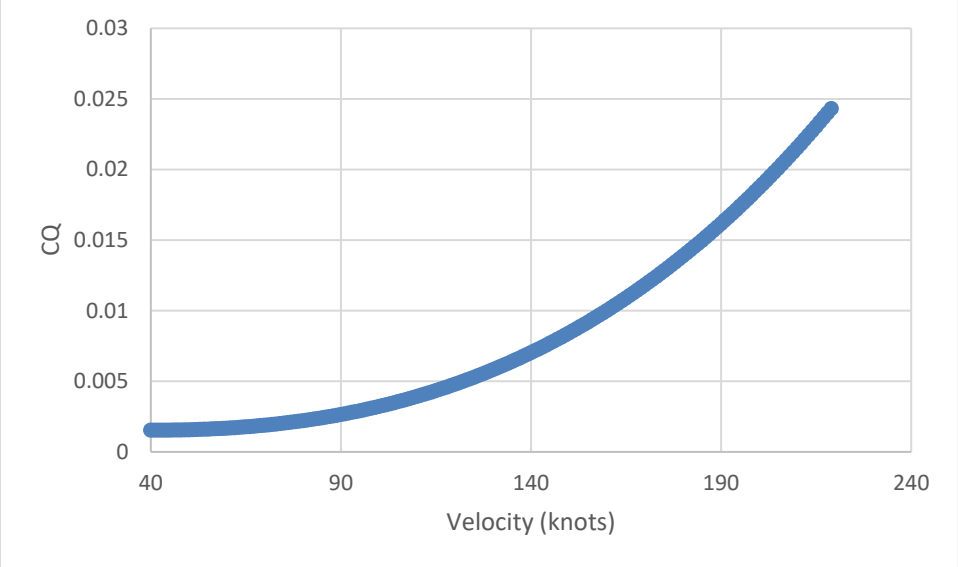


**Figure PROPTRQ - 3 Coefficient of Torque at Cruise**

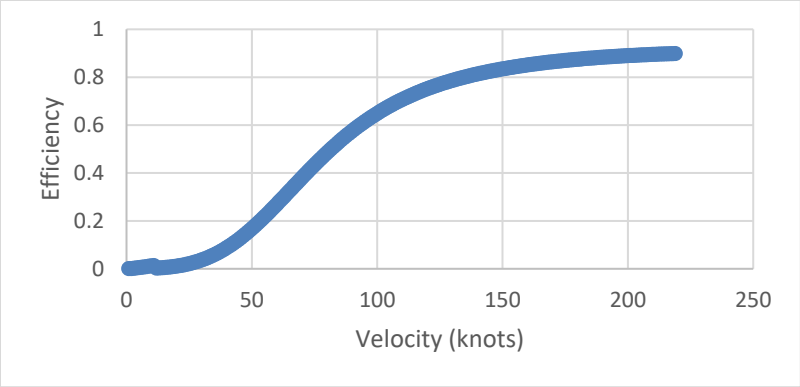


**Figure PROPTRQ - 4 Propulsive Efficiency Of Tecnam Propellers**

Using this data a spreadsheet of the power available, power required and rate of climb can be determined.

**Table PROPTRQ – 1 Speed/Power For Each Phase Along With ROC**

| | | | |
|---|---|---|---|
| | **Velocity climb** | 187.479 | ft/s |
| | **Velocity climb** | 111.0783078 | knots |
| | **ROC** | 900.6352576 | ft/min |
| | **ROC** | 15.01058763 | ft/s |
| | **Velocity Takeoff** | 101.34 | ft/s |
| | **Velocity Takeoff** | 60.04232856 | knots |
| | **Veclocity Cruise** | 236.46 | ft/s |
| | **Veclocity Cruise** | 140.0987666 | Knots |
| cruise | **Percent power needed for propeller** | 65.84524293 | |
| cruise | **Maximum Power available** | 162.5813548 | hp |
| cruise | **Power required** | 107.0389007 | hp |
| Takeoff | **Percent power needed for propeller** | 15.70069113 | |
| Takeoff | **Maximum Power available** | 53.67178197 | hp |
| Takeoff | **Power required** | 49.57599353 | hp |
| Climb | **Percent power needed for propeller** | 37.51259897 | |
| Climb | **Maximum Power available** | 142.2338017 | |
| Climb | **Power required** | 67.27226469 | |
| Landing | **Landing Speed** | 81.072 | ft/s |
| Landing | **Landing Speed** | 48.03386285 | knots |
| Landing | **Percent power needed for propeller** | 14.52552984 | |
| Landing | **Maximum Power available** | 29.70316722 | hp |
| Landing | **Power required** | 56.81204096 | hp |
| Descent | **Descent Speed** | 236.46 | ft/s |
| Descent | **Descent Speed** | 140.0987666 | Knots |
| Descent | **Percent power needed for propeller** | 65.84524293 | |
| Descent | **Maximum Power available** | 162.5813548 | hp |
| Descent | **Power required** | 107.0389007 | hp |

What this data shows compared with the speed requirement constraints is that the power percent of the engines needed to fly is 10% than the maximum 75% required, this shows that there is 10% of power room to still maintain the requirements even if there is non-ideal atmospheric conditions.

From that data the fuel consumption for the entire mission and the flight time can be determined now as shown below.

**Table PROPTRQ – 2 Flight Time and Fuel Used**

| | | | | |
|---|---|---|---|---|
| Warmup/taxi power percent | 0.2 | 5 | 0.072029609 | |
| Take off power percent | 1 | 1 | 0.121424607 | |
| Climb power percent | 0.8 | 2.7758185 | 0.193819172 | |
| Cruise power percent | 0.75 | 313.2295 | 19.11716543 | **Flt Time (min)** |
| Descent power percent | 0.6 | 5 | 0.20931964 | **323.005** |
| landing power percent | 0.3 | 1 | 0.021029669 | **Fuel used (lb)** |
| | | | 19.73478812 | **250.6318092** |

This data shows that the fuel used is almost 100 lbs. less than the maximum fuel that can be stored with an average 3 passenger and 3 luggage weight.

## Hybrid Research

Now that codes have been created to analysis the engine and propeller the next step is to take a leap of technology for alternative power solutions other than the standing fuel to internal combustion engine to propeller blades. The research in this report includes a hybrid propulsion system which includes the combustion system for the standard aircraft as well as an electric motor, battery system, and generator for recharging during flight. Given current technologies the new mechanical system analysis can be determined as shown in the following table.

**Table PROPTRQ – 3 Technology Constraints**

| Used in analysis | kW/kg | hp/lb | | Todays Tech | |
|---|---|---|---|---|---|
| Electric Motor | **4** | 2.4331087 | | ~ 3.75 - 5 | kW/kg |
| | kWh/kg | hp*hr/lb | | | |
| Battery Energy density | **0.5** | 0.3041386 | | ~ 100 - 250 | Wh/kg |
| | kWh/L | hp*h/in^3 | | | |
| Battery Volume | **0.6** | 0.0131852 | | ~ 250 - 620 | Wh/L |
| | kW/kg | hp/lb | | | |
| Generator output | **5.7** | 3.4671798 | | ~ 5.7 | kW/kg |

Knowing this, as well as a few other constraints shown below, a new weight analysis can be determined for any power requirement needed.

**Table PROPTRQ – 4 Weight Analysis For Hybrid Components**

| | | | | |
|---|---|---|---|---|
| Electric motor efficiency | **91** | % | from empircal data | |
| Electric motor Power output | **75** | kW | 100.5765 | hp |
| Electric motor weight | 18.75 | kg | 41.336625 | lb |
| battery efficiency | **99** | % | from empircal data | |
| Battery Capacity | **10** | kWh | 13.4102 | hp hr |
| Battery Weight | 20 | kg | 44.0924 | lb |
| % before charge | **50** | % | ~ 30-70 | % |

| | | | | |
|---|---|---|---|---|
| generator efficiency | 99 | % | from empircal data | |
| lapse rate | 0.8467 | 5000 ft | 0.7774 | 7500 ft |
| Generator Power required | 108.1695307 | kW | 145.0575041 | hp |
| Generator Weight | 18.97711065 | kg | 41.83731769 | lb |
| $\eta_{ELECTRONICS}$ | 0.891891 | | | |
| weight per engine added | 57.72711065 | kg | 127.2663427 | lb |
| Total Weight added | 115.4542213 | kg | 254.5326854 | lb |

Now knowing the constraints for the system a performance model of the aircraft can be calculated. As well as the increase in weight for this particular aircraft design being around 17%.

## Battery Performance

From the data and constraints in the previous tables the battery performance model can be calculated and coded. This is assuming the same mission flight time as the non-hybrid aircraft and the performance of charging and recharging is shown below with the internal combustion engine recharging at the 90% continuous engine power.

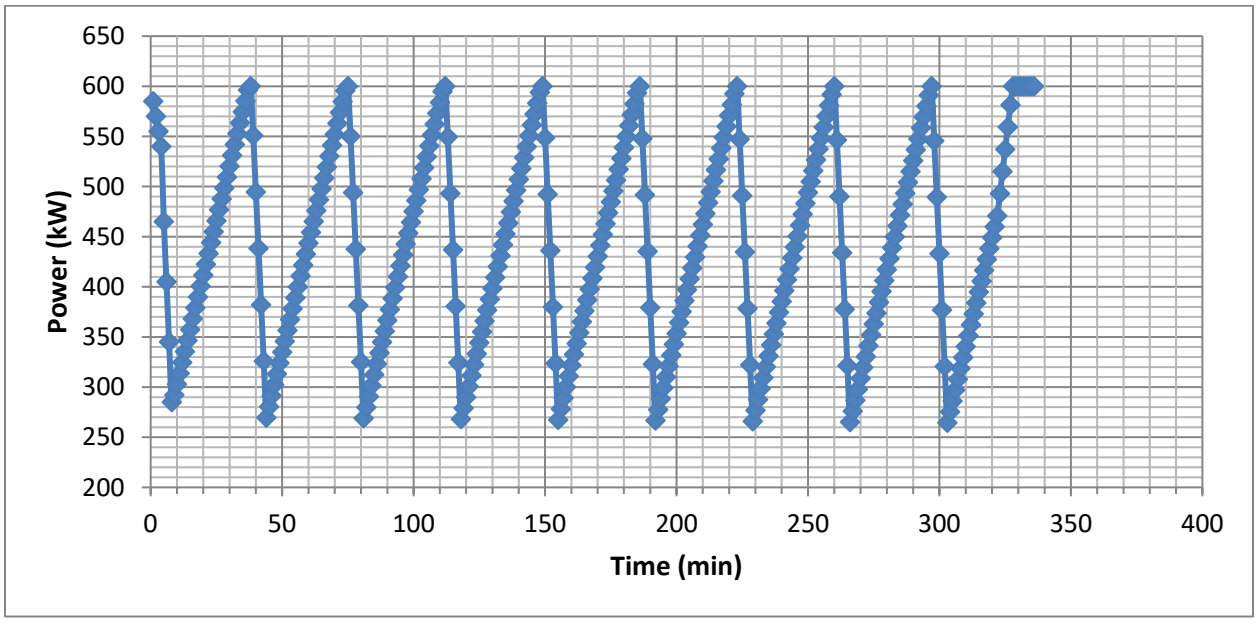


**Figure PROPTRQ - 5 Battery Cycling For Mission**

Now what this shows is the stored power inside the battery at any given minute during the entire phases of a flight with each single dot being 1 minute. What can be seen here is that with current battery technologies and the same type ICE engine that the recharge time is almost three times higher than the recharge, and that increasing the discharge time by adding more batteries will increase weight, while increasing the engine horsepower to decrease the recharge time is almost counter-productive in terms of a fuel efficient aircraft since a higher horsepower engine will increase the fuel consumption.

## Fuel Consumption

Since it has been determined that adding the electric components to the aircraft will increase weight and are borderline counter-productive in terms of recharging, so the next topic to be looked at is the fuel consumption between the hybrid, and standard propulsion aircraft, as shown below through calculations of recharging at 90% power for the hybrid and then using the synthesis tables for the standard.

**Table PROPTRQ – 5 Fuel Consumption between Aircraft Designs**

| Standard Aircraft | Hybrid Aircraft |
|---|---|
| Fuel Used (lb) | Fuel Used (lb) |
| 250.7997 | 317.8253 |
| **% Fuel Change Used** | 26.72 Increase |

Now not only does the last few tables and data show that weight will be increases, the fuel consumption will as well. However there is a silver lining so far, non-hybrid, purely electric aircraft with an added ICE engine for a single recharge, with current technologies the fuel consumption can decrease by 44%, the downside would be that weight would increase by 205%. However all the data shown is hypothetical that the mission can still be performed to the customers demand.

## Hybrid Performance

For this analysis the battery weight used will be for the 10 kWH battery will be used, and even with the small weight change from that the cruise speed will be increased to 147 knots for a 74% power to have the maximum efficiency with zero loss or additive in ROC by using a varying angle of attack. That is for the 75% cruise requirement but for the maximum available power available the graph is shown along with the power percent needed below

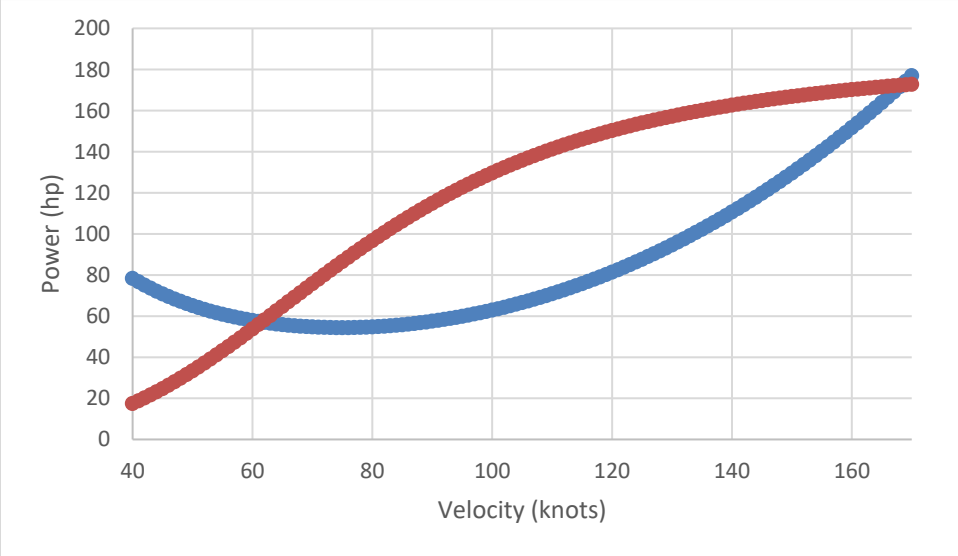


**Figure PROPTRQ - 6 Maximum Power vs. Required, Hybrid aircraft**

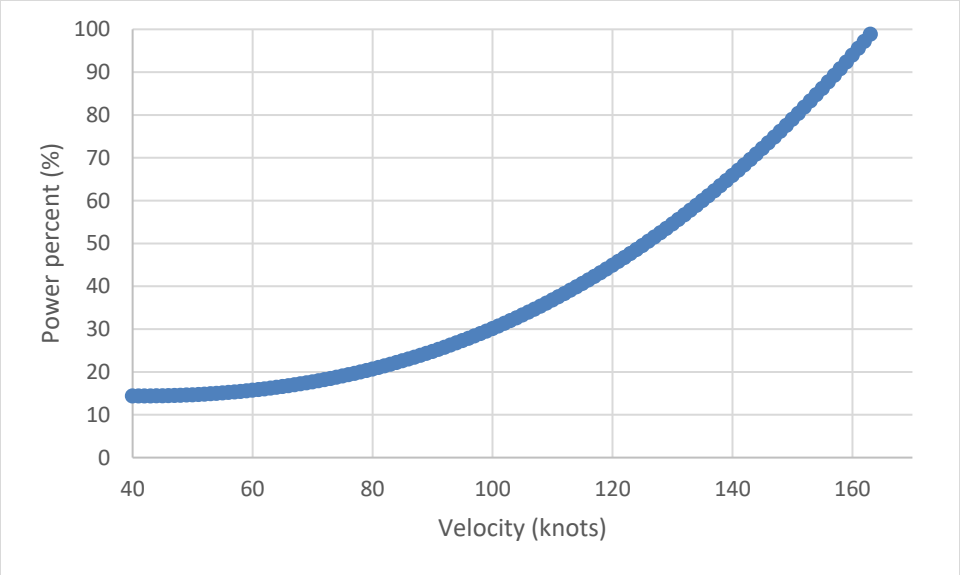


**Figure PROPTRQ - 7 Power Percent Needed to Run, Hybrid aircraft**

As it can be seen the power needed increased instead of with the synthesis Tecnam configuration the mission criteria of 140 knots being met at only 65% power, what else can be shown is that any more increase in battery weight will break the constraint that 75% of motor power will be used. So in addition to the added fuel consumption, and weight, an increase in basic percent power needed is required, which leaves almost zero room for headwinds or other weather phenomenon.

## Hybrid Conclusions

What can be concluded from the comparison between the hybrid aircraft and the standard aircraft are shown below

**Table PROPTRQ – 6 Comparison Between Standard To Hybrid Aircraft**

| | % increase |
|---|---|
| Weight increase | **14.16706342** |
| Fuel consumption change | **26.80964987** |

What this shows is that as well as a weight increase from the electronics an increase in fuel consumption will also happen. So while being able to be done it is counter intuitive to using an electrical hybrid machine if it will increase the fuel being used. The only way to overcome this would be to increase the battery energy density to increase the energy stored per kg to decrease the weight and with an aircraft the only way to save fuel would be to turn the aircraft into a sole electric aircraft or find another way of recharging the battery without using the internal combustion engine as the sole recharger. Maybe solar panels or some sort of regenerative charging because as it stands, using just an engine to recharge a battery to fly an aircraft just adds an extra step of losses instead of just using an engine to power the aircraft.

**Stability and Control Derivatives with Handling Qualities**

For the stability derivative calculations, some of the CFD (Computational Fluid Dynamics) data were used. But CFD was unable to provide the complete sets of the derivatives. Roskam's aircraft design Volume 6 (Reference 1) were used to obtain the rest of the stability derivatives. In addition, the known stability derivatives were also calculated to see if they match with CFD data. The values matched to a satisfactory level with less than one percent error. For the calculation of handling qualities, the cruise phase of the aircraft was chosen. It was assumed that the aircraft was operating at 7500 $ft$ and with 95% of the maximum takeoff weight. Straight and level flight conditions were maintained during cruise and the aircraft was in trimmed condition. These assumptions were necessary go get started with the calculations. The most important assumption was the aircraft center of gravity, which was taken to be at 23% of the wing m.g.c. This was an educated guess based upon the c.g. range obtained from the Tecnam P 2006T manual (Reference 2) which was from 16.5% to 31% of m.g.c. Using the assumed the stability derivatives were calculated which is described below in step-by-step process.

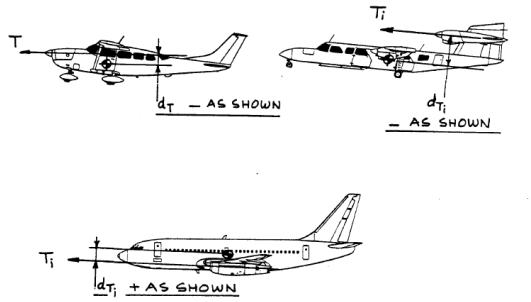


Figure 1. Geometry of the thrust line offset. [1]

**Steady state coefficients:** Since the aircraft is in a steady state (trimmed condition) the steady state lift coefficient is given as,

$$C_{L_1} = nW/\bar{q}S \tag{1}$$

It was noticed that, for a $1g$ flight $n = 1$. From the assumed data and calculations $C_{L_1} = .293$.
The steady state drag coefficient was obtained directly from the CFD data as it was a better and less complex method. From the CFD data $C_{D_1} = .0293$.
For the steady state thrust coefficient Eqn. (2) is usually satisfied.

$$C_{T_{X_1}} = -C_{D_1} \tag{2}$$

So, $C_{T_{X_1}} = -.0293$. Next, the aircraft steady state pitching moment coefficient is obtained from Eqn. (3).

$$C_{m_1} = -C_{m_{T_1}} \tag{3}$$

Also, the aircraft steady state pitching moment coefficient due to thrust is found from Eqn. (4).

$$C_{m_{T_1}} = \Delta C_{m_{T_L}} \tag{4}$$

Where,

$$\Delta C_{m_{T_L}} = \sum_{i-1}^{n} (T_{av_i} d_{T_i}/\bar{q}S\bar{c}) \tag{5}$$

Here, $T_{av_i}$ is the available installed thrust from a propeller and $d_{T_i}$ is the thrust line offset relative to the reference point shown in Fig. 1. It is counted positive if the thrust line is located beneath the reference point. The necessary locations and distances were calculated from the SolidWorks model of the Tecnam P 2006 T aircraft. Then using Eq. (4) $C_{m_{T_1}} = .0377$. Similarly, from Eqn. (3) $C_{m_1} = -.0377$.

**Speed Derivatives:**

1) The drag-due-to-speed derivative: It is determined in all speed regimes from the following formula:

$$C_{D_u} = M_1\left(\frac{\partial C_D}{\partial M}\right) \tag{6}$$

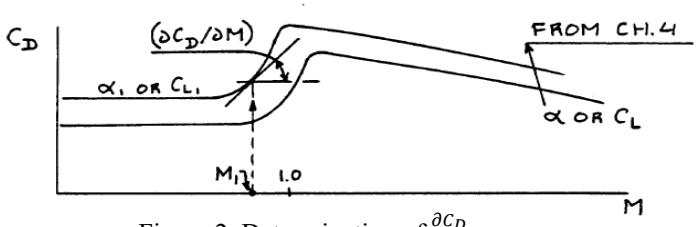


Figure 2. Determination of $\frac{\partial C_D}{\partial M}$

$M_1$ is the mach number of the flight obtained from the Tecnam manual and $\frac{\partial C_D}{\partial M}$ is the derivative of the aircraft drag coefficient found from Fig. 2. As seen from the figure, for low speed cruise, the derivative is zero. So using Eqn. (6), $C_{D_u} = 0$.

2) The lift-due-to-speed derivative: The formula for obtaining this values is given below:

$$C_{L_u} = \frac{M_1^2(cos\Lambda_{c/4})^2 C_{L_1}}{1 - M_1^2(cos\Lambda_{c/4})^2} \tag{7}$$

Using the appropriate values in Eqn. (7) $C_{L_u} = .01455$.

3) Pitching-moment-due-to-speed derivative: This is also known as Mach tuck derivative. This is nonzero for cases where a thrust pitching moment must be counteracted by an aerodynamic pitching moment to trim the aircraft to a total pitch moment of zero. The data obtained from the CFD is directly used in this case since its calculation is complex and time consuming. So, $C_{m_u} = -.0001$.

4) Thrust-due-to-speed derivative: For a variable pitch, constant speed propeller aircrafts, Roskam presents a simplified equation:

$$C_{T_{X_u}} = -3C_{T_{X_1}} \tag{8}$$

Using the previously obtained values, $C_{T_{X_u}} = .0877$.

5) Thrust-moment-due-to-speed derivative: Using Eqn. (9) this number can be calculated:

$$C_{m_{T_u}} = (d_T/\bar{c})C_{T_{X_u}} \tag{9}$$

Here, $d_T$ is the thrust moment arm relative to the center of gravity as indicated in Fig. 1. This value is also calculated from the Tecnam SolidWorks model. So, Eqn. 9 gives us $C_{m_{T_u}} = .0416$.

**Angle of attack derivatives:**

1) Lift-due-to-angle-of-attack derivatives: This is also known as the airplane lift curve slope. was calculated theoretically following the equations in Roskam Vol. 6. CFD data were also considered. The two numbers were close, having less than 5 percent error. So CFD data was used in this case. From CFD, $C_{L_\alpha} = 5.08$.

2) Drag-due-to-angle-of-attack derivative: This is calculated using Eqn. (10)

$$C_{D_\alpha} = (\partial C_D/\partial C_L)C_{L_\alpha} \tag{10}$$

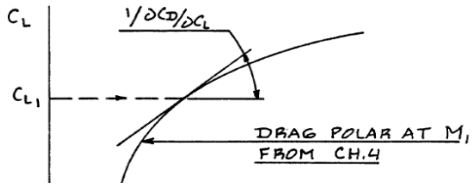


Figure 3. Determination of $\partial C_D/\partial C_L$ from drag polar

Here, $(\partial C_D/\partial C_L)$ is obtained from Fig. 3. The drag polar equation obtained from the CFD results was differentiated and the value was obtained from the differentiation. Using the value obtained from Fig. 3 and then using Eqn. (10) we get, $C_{D_\alpha} = .092$.

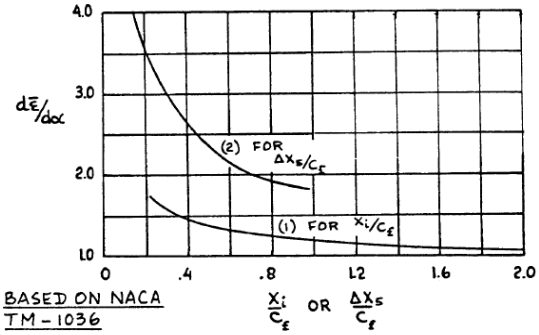


Figure 4. Effect of fuselage segment location on Upwash Gradient

3) Pitching-moment-due-to-angle-of-attack derivative: This is also called the static longitudinal stability. The formula for finding this value is:

$$C_{m_\alpha} = (dC_m/dC_L)C_{L_\alpha} \tag{11}$$

Where,
$$dC_m/dC_L = \bar{x}_{ref} - \bar{x}_{ac_A} \tag{12}$$

And,
$$\bar{x}_{ac_A} = [\bar{x}_{ac_{wf}}C_{L_{\alpha_{wf}}} + \eta_h C_{L_{\alpha_h}}\left(1 - \frac{d\varepsilon}{d\alpha}\right)\left(\frac{S_h}{S}\right)\bar{x}_{ac_h} - \eta_c C_{L_{\alpha_c}}\left(1 - \frac{d\varepsilon_c}{d\alpha}\right)\left(\frac{S_c}{S}\right)\bar{x}_{ac_c}]/\, C_{L_\alpha} \tag{13}$$

Also,
$$\bar{x}_{ac_{wf}} = \bar{x}_{ac_w} + \Delta\bar{x}_{ac_f} \tag{14}$$

Here, $\Delta\bar{x}_{ac_f}$ is the shift in aerodynamic center caused by adding the fuselage to the wing. The canard contribution in Eqn. (13) was zero since the given aircraft is not canard. The horizontal tail efficiency, $\eta_h = 1$ was considered since the exact value is very hard to get and the assumption is sufficient for preliminary calculation. $C_{L_{\alpha_h}}$ is the horizontal tail lift curve slope which was obtained from CFD. The value of downwash gradient of the horizontal tail $d\varepsilon/d\alpha$ was calculated from Eqn. (20).

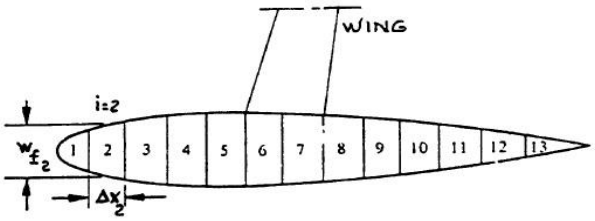


Figure 5. Definition of $W_{f_i}$ and $\Delta x_i$

Again,
$$C_{L_{\alpha_{wf}}} = K_{wf}C_{L_{\alpha_w}} \tag{15}$$

And,
$$K_{wf} = 1 + .025(d_f/b) - .25(d_f/b)^2 \tag{16}$$

$d_f$ is the equivalent fuselage diameter obtained from SolidWorks and wing lift curve slope $C_{L_{\alpha_w}}$ was obtained from CFD. Using the known values, Eqns. (15) and (16) were solved.

Next, $$\Delta\bar{x}_{ac_f} = -(dM/d\alpha)/\bar{q}S\bar{c}C_{L_{\alpha_w}} \quad (17)$$

And, $$\frac{dM}{d\alpha} = \left(\frac{\bar{q}}{36.5}\right)\left(\frac{C_{L_{\alpha_w}}}{.08}\right)\sum_{i=1}^{13} w_{f_i}^2 \left(\frac{d\varepsilon}{d\alpha}\right)_i \Delta x_i \quad (18)$$

$W_{f_i}$ and $\Delta x_i$ are defined in Fig. 4 and $\left(\frac{d\varepsilon}{d\alpha}\right)_i$ is defined in Fig. 5. Going through Eqns. (11) to (18), $C_{m_\alpha} = -6.32$.

4) Thrust versus angle-of-attack derivative: The equation to obtain this values is difficult to calculate and needs much more unknown values. However, going through flight dynamics books and historical data it was seen that for most of the cases, $C_{m_{T_\alpha}} = 0$.

**Rate of angle-of-attack derivatives:**

1) Drag-due-to-rate-of-angle-of-attack derivative: This term is usually neglected so, $C_{D_{\dot{\alpha}}} = 0$.

2) Lift-due-to-rate-of-angle-of-attack derivative: This may be computed from:

$$C_{L_{\dot{\alpha}}} = 2C_{L_{\alpha_h}}\eta_h\bar{V}_h(d\varepsilon/d\alpha) \quad (19)$$

Where, $$\frac{d\varepsilon}{d\alpha} = 4.44\left[\left\{K_A K_\lambda K_h (cos\Lambda_{\frac{c}{4}})^{\frac{1}{2}}\right\}^{1.19}\right] \times \left[\left(C_{L_{\alpha_w}}\right)_{at\ M} / \left(C_{L_{\alpha_w}}\right)_{at\ M=0}\right] \quad (20)$$

And, $K_A = \left(\frac{1}{A}\right) - \frac{1}{1+A^{1.7}}$; $K_\lambda = \frac{10-3\lambda}{7}$; $K_h = \frac{1-\frac{h_h}{b}}{\left(\frac{2l_h}{b}\right)^{\frac{1}{3}}}$; The quantities $h_h$ and $l_h$ are defined in the Fig. 6. $\left(C_{L_{\alpha_w}}\right)_{at\ M}$ was taken from the CFD model of the wing and Eqn. (21) was used to calculate $\left(C_{L_{\alpha_w}}\right)_{at\ M=0}$. In the equation, the mach corection factor $\beta = 1$, since $M = 0$. Also, $\kappa = \frac{(c_{l_\alpha})_{at\ M}}{2\pi}$. Sweep angle, $\Lambda_{c/2} = 0$.

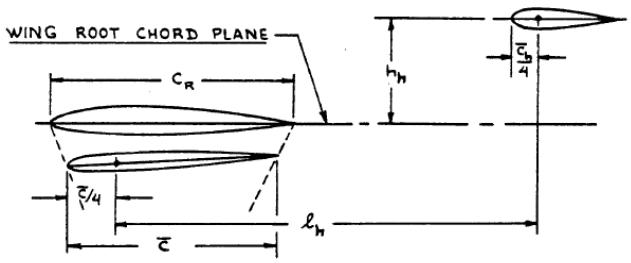


Figure 6. Geometric parameters for horizontal tail locations

Now, the wing section lift curve slope $(c_{l_\alpha})_{at\ M}$ was approximated from Fig. (7). Care was taken to ensure the units matched in both cases and for that reason, approporiate conversion factors were used. The horizontal tail volume coefficient was determined as:

$$C_{L_{\alpha_w}} = \frac{2\pi A}{2 + \left[A^2\beta^2/\kappa^2(1 + tan^2\Lambda_{c/2}/\beta^2) + 4\right]^{1/2}} \tag{21}$$

$$\bar{V}_h = (\bar{x}_{ac_h} - \bar{x}_{cg})(S_h/S) \tag{22}$$

As mentioned earlier, the c.g. location was taken to be at 23% of the wing chord and $\bar{x}_{ac_h}$ was determined from the 3-D model. Sweeping through Eqns. (19) to (22) the value obtained was: $C_{L_{\dot{\alpha}}} = 11.76$.

| Airfoil | $\alpha_{0_l}$ (deg) | $c_{m_o}$ | $c_{l_\alpha}$ (deg$^{-1}$) | a.c. (tenths c) | $\alpha_{c_{l_{max}}}$ (deg) | $c_{l_{max}}$ | $\alpha^*$ (deg) |
|---|---|---|---|---|---|---|---|
| 65-006 | 0 | 0 | .105 | .258 | 12.0 | .92 | 7.6 |
| 65-009 | 0 | 0 | .107 | .264 | 11.0 | 1.08 | 9.8 |
| 65-206 | -1.6 | -.031 | .105 | .257 | 12.0 | 1.03 | 6.0 |
| 65-209 | -1.2 | -.031 | .106 | .259 | 12.0 | 1.30 | 10.0 |
| 65-210 | -1.6 | -.034 | .108 | .262 | 13.0 | 1.40 | 9.6 |
| $65_1$-012 | 0 | 0 | .110 | .261 | 14.0 | 1.36 | 10.0 |
| $65_1$-212 | -1.0 | -.032 | .108 | .261 | 14.0 | 1.47 | 9.4 |
| $65_1$-412 | -3.0 | -.070 | .111 | .265 | 15.5 | 1.66 | 10.5 |
| 63A010 | 0 | .005 | .105 | .254 | 13.0 | 1.20 | 10.0 |
| 63A210 | -1.5 | -.040 | .103 | .257 | 14.0 | 1.43 | 10.0 |
| 64A010 | 0 | 0 | .110 | .253 | 12.0 | 1.23 | 10.0 |
| 64A210 | -1.5 | -.040 | .105 | .251 | 13.0 | 1.44 | 10.0 |
| 64A410 | -3.0 | -.080 | .100 | .254 | 15.0 | 1.61 | 10.0 |
| $64_1$A212 | -2.0 | -.040 | .100 | .252 | 14.0 | 1.54 | 11.0 |
| $64_2$A215 | -2.0 | -.040 | .095 | .252 | 15.0 | 1.50 | 12.0 |

Figure 7. Experimental low speed data for 6-digit NACA airfoils

3) Pitching-moment-due-to-rate-of-angle-of-attack derivative: An important assumption was made while calculating $C_{L_{\dot{\alpha}}}$ that the horizontal tail made the most important contribution to these derivatives. This assumption is frequently satisfied and hence used here as well.

$$C_{m_{\dot{\alpha}}} = -2C_{L_{\alpha_h}}\eta_h\bar{V}_h(d\varepsilon/d\alpha)(\bar{x}_{ac_h} - \bar{x}_{cg}) \tag{23}$$

Since, all the values were known previously, $C_{m_{\dot{\alpha}}} = -42.81$.

**Angle-of-sideslip derivatives:**

1) Sideforce-due-to-sideslip derivative: It includes contributions from wing, fuselage and vertical tail.

$$C_{y_\beta} = C_{y_{\beta_w}} + C_{y_{\beta_f}} + C_{y_{\beta_v}} \tag{24}$$

Where,

$$C_{y_{\beta_w}} = -.00573|\Gamma|$$

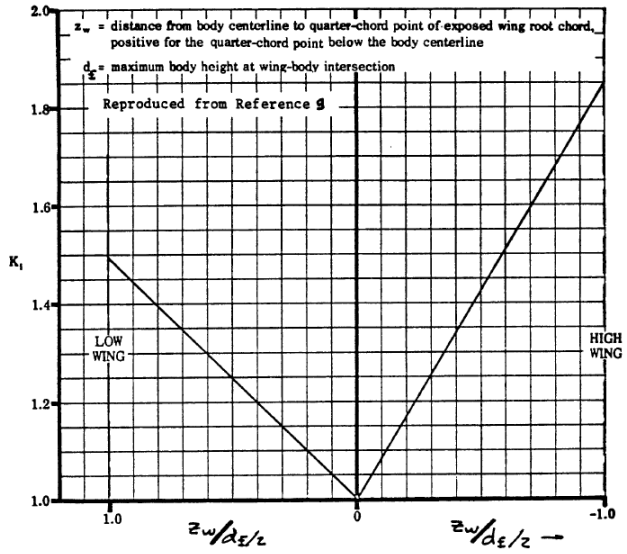


Figure 8. Wing-fuselage interference factor

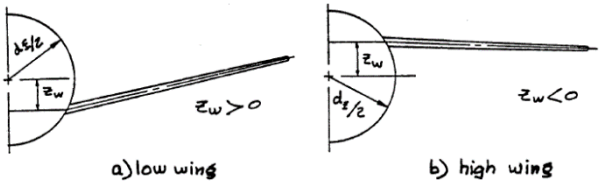


Figure 9. Definition of wing-fuselage parameters

$\Gamma = 1°$ is the geometric dihedral angle in degrees obtained from Reference 2. The fuselage contribution is given by, $C_{y_{\beta_f}} = -2k_i(S_o/S)$. $k_i$ is defined in Fig. 8 and the necessary inputs required is shown in Fig. 9. Both the figures contain high wing and low wing values. Since Tecnam P 2006T is a high wing aircraft, the high wing data were chosen. $S_o$ is the cross-sectional area of the fuselage station where the flow ceases to be potential. Due to lack of information, this region was approximated form different CFD models. The formula used for calculating this number was $\frac{x_o}{l_f} = .378 + .527\frac{x_1}{l_f}$. The geometric values for this equation is given in Fig. 10. After obtaining the approximate locations, $S_o$ was calculated from the CAD model. Finally, the vertical tail contribution was calculated using:

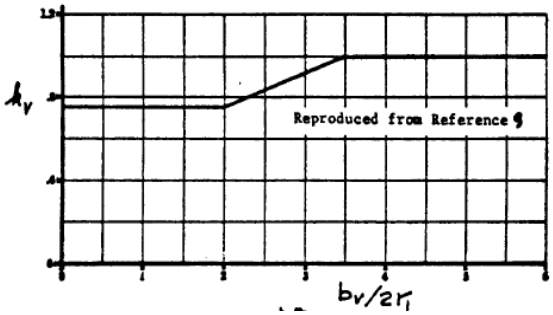


Figure 11. Empirical for estimation of side force due to sideslip of a single vertical tail

$$C_{y_{\beta_v}} = -\kappa_v C_{L_{\alpha_v}}(1 + d\sigma/d\beta)\eta_v(S_v/S) \tag{25}$$

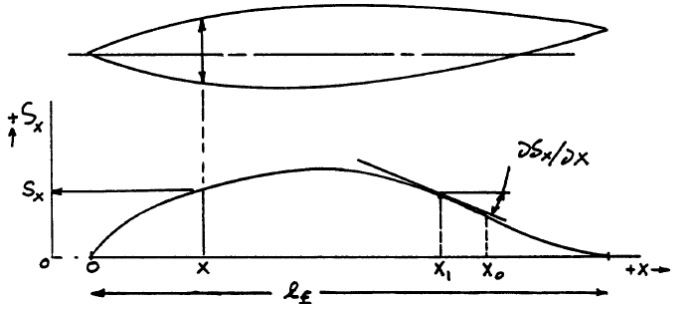


Figure 10. Geometric parameters

The vertical tail lift-curve-slope, $C_{L_{\alpha_v}}$, was obtained from CFD data of the vertical tail. $\kappa_v$ was obtained from Fig. 11. From the figure, $b_v$ is the vertical tail soan measured from the fuselage centerline and $2r_1$ is the fuselage depth in region of vertical tail. The entire quantity,

$$(1 + d\sigma/d\beta)\eta_v = .724 + 3.06[(S_v/S)/(1 + cos\Lambda_{c/4})] + .4z_w/z_f + .009A.$$

Here, $\Lambda_{c/4} = 0$ is the quarted chord sweep angle. The quantities $z_w$ and $z_f$ were obtained from CAD model (*describe in Nomenclature*).

Knowing all the quantities in Eqn. (24) the sideslip derivative was obtained to be $C_{y_\beta} = .5495$.

2) Rolling-moment-due-to-sideslip derivative: This is called the dihedral effect, and is described in Eqn. (26)

$$C_{l_\beta} = C_{l_{\beta_{wf}}} + C_{l_{\beta_h}} + C_{l_{\beta_v}} \quad (26)$$

Where,

$$C_{l_{\beta_{wf}}} = 57.3[C_{L_{wf}}\{(C_{l_\beta}/C_L)_{\Lambda_{c/2}} K_{M_\Lambda} K_f + (C_{l_\beta}/C_L)_A\} + \Gamma\{(C_{l_\beta}/\Gamma)K_{M_\Gamma} + (\Delta C_{l_\beta}/\Gamma)\} + (\Delta C_{l_\beta})_{z_w} + (\varepsilon_t tan\Lambda_{c/4})\{(\Delta C_{l_\beta})/\varepsilon_t tan\Lambda_{c/4}\}] \quad (27)$$

Here, the sweep and dihedral effects were very small, because there were no sweep and minimum dihedral, and thus were neglected. It was assumed that the wing fuselage lift coefficient $C_{L_{wf}} = C_{L_1}$ for preliminary design purposes. $(C_{l_\beta}/C_L)_{\Lambda_{c/2}}$ is the wing sweep contribution obtained from Fig. 12. Obtaining the values from both the graphs in Fig. 12, linear estimation was done to obtain the value at the exact taper ratio of Tecnam. The compressibility correction due to sweep $K_{M_\Lambda}$ was obtained from Fig. 13. The fuselage correction factor $K_f$ was obtained from Fig. 14. The geometric inputs were determined from CAD models for this graph. $(C_{l_\beta}/C_L)_A$ is the aspect ratio contribution.

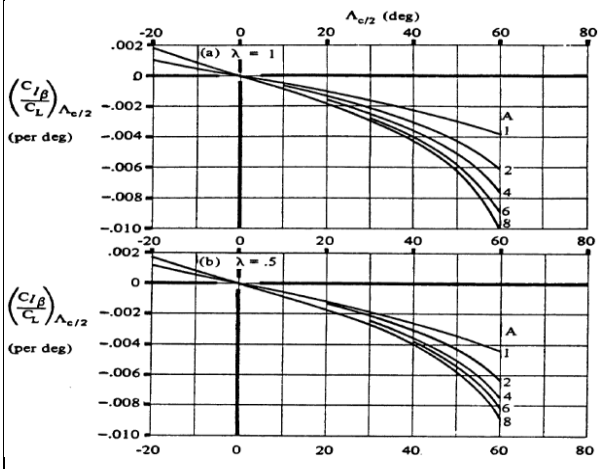


Figure 12. Wing sweep contribution to

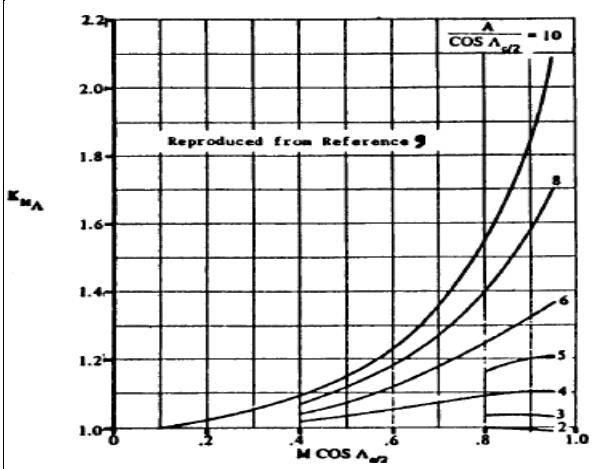


Figure 13. Compressibility correction

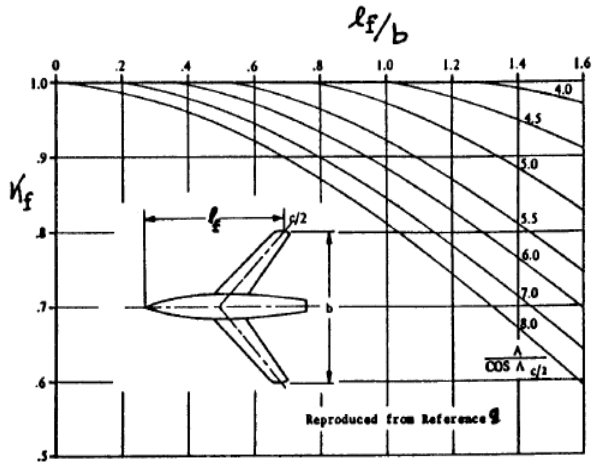


Figure 14. Fuselage correction

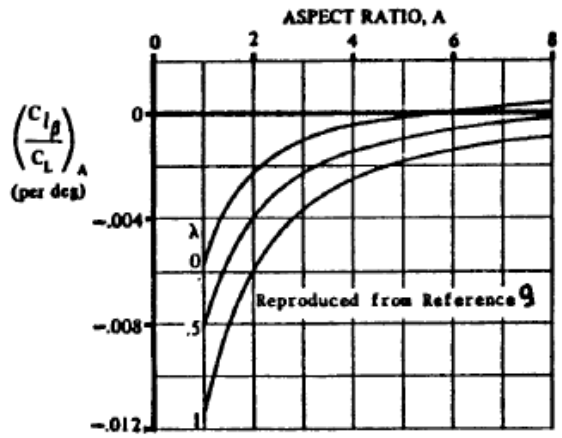


Figure 15. Aspect ratio contribution

This was very close to zero as seen from Fig. 15. The last unknown term of Eqn. (27) was obtained from the relation:

$$(\Delta C_{l_\beta})_{z_w} = .042A^{1/2}(z_w/b)(d_{f_{ave}}/b)$$

Where, $d_{f_{ave}} = \sqrt{Avg.\,fuselage\ cross\ section\ area/.7854}$.

Finally, using all the graphs and equations presented in this page, $C_{l_{\beta_{wf}}}$ was calculated. After that, the horizontal tail contribution was calculated using the following equation:

$$C_{l_{\beta_h}} = C_{l_{\beta_{hf}}}(S_h b_h / Sb) \tag{28}$$

$C_{l_{\beta_{hf}}}$ in Eqn. (28) is the horizontal tail dihedral effect as computed from Eqn. (27) with appropriate substitution of tail-fuselage for wing-fuselage parameters. Finally, the vertical tail contribution was obtained from Eqn. (29).

$$C_{l_{\beta_v}} = C_{y_\beta}[z_v cos\alpha - l_v sin\alpha]/b \tag{29}$$

The definitions of $z_v$ and $l_v$ are described in Fig. 16. $\alpha = 0$ for a straight and level flight, which was assumed in beginning and $C_{y_\beta}$ was previously obtained from Eqn. (24). Sweeping through Eqns. (26) to (29) $C_{l_\beta} = -.0458$.

3) Yawing-moment-due-to-sideslip derivative: This is also known as the static directional stability and is computed from Eqn. (30).

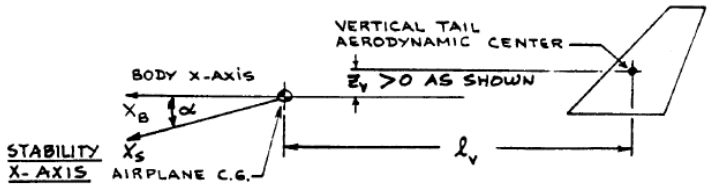


Figure 16. Geometrical inputs $z_v$ and $l_v$

$$C_{n_\beta} = C_{n_{\beta_w}} + C_{n_{\beta_f}} + C_{n_{\beta_v}} \tag{30}$$

In Eqn. (30) the wing contribution is only important at high angles of attack. For the cruise condition $C_{n_{\beta_w}} = 0$ was an educated assumption. The fuselage contribution was obtained from the following equation:

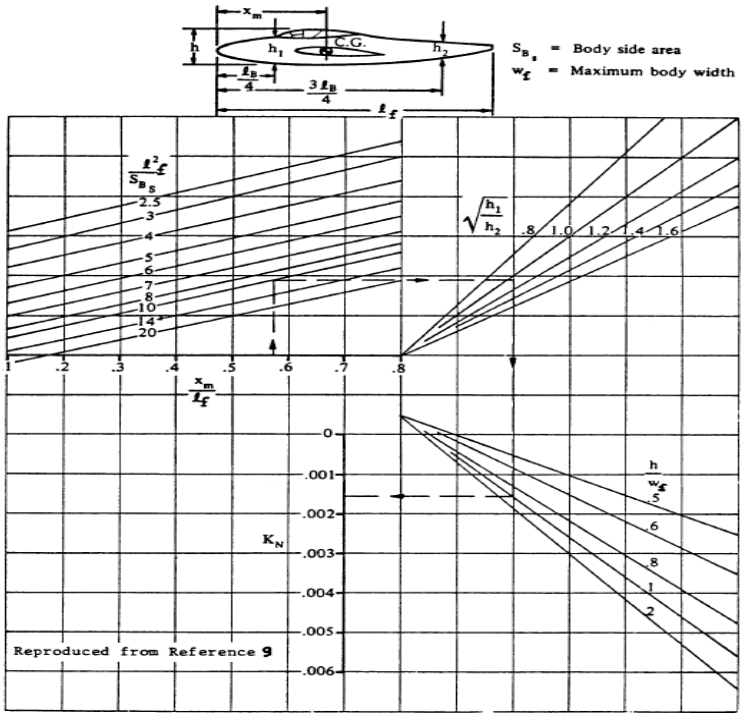


Figure 17. Empirical factor $K_N$ determination

$$C_{n_{\beta_f}} = -57.3 K_N K_{R_1} (S_{f_s} l_f / Sb)$$

With the empirical factor $K_N$ determined from Fig. 16. All the necessary geometric inputs were described in Fig. 17 and the values were obtained from CAD model. $K_{R_1}$ is obtained from Fig. 18. After knowing all the values, $C_{n_{\beta_f}}$ was calculated. Finally, the vertical tail contribution was found from the following relation:

$$C_{n_{\beta_v}} = -C_{y_{\beta_v}}[z_v sin\alpha + l_v cos\alpha]/b$$

Here, $C_{y_{\beta_v}}$ was obtained from Eqn. (25), $z_v$ and $l_v$ were described in Fig. 16. Using all the calculated values, $C_{n_\beta} = .1216$.

**Roll rate derivatives:**

1) Side force-due-to-toll-rate derivative: This value is primarily influenced by the vertical tail and is determined

from Eqn. (31) where all the quantities were described previously. Using Eqn. (31) $C_{y_p} = -.08$.

| | | |
|---|---|---|
| | $C_{y_p} = 2C_{y_{\beta_v}}[z_v cos\alpha - l_v sin\alpha]/b$ | (31) |

2) Rolling-moment-due-to-roll-rate derivative: This is also known as the roll damping derivative and is found from the following relation:

| | | |
|---|---|---|
| | $C_{l_p} = C_{l_{p_w}} + C_{l_{p_h}} + C_{l_{p_v}}$ | (32) |
| | | |
| Where, | $C_{l_{p_w}} = (\beta C_{l_p}/\kappa)_{C_L=0}(\kappa/\beta) \times \{(C_{L_{\alpha_w}})_{C_L}/(C_{L_{\alpha_w}})_{C_L=0}\} \times \{(C_{l_p})_\Gamma/(C_{l_p})_{\Gamma=0}\} + (\Delta C_{l_p})_{Drag}$ | (33) |

Here, $(\beta C_{l_p}/\kappa)_{C_L=0}$ is the roll damping parameter at zero lift, obtained from Fig. A19 (put this in appendix) with correct taper ratio approximation. It was noted that $\beta$ was not the sideslip angle in the above equation rather it was the mach correction factor,

$$\beta = \sqrt{1 - M^2}$$

And, $\kappa = (c_{l_\alpha})_M \beta/2\pi$

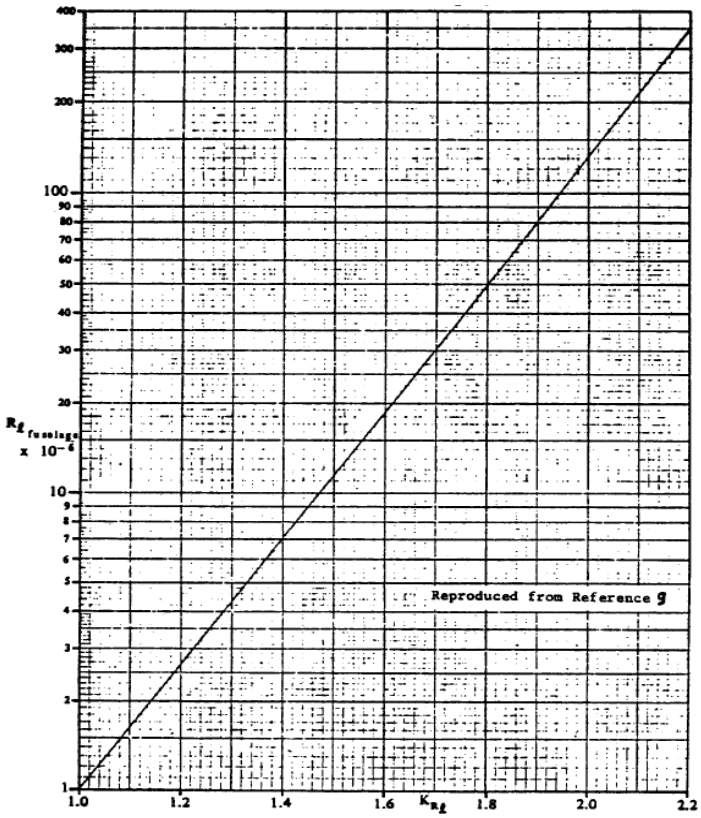


Figure 18. Effect of fuselage Reynold's number on wing fuselage directional stability

The term $(C_{L_{\alpha_w}})_{C_L}/(C_{L_{\alpha_w}})_{C_L=0} = 1$ was assumed since the wing lift curve slope is almost constant if the angle of attack is very small (zero in this case) (Reference 1, Section 8.1.3.5).

$$\left\{\frac{(C_{l_p})_\Gamma}{(C_{l_p})_{\Gamma=0}}\right\} = 1 - \frac{4z_w}{b} sin\Gamma + 12\left(\frac{z_w}{b}\right)^2 (sin\Gamma)^2$$

All the quantities were described previously. Then, the wing drag contribution to roll damping was found out using:

$$(\Delta C_{l_p})_{Drag} = \left(\frac{(C_{l_p})_{C_{D_L}}}{(C_{L_w})^2}\right)(C_{L_w})^2 - .125C_{D_{o_w}}$$

$\frac{(C_{l_p})_{C_{D_L}}}{(C_{L_w})^2}$ is the drag-due-to-lift roll damping parameter found from Fig. 19. In the preliminary design, it is acceptable to set $C_{L_w} = C_{L_1}$. The

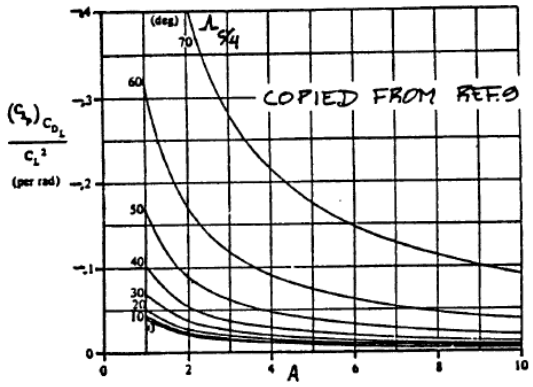


Figure 19. Drag-due-to-lift roll damping parameter

wing zero-lift drag coefficient $C_{D_{o_w}}$ was obtained from the CFD model. The fuselage contribution to $C_{l_p}$ tends to be negligible for airplanes for which $\frac{d_f}{b} < .3$. Tecnam P 2006T satisfied this criterion so the fuselage contribution was not shown in Eqn. (32). Next, the vertical tail contribution is given by:

$$C_{l_{p_v}} = 2(z_v/b)^2 C_{y_{\beta_v}}$$

Where, all the quantities were known from previous calculations. Finally, the horizontal tail contribution was obtained from:

$$C_{l_{p_h}} = .5\left(C_{l_p}\right)_h \left(\frac{S_h}{S}\right)\left(\frac{b_h}{b}\right)$$

Where, $\left(C_{l_p}\right)_h$ is the roll-damping derivative of the horizontal tail obtained from Eqn. (33) with appropriate substitution of horizontal tail parameters. After obtaining all the required values, using Eqn. (32) $C_{l_p} = -.8538$.

3) Yawing-moment-due-to-roll-rate derivative: This is determined from the following equation:

| | | |
|---|---|---|
| | $C_{n_p} = C_{n_{p_w}} + C_{n_{p_v}}$ | (34) |
| | | |
| Where, | $C_{n_{p_w}} = -\left\{\left(\frac{C_{n_p}}{C_L}\right)_{C_L=0,M}\right\} C_L + \left(\frac{C_{n_p}}{\varepsilon_t}\right)\varepsilon_t + \left\{\left(\frac{\Delta C_{n_p}}{\alpha_{\delta_f}}\right)(\delta_f)\right\}\left(\alpha_{\delta_f}\right)\delta_f$ | (35) |
| | | |
| With, | $\left(\frac{C_{n_p}}{C_L}\right)_{C_L=0,M} = \left(\frac{C_{n_p}}{C_L}\right)_{C_L=0,M=0}\left(\frac{A+4cos\Lambda_{c/4}}{AB+4cos\Lambda_{c/4}}\right)\left[\frac{AB+\frac{1}{2}(AB+cos\Lambda_{c/4})tan^2\Lambda_{c/4}}{A+\frac{1}{2}(A+cos\Lambda_{c/4})tan^2\Lambda_{c/4}}\right]$ | |

Here, $B = \sqrt{1-M^2(cos\Lambda_{C/4})^2}$ and, $\left(\frac{C_{n_p}}{C_L}\right)_{C_L=0,M=0} = -\frac{1}{6}\frac{A+6(A+cos\Lambda_{c/4})(\frac{\bar{x}}{c}\frac{tan\Lambda_{c/4}}{A}+\frac{tan^2\Lambda_{c/4}}{12})}{A+4cos\Lambda_{c/4}}$

The wing twist term was zero since there were no twist in the wing. As no flaps were necessary during cruise $\delta_f = 0$, the flap deflection term becomes zero. Then, the vertical tail contribution was obtained from:

$$C_{n_{p_v}} = -2/b^2(z_v cos\alpha - l_v sin\alpha - z_v)(z_v sin\alpha + l_v cos\alpha)C_{y_{\beta_v}}$$

All the terms in the above equation were known. So, using Eqn. (34) $C_{n_p} = -.0333$.

**Yaw rate derivatives:**

1) Side-force-due-to-yaw-rate derivative: This is primarily influenced by the vertical tail and may be determined form:

| | | |
|---|---|---|
| | $C_{y_r} = -2C_{y_{\beta_v}}[z_v sin\alpha + l_v cos\alpha]/b$ | (36) |

All the quantities were defined before. So, $C_{y_r} = .3428$.

2) Rolling-moment-due-to-yaw-rate derivative: This was estimated from:

| | | |
|---|---|---|
| | $C_{l_r} = C_{l_{r_w}} + C_{l_{r_v}}$ | (37) |
| Where, | $C_{l_{r_w}} = \left\{\left(\frac{C_{l_r}}{C_L}\right)_{C_L=0,M}\right\} C_{L_w} + \frac{\Delta C_{l_r}}{\Gamma}\Gamma + \left(\frac{\Delta C_{l_r}}{\varepsilon_t}\right)\varepsilon_t + \left(\frac{\Delta C_{l_r}}{\alpha_{\delta_f}}\right)\left(\alpha_{\delta_f}\right)\delta_f$ | (38) |

The dihedral, sweep and flap deflection terms in Eqn. (38) were zeroes and were neglected. The slope of the rolling moment due to roll rate at zero lift was found from:

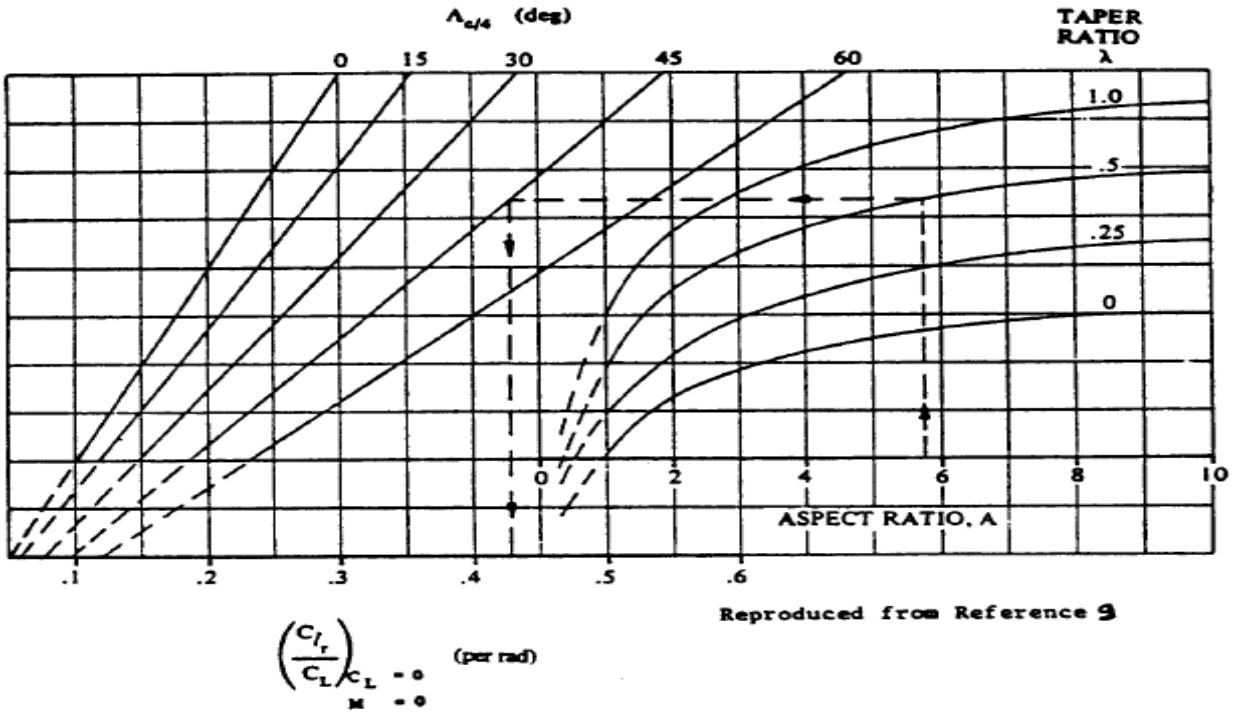


Figure 20. Wing rolling moment due to yaw rate derivative: Lifting effect

$$\left(\frac{C_{l_r}}{C_L}\right)_{C_L=0,M} = \frac{1 + \frac{A(1-B^2)}{2B(AB+2cos\Lambda_{c/4})} + \frac{AB+2cos\Lambda_{c/4}}{AB+4cos\Lambda_{c/4}}\frac{tan^2\Lambda_{c/4}}{8}}{1 + \frac{A+2cos\Lambda_{c/4}}{A+4cos\Lambda_{c/4}}\frac{tan^2\Lambda_{c/4}}{8}}\left(\frac{C_{l_r}}{C_L}\right)_{C_L=0,M=0}$$

Here, $\left(\frac{C_{l_r}}{C_L}\right)_{C_L=0,M=0}$ was the slope of the low-speed rolling moment due to yaw rate at zero lift found from Fig. (20). All the other terms were previously defined and obtained. Finally, the vertical tail contribution term was found out from with all the know quantities:

$$C_{l_{r_v}} = -(2/b^2)(z_v cos\alpha - l_v sin\alpha)(z_v sin\alpha + l_v cos\alpha)C_{y_{\beta_v}}$$

Knowing all the terms in Eqn. (37) $C_{l_r} = .1142$.

3) Yawing-moment-due-to-yaw-rate derivative: This is also known as the yaw-damping derivative and is found from:

| | | |
|---|---|---|
| | $C_{n_r} = C_{n_{r_w}} + C_{n_{r_v}}$ | (39) |
| | | |
| Where, | $C_{n_{r_w}} = (C_{n_r}/C_L^2)(C_{L_w})^2 + (C_{n_r}/C_{D_0})C_{D_{0_w}}$ | (40) |
| | | |
| And, | $C_{n_{r_v}} = (2/b^2)\,(z_v sin\alpha + l_v cos\alpha)^2 C_{y_{\beta_v}}$ | (41) |

All the terms in Eqn. (41) were know previously. $C_{L_w}$ was obtained from previous calculations and $C_{D_{0_w}}$ was obtained from the CFD model. $(C_{n_r}/C_L^2)$ was obtained from Fig. 21. $(C_{n_r}/C_{D_0})$ was obtained from Fig. A22 (put it in the appendix). Then, utilizing Eqn. (39) $C_{n_r} = -.14145$.

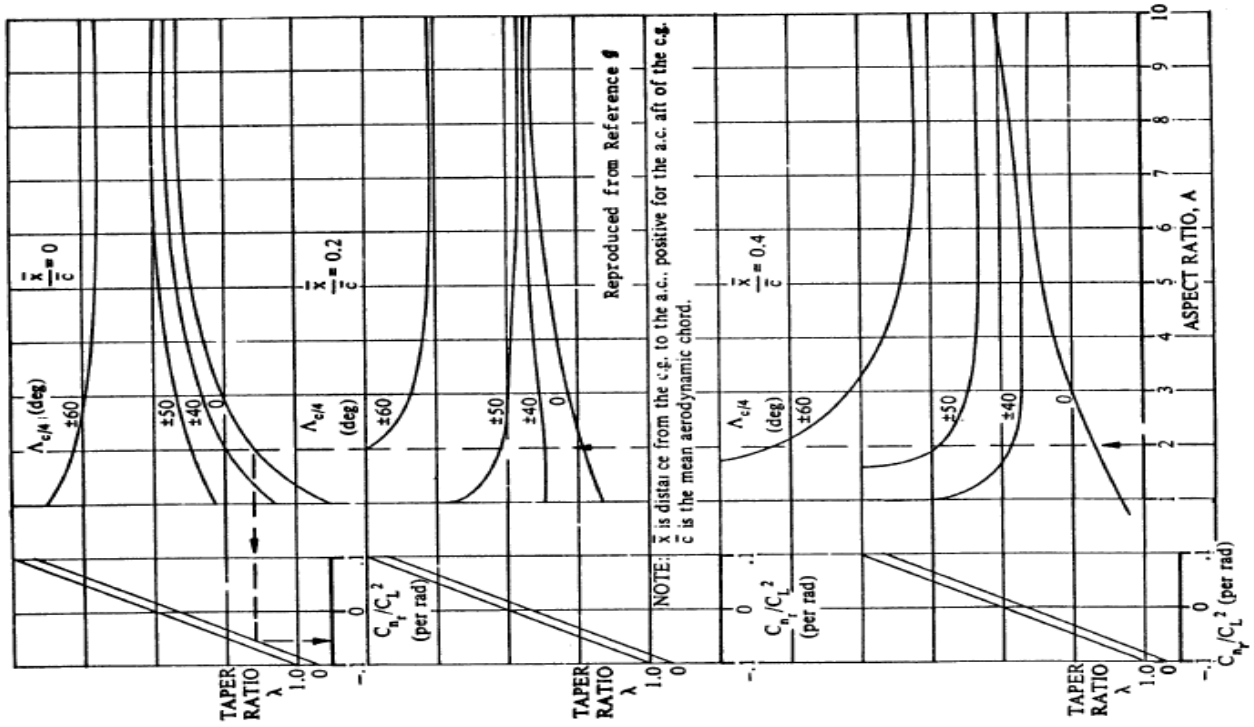


Figure 21. Wing yaw damping derivative: Lifting effect

**Pitch rate derivatives:**

1) Drag-due-to-pitch-rate derivative: This value is negligible for almost all the aircrafts. So, $C_{D_q} = 0$.

2) Lift-due-to-pitch-rate derivative: This was estimated from:

| | | |
|---|---|---|
| | $C_{l_q} = C_{l_{q_w}} + C_{l_{q_h}} + C_{l_{q_c}}$ | (42) |
| | | |
| Where, | $C_{l_{q_w}} = \{(A + 2cos\Lambda_{c/4})/(AB + 2cos\Lambda_{c/4})\}(C_{l_{q_w}})_{M=0}$ | |

Here, $B = \sqrt{1 - M^2(cos\Lambda_{C/4})^2}$ and, $(C_{l_{q_w}})_{M=0} = (.5 + 2x_w/\bar{c})C_{l_{\alpha_w}}$. $C_{l_{\alpha_w}}$ in the previous equation was obtained from the CFD data and $x_w$ was obtained from Fig. 22. The, the horizontal tail contribution was figured out using the following formula:

$$C_{l_{q_h}} = 2C_{l_{\alpha_h}}\eta_h\bar{V}_h$$

$\bar{V}_h$ in the above equation was obtained using Eqn. (22), $C_{l_{\alpha_h}}$ was obtained from the horizontal tail CFD and the procedure for getting $\eta_h$ was described in Eqn. (13). So, obtained all the required values Eqn. (42) gave $C_{l_q} = 3.598$. It should be noted that the canard contribution for the aircraft in consideration was zero.

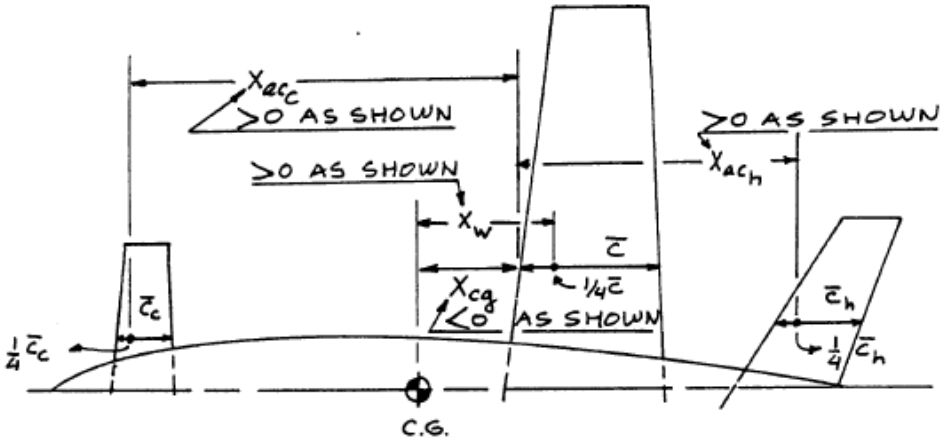


Figure 22. Definition of geometric parameter

3) Pitching-moment-due-to-pitch-rate derivative: This is also called pitch damping derivative and estimated From Eqn. (43).

| | | |
|---|---|---|
| | $C_{m_q} = C_{m_{q_w}} + C_{m_{q_h}} + C_{m_{q_c}}$ | (43) |

According to Reference 3 (pg. 286), the primary contributor to this derivative is the horizontal tail term. The canard contribution is zero for the current aircraft and the effect of wing and fuselage can be accounted for by increasing the horizontal tail contribution $C_{m_{q_h}}$ by 10%. The horizontal tail contribution thus was obtained from:

$$C_{m_{q_h}} = -2C_{l_{\alpha_h}}\eta_h\bar{V}_h(\bar{x}_{ac_h} - \bar{x}_{cg})$$

Finally, Eqn. (43) gave $C_{m_q} = -3.427$.

**Elevator control derivatives:**

1) Drag-due-to-elevator derivative: According to Reference 3 (pg. 287), $C_{D_{\delta_e}}$ is very small and usually assumed to be zero. So, $C_{D_{\delta_e}} = 0$.

2) Lift-due-to-elevator derivative: This was found from Eqn. (44).

| | | |
|---|---|---|
| | $C_{L_{\delta_e}} = (\alpha_{\delta_e}) C_{L_{i_h}}$ | (44) |
| | | |
| Where, | $\alpha_{\delta_e} = K_b \left\{ \frac{c_{l_\delta}}{(c_{l_\delta})_{theory}} \right\} (c_{l_\delta})_{theory} \times \left( \frac{k'}{c_{l_{\alpha_h}}} \right) \left[ \frac{(\alpha_\delta)_{c_L}}{(\alpha_\delta)_{c_L}} \right]$ | (45) |

Correction factor for elevator deflection, $k' = 1$ was assumed since no elevator deflection was done in cruise. $\left\{ \frac{c_{l_\delta}}{(c_{l_\delta})_{theory}} \right\}$ was obtained from Fig. 23. $(c_{l_\alpha})_{theory} = 2\pi$ was assumed for a 2D airfoil. The horizontal tail airfoil was taken to be NACA 0012. But NACA 0009 was used to obtain the approximate result as the data didn't include values for NACA 0012 airfoil. This gave $c_{l_\alpha} = .109\ (/deg)$. After obtaining the ratio form Fig. 23, $(c_{l_\delta})_{theory}$ was obtained from Fig. 24 presented below with the necessary input parameters. It was noted that although the data were

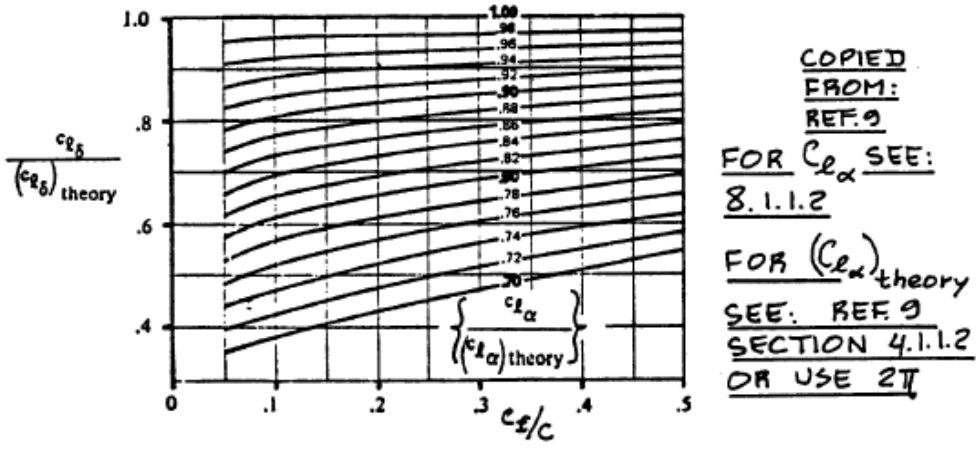


Figure 23. correction factor for a plain flap lift

described for plain flaps, they were used for elevators with necessary changes in size and dimensions. $K_b$ was estimated from Fig. 25. $\frac{(\alpha_\delta)_{c_L}}{(\alpha_\delta)_{c_L}}$ was obtained from Fig. 26. The necessary inputs were calculated previously from CAD models. $(\alpha_{\delta_e})$ was then calculated. Next, $C_{L_{i_h}}$ was calculated from the following equation with all previously known inputs:

$$C_{L_{i_h}} = \eta_h (S_h/S) C_{L_{\alpha_h}}$$

Finally, from Eqn. (44) $C_{L_{\delta_e}} = .6853$.

3) Pitching-moment-due-to-elevator derivative: This is also known as the elevator control power and may be computed from:

| | | |
|---|---|---|
| | $C_{m_{\delta_e}} = (\alpha_{\delta_e}) C_{m_{i_h}}$ | (46) |

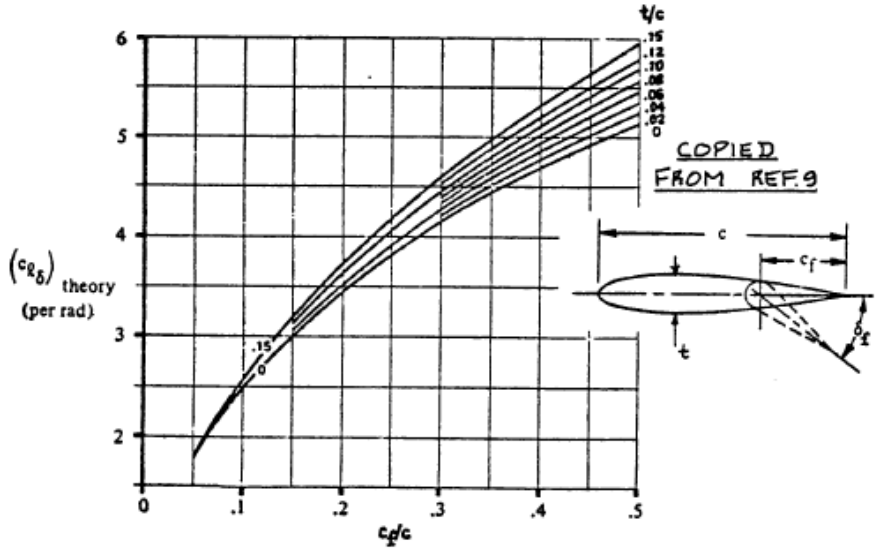


Figure 24. Lift effectiveness for a plain flap

Where, $(\alpha_{\delta_e})$ was obtained from Eqn. (45) and $C_{m_{i_h}}$ was obtained from:

$$C_{m_{i_h}} = -C_{L_{\alpha_h}} \eta_h \bar{V}_h$$

All the input values were previously obtained. This gave the value using Eqn. (46) of $C_{m_{\delta_e}} = -2.4945$.

**Aileron control derivatives:**

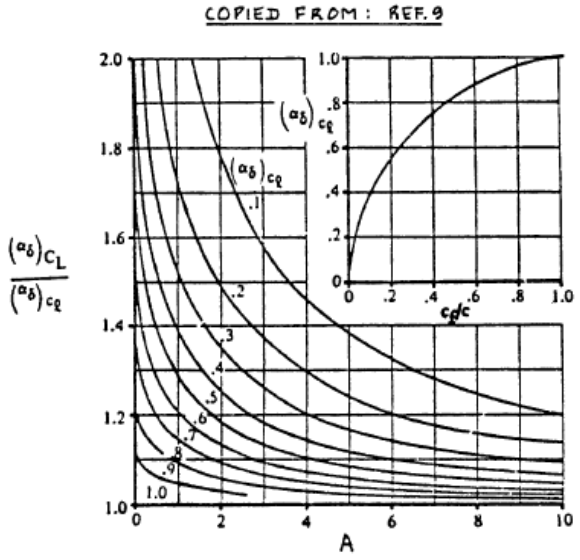


Figure 26. Effect of aspect ratio and flap-chord ratio on flap effectiveness

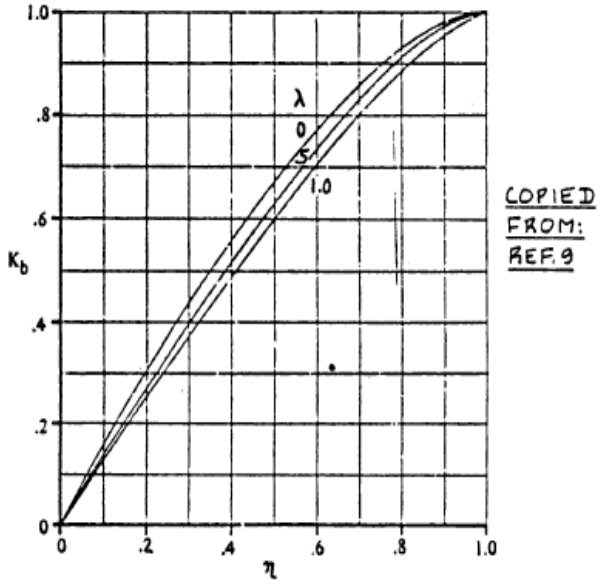


Figure 25. Effect of taper ratio and flap span on $K_b$

1) Side-force-due-to-aileron derivative: This values is negligible for most conventional aileron arrangements. Only if ailerons are near a vertical tail (Example, F-106) a significant side-force due to aileron deflection may arise and wind tunnel data are required for such cases. For this case: $C_{y_{\delta_a}} = 0$.

2) Rolling-moment-due-to-aileron derivative: This is also called the roll control power. This was estimated using the methods presented in Reference 1 (Section 10.3.5) since the methods were much more complex and broader to describe here properly. The analysis gave $C_{l_{\delta_a}} = .1457$.

3) Yawing-moment-due-to-aileron derivative: This is also called the adverse aileron yaw and was computed from the following equation:

$$C_{n_{\delta_a}} = K_a C_{L_w} C_{l_{\delta_a}}$$

For preliminary purposes, $C_{L_w} = C_{L_1}$ as described earlier and $K_a$ was obtained from Fig. 27. This gave from the above equation: $C_{n_{\delta_a}} = -.00576$.

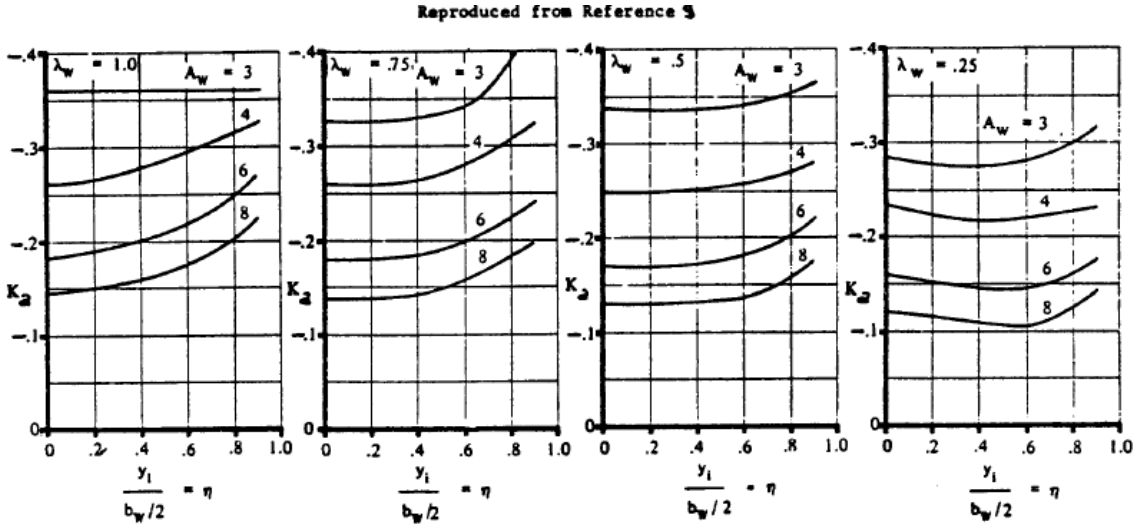


Figure 27. Correlation constant for yawing moment due to aileron deflection

**Rudder control derivatives:**

1) Side-force-due-to-rudder derivative: This was calculated from Eqn. (47):

$$C_{y_{\delta_r}} = C_{L_{a_v}} K' K_b \times \left\{ \frac{c_{l_\delta}}{(c_{l_\delta})_{theory}} \right\} (c_{l_\delta})_{theory} \times (S_v/S) \quad (47)$$

Where, $C_{L_{a_v}}$ was obtained from the CFD data. Correction factor for rudder deflection, $k' = 1$ was assumed since no rudder deflection was done in cruise. $\left\{ \frac{c_{l_\delta}}{(c_{l_\delta})_{theory}} \right\}$ was obtained from Fig. 23 and had the same values as in Eqn. (45) because the vertical tail airfoil was assumed to be the same as the horizontal tail airfoil (NACA 0012). $K_b$ was calculated from Fig. 25 with appropriate substitution of rudder parameters. Finally, from Eqn. (47) $C_{y_{\delta_r}} = .1$.

2) Rolling-moment-due-to-rudder derivative: This was found from:

$$C_{l_{\delta_r}} = C_{y_{\delta_r}}\{(z_v cos\alpha - l_v sin\alpha)/b\} \quad (48)$$

Where, $z_v$ and $l_v$ were described in Fig. 16. So, Eqn. (48) gave $C_{l_{\delta_r}} = .0095$.

3) Yawing-moment-due-to-rudder derivative: This is also called the rudder control power and estimated from:

$$C_{n_{\delta_r}} = -C_{y_{\delta_r}}\{(l_v cos\alpha + z_v sin\alpha)/b\} \quad (49)$$

The above equation gave $C_{n_{\delta_r}} = -.0408$.

**Moment of inertia calculation:** Reference 2 was unable to provide the mass inertias of the aircraft during cruise. So, historical data was considered while figuring out the inertias. This process involved a lot of errors in calculation as the data obtained from Fig. 28 did not have a clear trend line.

| Airplane Type | GW lbs | Wing Span, b, ft | Total Length, L, ft | e = (b+L)/2, ft | $\bar{R}_x$ | $\bar{R}_y$ | $\bar{R}_z$ | Number of engines and disposition |
|---|---|---|---|---|---|---|---|---|
| Beech 55 | 4,880 | 37.8 | 25.7 | 31.8 | 0.260 | 0.329 | 0.399 | 2 on wing |
| Beech 95 | 4,000 | 37.8 | 25.3 | 31.6 | 0.251 | 0.327 | 0.391 | 2 on wing |
| Beech D-50 | 6,500 | 45.9 | 31.5 | 38.7 | 0.240 | 0.313 | 0.384 | 2 on wing |
| Beech D18S | 9,000 | 47.7 | 34.2 | 41.0 | 0.232 | 0.360 | 0.396 | 2 on wing |
| Cessna 402* | 5,000 | 39.9 | 36.3 | 38.1 | 0.414 | 0.278 | 0.502 | 2 on wing |
| Cessna 402 | 6,200 | 39.9 | 36.3 | 38.1 | 0.373 | 0.269 | 0.461 | 2 on wing |
| Cessna 404* | 4,851 | 46.7 | 39.5 | 43.1 | 0.324 | 0.318 | 0.446 | 2 on wing |
| Cessna 404 | 8,400 | 46.7 | 39.5 | 43.1 | 0.340 | 0.284 | 0.445 | 2 on wing |
| Cessna 441* | 5,642 | 49.3 | 39.0 | 44.2 | 0.285 | 0.345 | 0.429 | 2 on wing |
| Cessna 441 | 9,925 | 49.3 | 39.0 | 44.2 | 0.256 | 0.212 | 0.336 | 2 on wing |

*at $W_E$

Figure 28. Non-dimensional radii of gyration for twin engine propeller driven airplanes [4]

Reference 4 presented the Class I methods for estimating the inertia. The moment inertia was found using Eqn. (50)

$$I_{xx} = (R_x)^2 W/g$$
$$I_{yy} = (R_y)^2 W/g \quad (50)$$
$$I_{zz} = (R_z)^2 W/g$$

Where,

$$\bar{R}_x = 2R_x/b$$
$$\bar{R}_y = 2R_y/b \quad (51)$$
$$\bar{R}_z = 2R_z/e$$

$\bar{R}_x, \bar{R}_y$ and $\bar{R}_z$ in Eqn. (51) were obtained from the average data in Fig. 28 removing the outliers first. The normalized data was then standardized using $b$ and $e$ from Tecnam P 2006T. The standardized radii of gyration $R_x, R_y$ and $R_z$were then obtained using Eqn. (51). Thus, the aircraft inertias were obtained from Eqn. (50) and using cruise weight (95% of maximum takeoff weight). The calculation provided the following values:

$$I_{xx} = 2915\ (slug \cdot ft^2);\ I_{yy} = 1788\ (slug \cdot ft^2);\ I_{zz} = 4480\ (slug \cdot ft^2);\ I_{xz} = 0\ (slug \cdot ft^2)$$

It was noted that there was no rapid method for the calculation of $I_{xz}$. This product of inertia could be realistically evaluated only from Class II weight and balance analysis which was out of the scope of this course. Moreover, this was not important for a preliminary estimation. [Reference 4]

**MATLAB code and transfer functions:** The MATLAB code (Appendix A1) for calculating the transfer functions took in as inputs the above calculations that were done and produced the transfer functions required as well as the longitudinal and lateral characteristic equations which were required for performing the handling quality analysis. The MATLAB code was based upon the calculations performed in McRuer Aircraft Dynamics and Automatic Controls textbook (Reference 5). The equations for converting the non-dimensional stability derivatives to dimensional stability derivatives were given in Figs. 29 and 30 for longitudinal and lateral-directional stabilities respectively.

| QUANTITY | IN TERMS OF BASIC STABILITY DERIVATIVES | | | IN TERMS OF NONDIMENSIONAL STABILITY DERIVATIVE PARAMETERS |
|---|---|---|---|---|
| | DIMENSIONAL | | NONDIMENSIONAL | |
| | DEFINITIONS | UNIT | | |
| $X_u$ | $\frac{1}{m}\frac{\partial X}{\partial u}$ | $\frac{1}{sec}$ | $\frac{\rho SU}{m}\left(-C_D - C_{D_u}\right)^*$ | $\frac{1}{\tau} x_u^*$ |
| $X_w$ | $\frac{1}{m}\frac{\partial X}{\partial w}$ | $\frac{1}{sec}$ | $\frac{\rho SU}{2m}\left(C_L - C_{D_\alpha}\right)$ | $\frac{1}{\tau} x_w$ |
| $X_\delta$ | $\frac{1}{m}\frac{\partial X}{\partial \delta}$ | $\frac{ft}{sec^2 rad}$ | $\frac{\rho SU^2}{2m}\left(-C_{D_\delta}\right)$ | $\frac{U}{\tau} x_\delta$ |
| $Z_u$ | $\frac{1}{m}\frac{\partial Z}{\partial u}$ | $\frac{1}{sec}$ | $\frac{\rho SU}{m}\left(-C_L - C_{L_u}\right)^*$ | $\frac{1}{\tau} z_u$ |
| $Z_w$ | $\frac{1}{m}\frac{\partial Z}{\partial w}$ | $\frac{1}{sec}$ | $\frac{\rho SU}{2m}\left(-C_{L_\alpha} - C_D\right)$ | $\frac{1}{\tau} z_w$ |
| $Z_{\dot{w}}$ | $\frac{1}{m}\frac{\partial Z}{\partial \dot{w}}$ | $\frac{1}{1}$ | $\frac{\rho Sc}{4m}\left(-C_{L_{\dot{\alpha}}}\right)$ | $\frac{c}{\tau U} z_{\dot{w}}$ |
| $Z_q$ | $\frac{1}{m}\frac{\partial Z}{\partial q}$ | $\frac{ft}{sec\text{-}rad}$ | $\frac{\rho SUc}{4m}\left(-C_{L_q}\right)$ | $\frac{c}{\tau} z_q$ |
| $Z_\delta$ | $\frac{1}{m}\frac{\partial Z}{\partial \delta}$ | $\frac{ft}{sec^2 rad}$ | $\frac{\rho SU^2}{2m}\left(-C_{L_\delta}\right)$ | $\frac{U}{\tau} z_\delta$ |
| $M_u$ | $\frac{1}{I_y}\frac{\partial M}{\partial u}$ | $\frac{1}{sec\text{-}ft}$ | $\frac{\rho SUc}{I_y}\left(C_M + C_{M_u}\right)$ | $\frac{2}{\tau c} m_u$ |
| $M_w$ | $\frac{1}{I_y}\frac{\partial M}{\partial w}$ | $\frac{1}{sec\text{-}ft}$ | $\frac{\rho SUc}{2I_y} C_{M_\alpha}$ | $\frac{1}{\tau c} m_w$ |
| $M_{\dot{w}}$ | $\frac{1}{I_y}\frac{\partial M}{\partial \dot{w}}$ | $\frac{1}{ft}$ | $\frac{\rho Sc^2}{4I_y} C_{M_{\dot{\alpha}}}$ | $\frac{1}{\tau U} m_{\dot{w}}$ |
| $M_q$ | $\frac{1}{I_y}\frac{\partial M}{\partial q}$ | $\frac{1}{sec}$ | $\frac{\rho SUc^2}{4I_y} C_{M_q}$ | $\frac{1}{\tau} m_q$ |
| $M_\delta$ | $\frac{1}{I_y}\frac{\partial M}{\partial \delta}$ | $\frac{1}{sec^2 rad}$ | $\frac{\rho SU^2 c}{2I_y} C_{M_\delta}$ | $\frac{U}{\tau c} m_\delta$ |

Figure 29. Longitudinal static stability [5]

Here, it was noted that the stability derivatives acted along the aircrafts stability axis system. So, the inertia calculations, performed in the body axis system of the aircraft was converted into the stability axis using the conversion matrix included in the MATLAB code. However, for zero angle-of-attack (straight and level flight) the two inertias were the same.

| QUANTITY | IN TERMS OF BASIC STABILITY DERIVATIVES | | | IN TERMS OF NONDIMENSIONAL STABILITY DERIVATIVE PARAMETERS |
|---|---|---|---|---|
| | DIMENSIONAL | | NONDIMENSIONAL | |
| | DEFINITIONS | UNIT | | |
| $Y_v$ | $\frac{1}{mU}\frac{\partial Y}{\partial \beta}$ | $\frac{1}{sec}$ | $\frac{\rho SU}{2m} C_{y_\beta}$ | $\frac{1}{\tau} y_v$ |
| $Y_{\dot{v}}$ | $\frac{1}{mU}\frac{\partial Y}{\partial \dot{\beta}}$ | $\frac{1}{1}$ | $\frac{\rho Sb}{4m} C_{y_{\dot{\beta}}}$ | $\frac{b}{\tau U} y_{\dot{v}}$ |
| $Y_r^*$ | $\frac{1}{mU}\frac{\partial Y}{\partial r}$ | $\frac{1}{rad}$ | $\frac{\rho Sb}{4m} C_{y_r}$ | $\frac{b}{\tau U} y_r$ |
| $Y_p^*$ | $\frac{1}{mU}\frac{\partial Y}{\partial p}$ | $\frac{1}{rad}$ | $\frac{\rho Sb}{4m} C_{y_p}$ | $\frac{b}{\tau U} y_p$ |
| $Y_\delta^*$ | $\frac{1}{mU}\frac{\partial Y}{\partial \delta}$ | $\frac{1}{sec\text{-}rad}$ | $\frac{\rho SU}{2m} C_{y_\delta}$ | $\frac{1}{\tau} y_\delta$ |
| $N_\beta$ | $\frac{1}{I_z}\frac{\partial N}{\partial \beta}$ | $\frac{1}{sec^2}$ | $\frac{\rho SU^2 b}{2I_z} C_{n_\beta}$ | $\frac{U}{\tau b} n_v$ |
| $N_{\dot{\beta}}$ | $\frac{1}{I_z}\frac{\partial N}{\partial \dot{\beta}}$ | $\frac{1}{sec}$ | $\frac{\rho SUb^2}{4I_z} C_{n_{\dot{\beta}}}$ | $\frac{1}{\tau} n_{\dot{v}}$ |
| $N_r$ | $\frac{1}{I_z}\frac{\partial N}{\partial r}$ | $\frac{1}{sec}$ | $\frac{\rho SUb^2}{4I_z} C_{n_r}$ | $\frac{1}{\tau} n_r$ |
| $N_p$ | $\frac{1}{I_z}\frac{\partial N}{\partial p}$ | $\frac{1}{sec}$ | $\frac{\rho SUb^2}{4I_z} C_{n_p}$ | $\frac{1}{\tau} n_p$ |
| $N_\delta$ | $\frac{1}{I_z}\frac{\partial N}{\partial \delta}$ | $\frac{1}{sec^2 rad}$ | $\frac{\rho SU^2 b}{2I_z} C_{n_\delta}$ | $\frac{U}{\tau b} n_\delta$ |
| $L_\beta$ | $\frac{1}{I_x}\frac{\partial L}{\partial \beta}$ | $\frac{1}{sec^2}$ | $\frac{\rho SU^2 b}{2I_x} C_{\ell_\beta}$ | $\frac{U}{\tau b} \ell_v$ |
| $L_{\dot{\beta}}$ | $\frac{1}{I_x}\frac{\partial L}{\partial \dot{\beta}}$ | $\frac{1}{sec}$ | $\frac{\rho SUb^2}{4I_x} C_{\ell_{\dot{\beta}}}$ | $\frac{1}{\tau} \ell_{\dot{v}}$ |
| $L_r$ | $\frac{1}{I_x}\frac{\partial L}{\partial r}$ | $\frac{1}{sec}$ | $\frac{\rho SUb^2}{4I_x} C_{\ell_r}$ | $\frac{1}{\tau} \ell_r$ |
| $L_p$ | $\frac{1}{I_x}\frac{\partial L}{\partial p}$ | $\frac{1}{sec}$ | $\frac{\rho SUb^2}{4I_x} C_{\ell_p}$ | $\frac{1}{\tau} \ell_p$ |
| $L_\delta$ | $\frac{1}{I_x}\frac{\partial L}{\partial \delta}$ | $\frac{1}{sec^2 rad}$ | $\frac{\rho SU^2 b}{2I_x} C_{\ell_\delta}$ | $\frac{U}{\tau b} \ell_\delta$ |

Figure 30. Lateral-directional static stability [5]

From the MATLAB code presented in appendix the following transfer functions were obtained:

Elevator control input transfer functions:

$$\frac{\theta(s)}{\delta_e(s)} = \frac{-47.48s^2 - 212.6s - 7.016}{s^4 + 10.4s^3 + 83.48s^2 + 2.418s + 2.485}$$
$$\frac{w(s)}{\delta_e(s)} = \frac{-75.13s^3 - 11850s^2 - 321.5s - 442.4}{s^4 + 10.4s^3 + 83.48s^2 + 2.418s + 2.485}$$
$$\frac{u(s)}{\delta_e(s)} = \frac{-6.994s^2 + 424.6s + 6797}{s^4 + 10.4s^3 + 83.48s^2 + 2.418s + 2.485}$$

Aileron control input transfer functions:

$$\frac{\beta(s)}{\delta_a(s)} = \frac{.4049s^2 + 8.014s + 1.633}{s^4 + 8.976s^3 + 28.36s^2 + 117.75s - 1.0963}$$
$$\frac{\varphi(s)}{\delta_a(s)} = \frac{15.75s^2 + 16.01s + 135.6}{s^4 + 8.976s^3 + 28.36s^2 + 117.75s - 1.0963}$$
$$\frac{r(s)}{\delta_a(s)} = \frac{-.4049s^3 - 5.974s^2 - 1.497s + 18.05}{s^4 + 8.976s^3 + 28.36s^2 + 117.75s - 1.0963}$$

Rudder control input transfer functions:

$$\frac{\beta(s)}{\delta_r(s)} = \frac{.0463s^3 + 3.245s^2 + 21.56s - .2715}{s^4 + 8.976s^3 + 28.36s^2 + 117.75s - 1.0963}$$
$$\frac{\varphi(s)}{\delta_r(s)} = \frac{1.028s^2 - 1.961s - 5.698}{s^4 + 8.976s^3 + 28.36s^2 + 117.75s - 1.0963}$$
$$\frac{r(s)}{\delta_r(s)} = \frac{-2.87s^3 - 21.48s^2 - 2.453s - .7347}{s^4 + 8.976s^3 + 28.36s^2 + 117.75s - 1.0963}$$

These transfer functions were then used in the Simulink to plot the response of the aircraft.

**Handling qualities:**

Classification of airplanes:

For the purpose of this specification, an airplane shall be placed in one of the following classes:

Class I

| | |
|---|---|
| Small, light airplanes | Light utility<br>Primary trainer<br>Light observation |

Class II

| | |
|---|---|
| Medium weight, low-to-medium maneuverability airplanes | Heavy utility/search and rescue<br>Light or medium transport/cargo/tanker<br>Early warning/electronic countermeasures/airborne command,<br>control, or communications relay<br>Antisubmarine<br>Assault transport<br>Reconnaissance<br>Tactical bomber<br>Heavy attack<br>Trainer for Class II |

Class III

| | |
|---|---|
| Large, heavy, low-to-medium maneuverability airplanes | Heavy transport/cargo/tanker<br>Heavy bomber<br>Patrol/early warning/electronic countermeasures/airborne command, control, or communications relay<br>Trainer for Class III |

Class IV

| | |
|---|---|
| High-maneuverability airplanes | Fighter/interceptor<br>Attack<br>Tactical reconnaissance<br>Observation<br>Trainer for Class IV |

TECNAM P 2006T is a Light utility/trainer aircraft which falls under CLASS I aircrafts.

Flight Phases:

| | |
|---|---|
| Category A<br>Those nonterminal Flight Phases that require rapid maneuvering, precision tracking, or precise flight-path control. | a. Air-to-air combat (CO)<br>b. Ground attack (GA)<br>c. Weapon delivery/launch (WD)<br>d. Aerial recovery (AR)<br>e. Reconnaissance (RC)<br>f. In-flight refueling (receiver) (RR)<br>g. Terrain following (TF)<br>h. Antisubmarine search (AS)<br>i. Close formation flying (FF). |

| | |
|---|---|
| Category B<br>Those nonterminal Flight Phases that are normally accomplished using gradual maneuvers and without precision tracking, although accurate flight-path control may be required. | a. Climb (CL)<br>b. Cruise (CR)<br>c. Loiter (LO)<br>d. In-flight refueling (tanker) (RT)<br>e. Descent (D)<br>f. Emergency descent (ED)<br>g. Emergency deceleration (DE)<br>h. Aerial delivery (AD). |

| | |
|---|---|
| Category C<br>Terminal Flight Phases are normally accomplished using gradual maneuvers and usually require accurate flight-path control. | a. Takeoff (TO)<br>b. Catapult takeoff (CT)<br>c. Approach (PA)<br>d. Wave-off/go-around (WO)<br>e. Landing (L) |

The handling qualities were evaluated at cruise condition since the stability derivatives were calculated at cruise. So the flight phase falls under CATEGORY B.

Levels of flying qualities:

| | |
|---|---|
| Level 1 | Flying qualities clearly adequate for the mission Flight Phase |

| | |
|---|---|
| Level 2 | Flying qualities adequate to accomplish the mission Flight Phase, but some increase in pilot workload or degradation in mission effectiveness, or both, exists |
| Level 3 | Flying qualities such that the airplane can be controlled safely, but pilot workload is excessive or mission effectiveness is inadequate, or both. Category A Flight Phases can be terminated safely, and Category B and C Flight Phases can be completed |

Longitudinal Characteristic Equation: $s^4 + 10.4s^3 + 83.48s^2 + 2.418s + 2.485$

Poles: $s = -5.19 \pm 7.5i;\ s = -.0127 \pm .172i$

Short Period mode:
It is characterized by complex conjugate roots with a moderate to relatively high damping ration and relatively high natural frequency and damped natural frequency. From the longitudinal characteristic equation $\zeta_{sp} = .569$ and $\omega_{nsp} = 9.12\ (rad/s)$. From Reference 3 (Eqn. 7.59): $\frac{n}{\alpha} \approx -\frac{z_\alpha}{g} \approx 37\ (g's/rad)$

Table 1. Short-period damping ratio limit

| Level | Category A and C Flight Phases | | Category B Flight Phases | |
|---|---|---|---|---|
| | Minimum | Maximum | Minimum | Maximum |
| 1 | 0.35 | 1.30 | 0.30 | 2.00 |
| 2 | 0.25 | 2.00 | 0.20 | 2.00 |
| 3 | 0.15* | - | 0.15* | - |

* May be reduced at altitudes above 20,000 feet if approved by the procuring activity

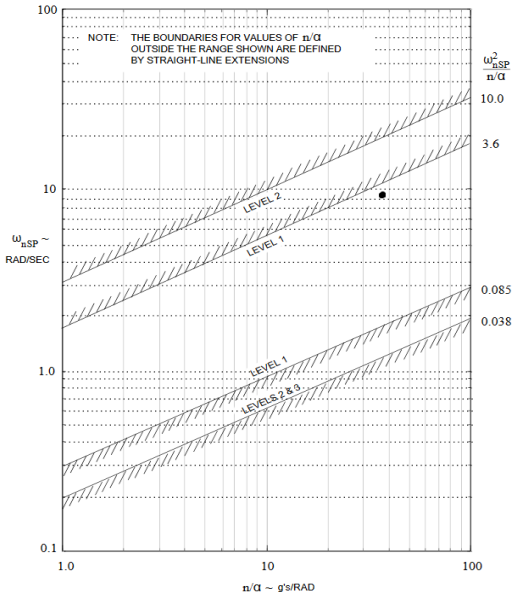


Figure 31. Short-period natural frequency requirements

(obtained from MATLAB code). From Fig. 31, the aircraft falls within the Level 1 requirements for MIL-F-8785C standard (indicated by the black dot). In the short period, there is also a damping ratio limit For Category B flight phases to be Level 1 the limit is $.3 \leq \zeta_{sp} \leq 2$ (Table 1). The aircraft has $\zeta_{sp} = .569$ and meets the Level 1 criterion. Overall, Tecnam P 2006T is Level 1 in short period mode.

Phugoid mode:
It is characterized by complex conjugate roots with a relatively low damping ratio and damped/natural frequency. From the longitudinal characteristic equation: $\zeta_p = .0733$ and $\omega_{np} = .173\ (rad/s)$. MIL-F-8785C only has a requirement on damping ratio for the phugoid mode. The requirement is:

a. Level 1 ----- $\zeta_p$ at least 0.04
b. Level 2 ----- $\zeta_p$ at least 0
c. Level 3 ----- $T_2$ at least 55 $seconds$

Obtained phugoid damping ratio $\zeta_p = .0733 > .04$. So Tecnam P 2006T passes Level 1 in phugoid mode.

Lateral Characteristic Equation: $s^4 + 8.976s^3 + 28.36s^2 + 117.75s - 1.0963$

Poles: $s = -.841 \pm 3.93i;\ s = -7.3;\ s = .00929$

Roll mode:

It has a real root and a first order (non-oscillatory) response that involves almost a pure rolling motion about the x-stability axis. It is usually stable at low angles of attack and can be unstable at high angles of attack. MIL-F-8785C specifies maximum limits on the roll mode time constant, which depends on class and category given in Table 2. The compliance region for roll mode root is: $s < -\frac{1}{\tau_{max}}$. From Table 2., for aircrafts of all classes with flight phase category B, $\tau_{max} = 1.4$ for Level 1. That means $s < -.714$. Above data indicates that our roll mode pole $s = -7.3 < -.714$. So Tecnam P 2006T is Level 1 in roll mode.

Spiral mode:

The spiral mode is a first order response (real root) that involves relatively slow roll and yawing motion of the aircraft. It can be stable or unstable. Spiral stability is usually compromised for good Dutch roll characteristics. MIL-8785C specifies that the spiral mode meet the requirements for time to double amplitude of the bank angle for bank angles up to 20 degrees presented in Table 3. Mathematically, the spiral root $s \leq \frac{.693}{T_{2min}}$. For all aircraft classes and for category B flight phase

Table 2. Maximum roll-mode time

| Flight Phase Category | Class | Level | | |
|---|---|---|---|---|
| | | 1 | 2 | 3 |
| A | I, IV | 1.0 | 1.4 | |
| | II,III | 1.4 | 3.0 | |
| B | All | 1.4 | 3.0 | 10 |
| C | I. II-C, IV | 1.0 | 1.4 | |
| | II-L, III | 1.4 | 3.0 | |

Table 3. Spiral stability: minimum time to double amplitude

| Flight Phase Category | Level 1 | Level 2 | Level 3 |
|---|---|---|---|
| A & C | 12 sec | 8 sec | 4 sec |
| B | 20 sec | 8 sec | 4 sec |

Table 4. Minimum Dutch-roll frequency and damping

| Level | Flight Phase Category | Class | Min $\zeta_d$* | Min $\zeta_d\omega_{nd}$* rad/sec. | Min $\omega_{nd}$ rad/sec. |
|---|---|---|---|---|---|
| 1 | A (CO and GA) | IV | 0.4 | - | 1.0 |
| | A | I, IV | 0.19 | 0.35 | 1.0 |
| | | II, III | 0.19 | 0.35 | 0.4** |
| | B | All | 0.08 | 0.15 | 0.4** |
| | C | I, II-C, IV | 0.08 | 0.15 | 1.0 |
| | | II-L, III | 0.08 | 0.10 | 0.4** |
| 2 | All | All | 0.02 | 0.05 | 0.4** |
| 3 | All | All | 0 | 0 | 0.4** |

MIL-F-8785C document requires minimum time to double amplitude be $T_{2min} = 20\ (s)$. That is, $s \leq .03465$. From the lateral characteristic equation $s = .00929 \leq .03465$. So Tecnam P 2006T passes Level 1 for spiral mode.

Dutch roll mode:

The Dutch roll mode is a second order response usually characterized by concurrent oscillations in the three lateral directional motion variables. From the lateral characteristic equation: $\zeta_{dr} = .209$ and $\omega_{ndr} = 4.02\ (rad/s)$. The MIL-F-8785C requirements for Dutch roll consists of a minimum $\zeta_{dr}$, a minimum $\omega_{ndr}$ and a minimum $\zeta_{dr}\omega_{ndr}$ described in Table 4. For aircrafts of all classes and for flight phase B the Level 1 minimum requirements are: $\zeta_{dr} = .08$; $\omega_{ndr} = .4\ (rad/s)$ and $\zeta_{dr}\omega_{ndr} = .15\ (rad/s)$. The aircraft has $\zeta_{dr} = .209 > .08$, $\zeta_{dr}\omega_{ndr} = .84 > .15\ (rad/s)$ and $\omega_{ndr} = 4.02 > .4\ (rad/s)$. So, Tecnam P 2006T passes level for Dutch roll mode as well.

**Simulink simulations:** The transfer functions obtained using Reference 5 were plotted in Simulink to obtain the response characteristics of the aircraft due to small aileron, rudder and elevator inputs. The response time history of an example airplane to an elevator pulse is shown in Fig. 32. Using two time scales in Fig. 32 the short period and the phugoid mode are emphasized. Here, it is seen that the maximum amplitudes of $u$ and $h$ are very much smaller in the short period than in the phugoid, and that the maximum amplitude of $w\ (= U_o\alpha)$ during the phugoid is very nearly

zero. Further, the maximum amplitudes of $\theta$ in each mode are comparable in magnitude. Plotting the transfer function in response to an impulse input, similar graphs were obtained for short period and phugoid mode. The graphs obtained were shown in Fig. 33.

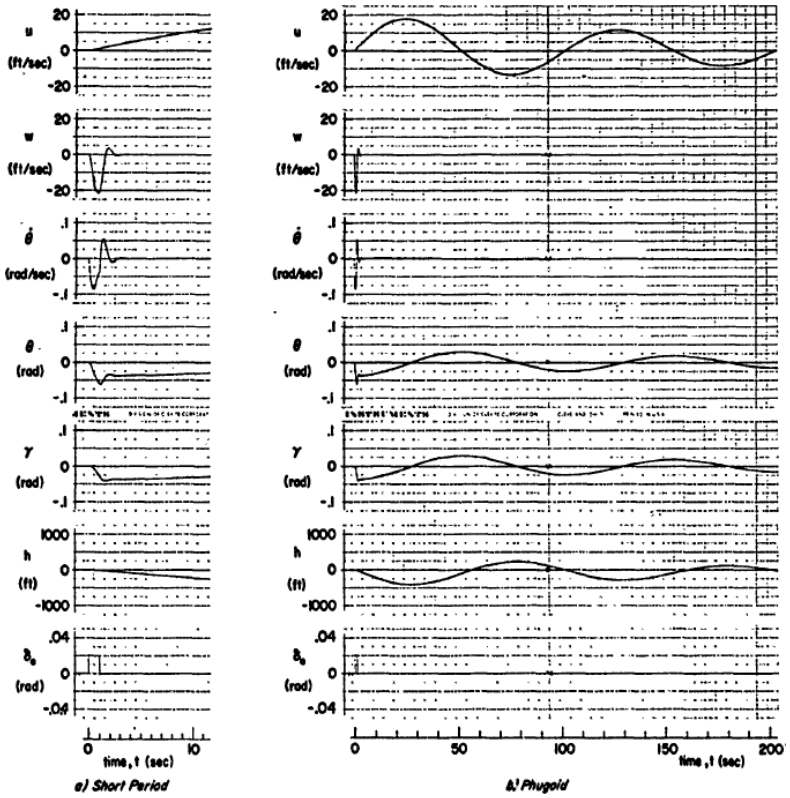


Figure 32. Time history for impulse elevator deflection [5]

| | | |
|---|---|---|
| $\frac{\theta(s)}{\delta_e(s)}$ | 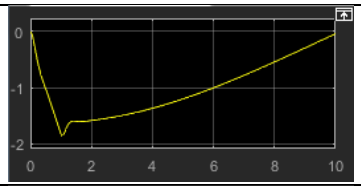 | 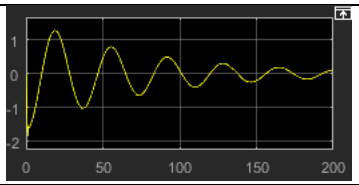 |
| $\frac{w(s)}{\delta_e(s)}$ | 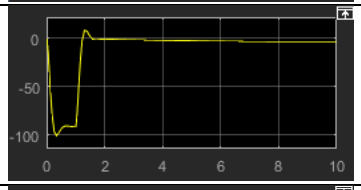 | 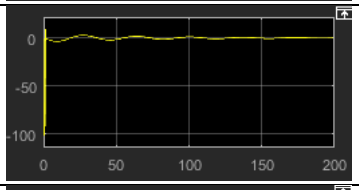 |
| $\frac{u(s)}{\delta_e(s)}$ | 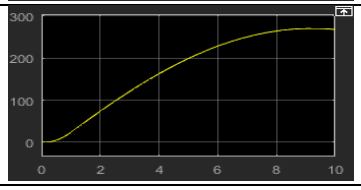 | 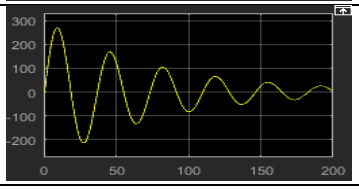 |

Figure 33. Response to an impulse elevator input to Short period(left) and Phugoid( right)

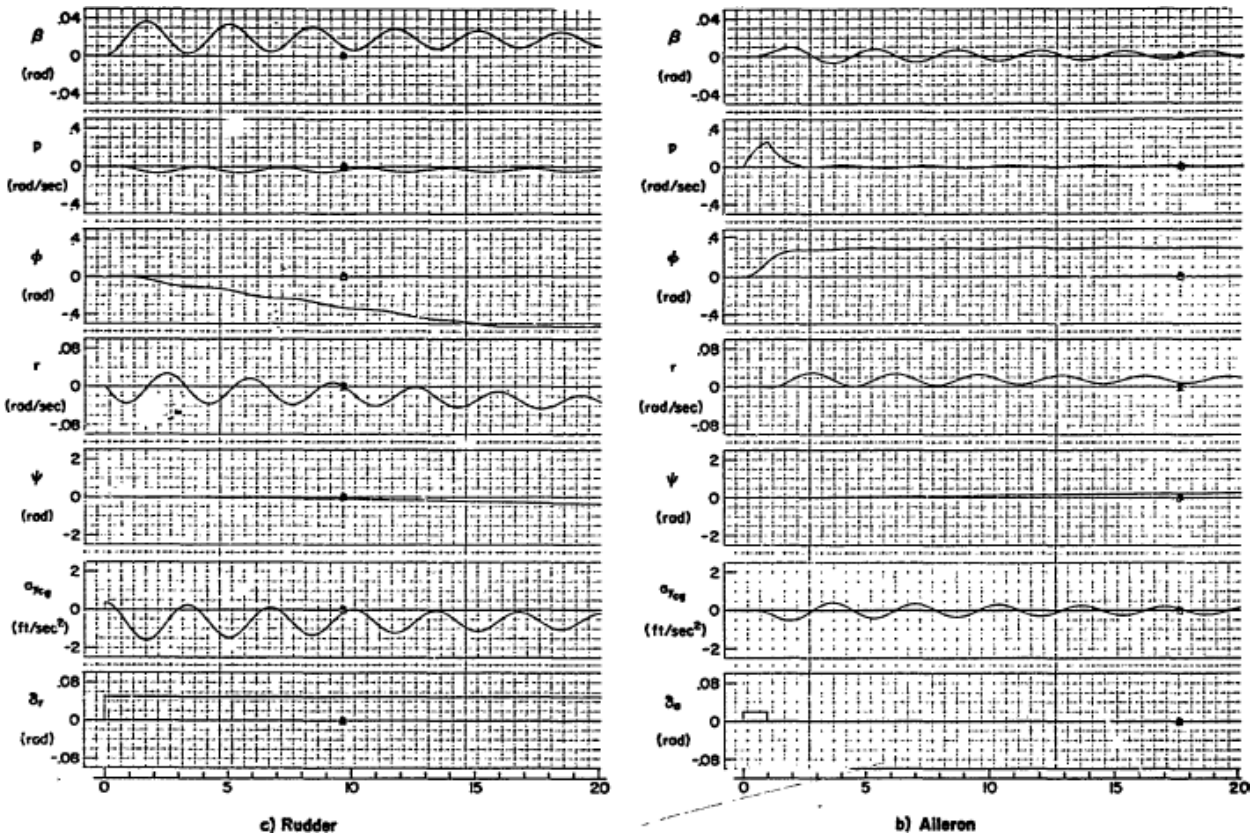


**Figure 34.** Time history for impulse rudder-aileron deflection [5]

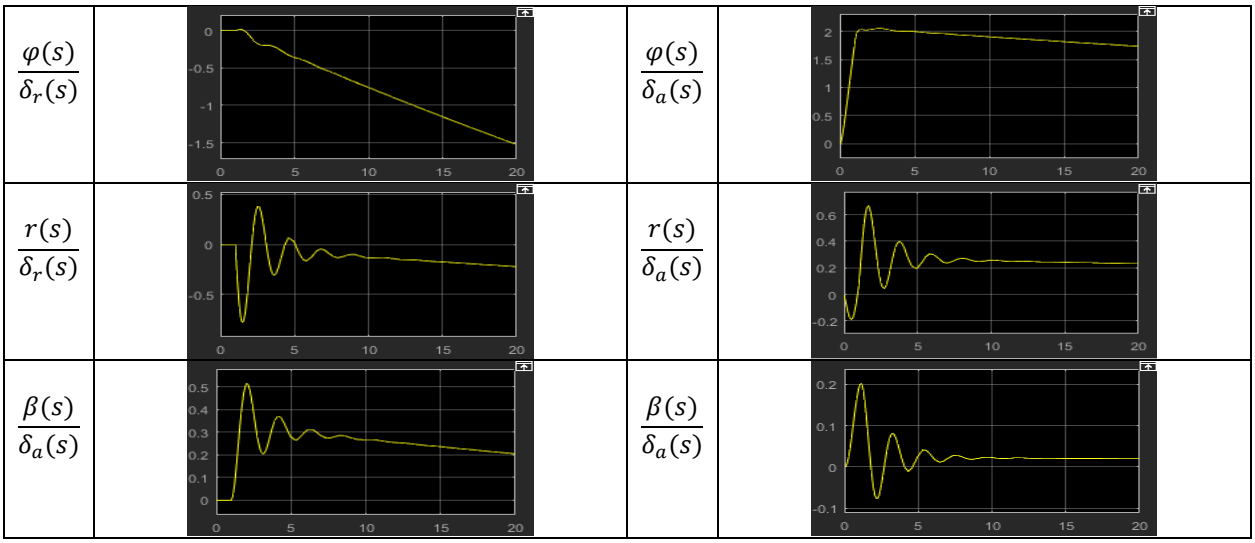


**Figure 35. Response of rudder(left) and aileron (right) to step and impulse inputs respectively**

Fig. 34 presents time histories of the responses to an aileron pulse and a rudder step. Here, it was seen that the primary response to an aileron input is in roll angle; and that nearly constant angle is achieved in a short time, corresponding to a response time $3T_R$ of the roll subsidence mode. The spiral mode divergence is not discernible due to its extremely large time constant, 738 sec. The Dutch roll excited by the aileron appears to be mostly in $\beta$ and $r$, but the much larger scale used for the $\varphi$ trace tends to mask its magnitude relative to $\beta$ and $r$. The magnitudes of these three motions in the Dutch roll mode are more easily seen in the time histories for a rudder step. These also show a relatively small average roll rate response, indicative of the reduced excitation of the roll subsidence mode by the rudder as compared to the aileron. Fig. 35 showed the responses for the given aircraft. The rudder was excited with a step input whereas the aileron was excited with an impulse just like the conditions depicted in Fig. 34. The response for both the inputs provided similar graphs for roll angle $\varphi$.

**{THESE WILL BE IN APPENDIX}**

Appendix

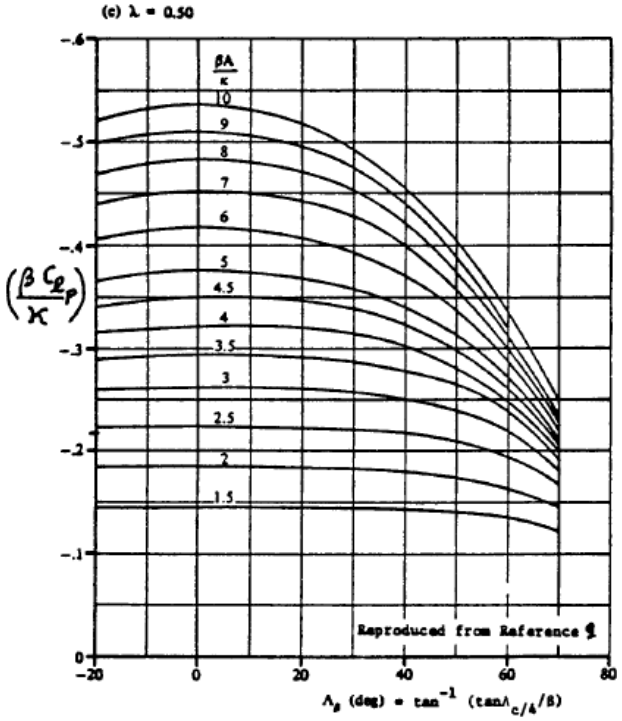


Figure A18. Effect of fuselage Reynold's number on wing fuselage directional stability

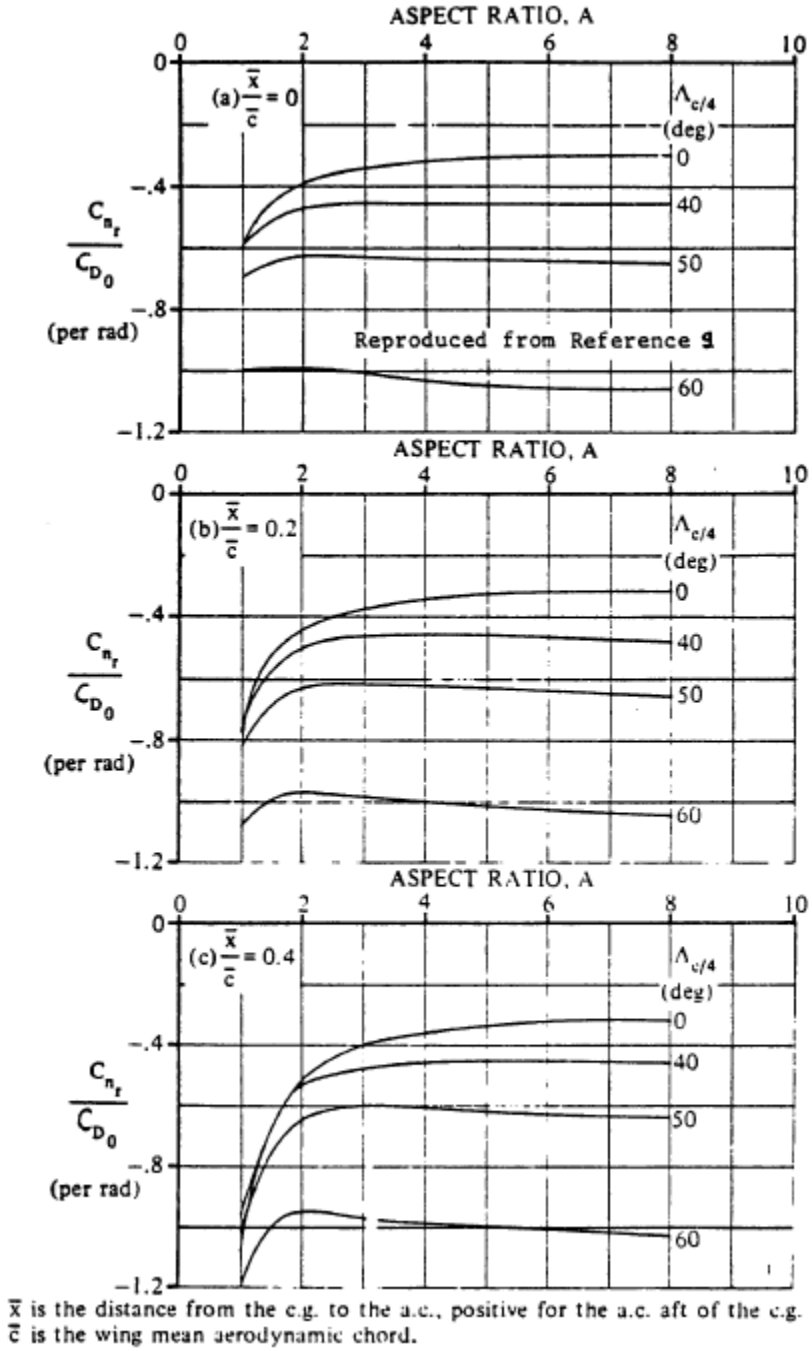


$\bar{x}$ is the distance from the c.g. to the a.c., positive for the a.c. aft of the c.g.
$\bar{c}$ is the wing mean aerodynamic chord.

Figure A22. Effect of fuselage Reynold's number on wing fuselage directional stability

## Appendix Tables

**Table A1. Jonathan's Empty Weight Preliminary Code**

Empty Weight Preliminary

| Inputs (lbs) | | | |
|---|---|---|---|
| Number of Passangers | 2 | 410 | 2740 |
| Number of Crew Members | 1 | 205 | |
| Weight limitations | | Fuel + Payload | W_Take Off (lbs) |
| Useful Load Limit (lbs) | 950 | | Landing Distance (ft) 2500 |

| Given (assumed from Historical Data) | | | | | | |
|---|---|---|---|---|---|---|
| Avg Weight/Person (lbs) | 175 | Propelent Efficiency | 0.82 | V_cr (Cruise Vel) (kts) | 140 |
| Avg Baggage/Person (lbs) | 30 | Cp | 0.5 | R_cr, Range (nm) | 725 |
| Total Payload (lbs) | 410 | L/D | 11 | h_cr (Cruis alt) (ft) | 5000 |
| | | | | V_stall Lndg (kts) | 48 |

| Phases | Fuel Fractions | Historical |
|---|---|---|
| 1 (Engine Start/ Warm Up) | W_1/W_to | 0.992 |
| 2 (Taxi) | W_2/W_1 | 0.996 |
| 3 (Take Off) | W_3/W_2 | 0.996 |
| 4 (Climb To Cruise) | W_4/W_3 | 0.99 |
| 5 (Cruise) | W_5/W_4 | 0.884 |
| 6 (Loiter) | W_6/W_5 | 1 |
| 7 (Descend) | W_7/W_6 | 0.992 |
| 8 (Land/Taxi/ Shut Down) | W_8/W_7 | 0.992 |
| **Mff** | **W_8/W_to** | **0.848** |

| FUEL WEIGHT Paramers | | |
|---|---|---|
| W_Take Off (lbs) | 2740.000 | |
| W_Trapped Fuel/Oil (lbs) | 137 | |
| W_Operating Empty (lbs) | 1912.195 | |
| W_Operating Empty, tentative (lbs) | 1912.206 | |
| W_Empty (lbs) | 1570.195 | |
| W_Empty, tentative (lbs) | 1570.206 | |
| Diff (lbs) | 0.011 | |
| W Availble for fuel (lbs) | 335 | |
| available Gallons of Fuel (Gal.) | 55.7 | |
| W_F_used (lbs) | 417.794 | |
| W_F_reserve (lbs) | 0 | |
| W_FUEL Total (lbs) | 417.794 | |

| HISTORICAL DATA (for Twin Engines) | | |
|---|---|---|
| A (Slope) | 0.113 | CL_max 1.4 |
| B (Intercept) | 1.0403 | CL_max T.O. 1.6 |
| C (We+D)/Wto) | 0.7975 | CL_max Ldng. 1.8 |
| D (PayLoad+Crew) | 615 | *SIZING TO CLIMB REQ.* |
| F (lbs) | 9414.9 | *fig. S_wet vs. W_to* |
| Y = Payload Weigth | 410 | c 0.8635 |
| d(C)/d(y) | 0 | d 0.5632 |
| d(D)/d(y) | 1 | |

should we subtract W_crew? W_TO = 3561.5 lbs

| Partial Derivatives (SENSITIVITY GRADIENTS) | | | | | |
|---|---|---|---|---|---|
| Airplane Growth | | | | | |
| d(Wto)/dR | d(Wto)/dy | d(Wto)/d(W_pL) | d(Wto)/d(cp) | d(Wto)/d(L/D) | d(Wto)/d(eta_prop) | d(Wto)/d(E) |
| 1.60 | 4.05 | 4.05 | 2321.3 | -105.51 | -1415.42 | 1.82 |

| | |
|---|---|
| Press Ratio, 'δ' | 0.832 |
| Temp Ratio, 'θ' | 0.966 |
| Dens Ratio, 'σ' | 0.862 |

**Table A2. Typical Values for Landing Weight to Takeoff Weight Ratio**

| | | $W_L/W_{TO}$ | | |
|---|---|---|---|---|
| Airplane Type | | Minimum | Average | Maximum |
| 1. | Homebuilts | 0.96 | 1.0 | 1.0 |
| 2. | Single Engine Propeller Driven | 0.95 | 0.997 | 1.0 |
| 3. | Twin Engine Propeller Driven | 0.88 | 0.99 | 1.0 |
| 4. | Agricultural | 0.7 | 0.94 | 1.0 |
| 5. | Business Jets | 0.69 | 0.88 | 0.96 |
| 6. | Regional TBP | 0.92 | 0.98 | 1.0 |
| 7. | Transport Jets | 0.65 | 0.84 | 1.0 |
| 8. | Military Trainers | 0.87 | 0.99 | 1.1 |
| 9. | Fighters (jets) | 0.78 | insufficient | 1.0 |
| | (tbp's) | 0.57 | data | 1.0 |
| 10. | Mil. Patrol, Bomb and Transports (jets) | 0.68 | 0.76 | 0.83 |
| | (tbp's) | 0.77 | 0.84 | 1.0 |
| 11. | Flying Boats, Amphibious and Float Airplanes (land) | 0.79 | insufficient | 0.95 |
| | (water) | 0.98 | data | 1.0 |
| 12. | Supersonic Cruise Airplanes | 0.63 | 0.75 | 0.88 |

**Table A3. Correlation Coefficients for Parasite Area vs. Wetted Area**

| Equivalent Skin Friction Coefficient, $c_f$ | a | b |
|---|---|---|
| 0.0090 | -2.0458 | 1.0000 |
| 0.0080 | -2.0969 | 1.0000 |
| 0.0070 | -2.1549 | 1.0000 |
| 0.0060 | -2.2218 | 1.0000 |
| 0.0050 | -2.3010 | 1.0000 |
| 0.0040 | -2.3979 | 1.0000 |
| 0.0030 | -2.5229 | 1.0000 |
| 0.0020 | -2.6990 | 1.0000 |

$$log_{10}(f) = a + b\ log_{10}(S_{wet}) \tag{30}$$

**Table A4. Regression Line Coefficients for Takeoff Weight Versus Wetted Area**

| Airplane Type | c | d |
|---|---|---|
| 1. Homebuilts | 1.2362 | 0.4319 |
| 2. Single Engine Propeller Driven | 1.0892 | 0.5147 |
| 3. Twin Engine Propeller Driven | 0.8635 | 0.5632 |
| 4. Agricultural | 1.0447 | 0.5326 |
| 5. Business Jets | 0.2263 | 0.6977 |
| 6. Regional Turboprops | -0.0866 | 0.8099 |
| 7. Transport Jets | 0.0199 | 0.7531 |
| 8. Military Trainers* | 0.8565 | 0.5423 |
| 9. Fighters* | -0.1289 | 0.7506 |
| 10. Mil. Patrol, Bomb and Transport | 0.1628 | 0.7316 |
| 11. Flying Boats, Amph. and Float | 0.6295 | 0.6708 |
| 12. Supersonic Cruise Airplanes | -1.1868 | 0.9609 |

$$log_{10}(S_{wet}) = c + d\ log_{10}(W_{TO}) \tag{31}$$

**Table A5. First estimates for $\Delta C_{D_0}$ and 'e' With Flaps and Gear Down**

| Configuration | $\Delta C_{D_0}$ | e |
|---|---|---|
| Clean | 0 | 0.80 - 0.85 |
| Take-off flaps | 0.010 - 0.020 | 0.75 - 0.80 |
| Landing Flaps | 0.055 - 0.075 | 0.70 - 0.75 |
| Landing Gear | 0.015 - 0.025 | no effect |

**Table A6. Group Weight Data for Twin Engine Propeller Driven Airplanes None Dimensional Data**

| NON - DIMENSIONAL DATA FOR A/C TYPE (LBS.) | | | | | | | | | | |
|---|---|---|---|---|---|---|---|---|---|---|
| | BEECH | | | | CESSNA | | | | ROCKWELL | |
| | 65 QA* | E-18S | G-50 TB* | 95 TA* | 310C | 404-3 | 414A | TP-441 | 690B | |
| FLIGHT DESIGN GROSS Weight, GW, lbs. | 7368 | 9700 | 7150 | 4000 | 4830 | 8400 | 6785 | 9925 | 10205 | AVERAGE (LBS.) 7596 |
| Structure/GW | 0.292 | 0.282 | 0.282 | 0.303 | 0.265 | 0.268 | 0.292 | 0.260 | 0.296 | 0.282 |
| Power Plan/GW | 0.219 | 0.235 | 0.224 | 0.218 | 0.259 | 0.194 | 0.206 | 0.128 | 0.164 | 0.205 |
| Fixed Equipment/GW | 0.123 | 0.128 | 0.114 | 0.122 | 0.103 | 0.134 | 0.167 | 0.194 | 0.187 | 0.141 |
| Empty Weight/GW | 0.638 | 0.651 | 0.624 | 0.649 | 0.628 | 0.596 | 0.665 | 0.582 | 0.647 | |
| Wing Group/GW | 0.091 | 0.090 | 0.092 | 0.115 | 0.094 | 0.102 | 0.094 | 0.088 | 0.098 | 0.096 |
| Empennage Group/GW | 0.021 | 0.019 | 0.022 | 0.020 | 0.024 | 0.022 | 0.024 | 0.023 | 0.020 | 0.022 |
| Fuselage Group/GW | 0.082 | 0.079 | 0.069 | 0.069 | 0.066 | 0.073 | 0.100 | 0.088 | 0.135 | 0.084 |
| Nacelle Group/GW | 0.039 | 0.034 | 0.037 | 0.045 | 0.027 | 0.034 | 0.029 | 0.026 | - | 0.034 |
| Land. Gear Group/GW | 0.060 | 0.060 | 0.063 | 0.055 | 0.054 | 0.038 | 0.045 | 0.035 | 0.043 | 0.051 |
| Take off Gross lbs. Wto | 7368 | 9700 | 7150 | 4000 | 4830 | 8400 | 6785 | 9925 | 10205 | 7270 |
| Empty Weight lbs. W_E | 4701 | 6318 | 4459 | 2595 | 3032 | 5006 | 4511 | 5781 | 6605 | 4779 |
| | Surface Areas, ft^2 | | | | | | | | | |
| Wing ,S | 277 | 361 | 277 | 194 | 175 | 242 | 226 | 254 | 266 | 252 |
| Horiz. Tail, Sh | 79.3 | 71.6 | 79.3 | 42.4 | 54.3 | 63.4 | 60.7 | 63.4 | 58.4 | 64 |
| Vert. Tail, Sv | 30.8 | 33.6 | 30.8 | 23.3 | 25.9 | 43.5 | 41.2 | 43.5 | 44.8 | 35 |
| Empennage Area, Semp | 110 | 105 | 110 | 66 | 80 | 107 | 102 | 107 | 103 | 99 |
| Wing Group/S , psf | 2.4 | 2.4 | 2.4 | 2.4 | 2.6 | 3.6 | 2.8 | 3.4 | 3.8 | 3 |
| Empennage/Semp , psf | 1.4 | 1.7 | 1.4 | 1.2 | 1.5 | 1.7 | 1.6 | 2.2 | 2.0 | 2 |
| Ultimate Load, g's | 6.60 | | 7.10 | | 5.70 | 3.75 | 3.75 | 3.75 | 3.75 | 4 |

## Appendix Figures

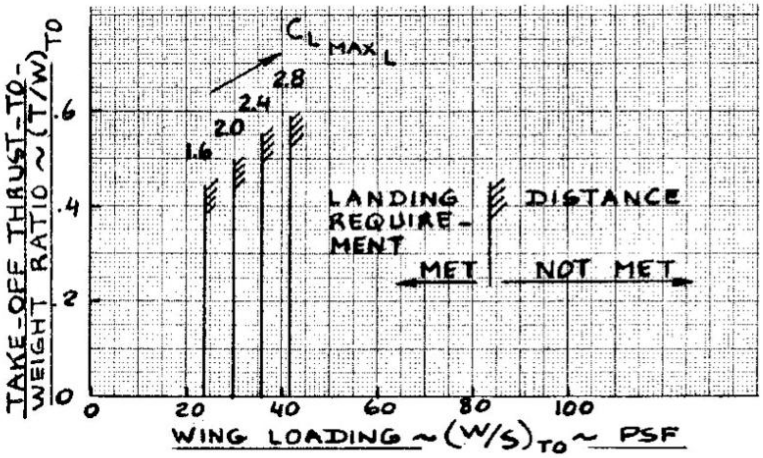


**Fig. A1. Allowable Wing Loadings to Meet a Landing Distance Requirement**

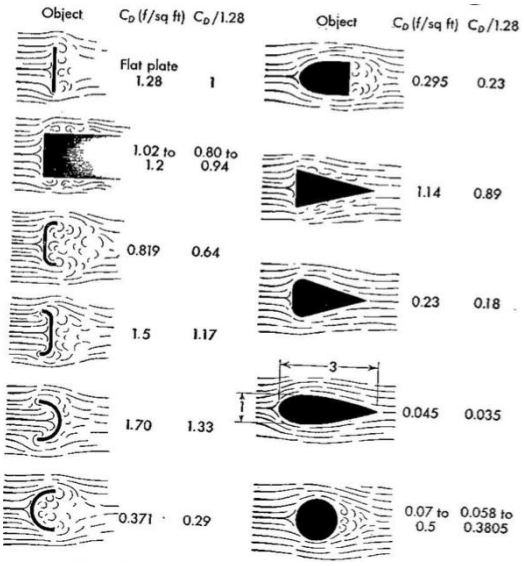


**Fig. A2. Relative Drag of Various Objects a Low Mach Numbers**

Table 8.3b) Twin Engine Propeller Driven Airplanes: Vertical Tail, Rudder and Aileron Data

| Type | Wing Area $S$ $ft^2$ | Wing Span $b$ ft | Vert. Tail Area $S_v$ $ft^2$ | $S_r/S_v$ | $x_v$ ft | $\bar{V}_v$ | Rudder Chord root/tip fr.$c_v$ | $S_a/S$ | Ail. Span Loc. in/out fr.b/2 | Ail. Chord in/out fr.$c_w$ |
|---|---|---|---|---|---|---|---|---|---|---|
| CESSNA | | | | | | | | | | |
| 310R | 179 | 36.9 | 26.1 | 0.45 | 15.9 | 0.063 | .48/.41 | 0.064 | .60/.90 | .30/.29 |
| 402B | 196 | 39.9 | 37.9 | 0.47 | 16.5 | 0.080 | .48/.40 | 0.058 | .64/.91 | .29/.27 |
| 414A | 226 | 44.1 | 41.3 | 0.38 | 17.0 | 0.071 | .49/.37 | 0.061 | .62/.87 | .30/.28 |
| T303 | 189 | 39.0 | 23.2 | 0.44 | 16.5 | 0.052 | .46/.39 | 0.087 | .64/.97 | .31/.30 |
| ConquestI | 225 | 44.1 | 41.3 | 0.38 | 17.1 | 0.071 | .47/.34 | 0.060 | .61/.86 | 0.29 |
| PIPER | | | | | | | | | | |
| PA-31P | 229 | 40.7 | 30.1 | 0.38 | 17.2 | 0.056 | .37/.40 | 0.056 | .59/.97 | .24/.29 |
| PA44-180T | 184 | 38.6 | 21.5 | 0.37 | 14.4 | 0.044 | .30/.30 | 0.077 | .45/.90 | .19/.18 |
| Chieftain | 229 | 40.7 | 29.5 | 0.40 | 17.3 | 0.055 | .40/.38 | 0.060 | .66/.98 | .24/.30 |
| Cheyen. I | 229 | 42.7 | 26.5 | 0.40 | 16.5 | 0.045 | .37/.42 | 0.057 | .62/.93 | .24/.29 |
| Cheye.III | 293 | 47.7 | 43.6 | 0.46 | 20.8 | 0.065 | 0.33 | 0.046 | .66/.94 | .23/.26 |
| BEECH | | | | | | | | | | |
| Duchess | 181 | 38.0 | 25.6 | 0.29 | 14.2 | 0.053 | .34/.42 | 0.059 | .67/.97 | 0.28 |
| Duke B60 | 213 | 39.3 | 28.8 | 0.43 | 17.4 | 0.060 | .44/.46 | 0.054 | .50/.84 | .24/.26 |
| Lear Fan | | | | | | | | | | |
| 2100 | 163 | 39.3 | 44.4 | 0.17 | 14.0 | 0.097 | .32/.34 | 0.044 | .72/.98 | .31/.24 |
| Rockwell | | | | | | | | | | |
| Comdr 700 | 200 | 42.5 | 39.9 | 0.38 | 20.5 | 0.096 | .37/.38 | 0.087 | .58/.99 | .28/.24 |
| Piaggio | | | | | | | | | | |
| P166-DL3 | 286 | 48.2 | 30.7 | 0.43 | 18.3 | 0.041 | .38/.43 | 0.073 | .61/.94 | .19/.22 |
| EMB-121 | 296 | 46.4 | 42.6 | 0.45 | 17.8 | 0.055 | .42/.41 | 0.052 | .71/.97 | 0.22 |

**Fig. A3. Vertical Tail Rudder and Aileron Data.**

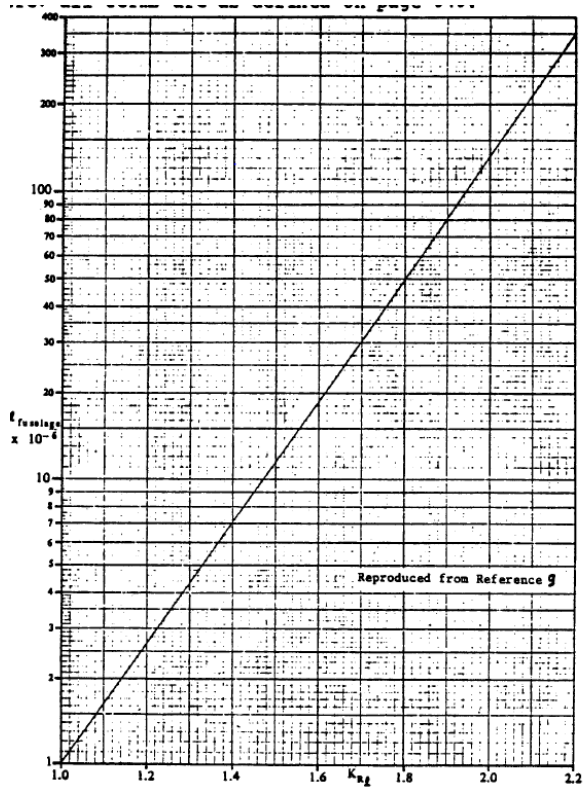


**Fig. A4. Fuselage Reynold's number calculation**

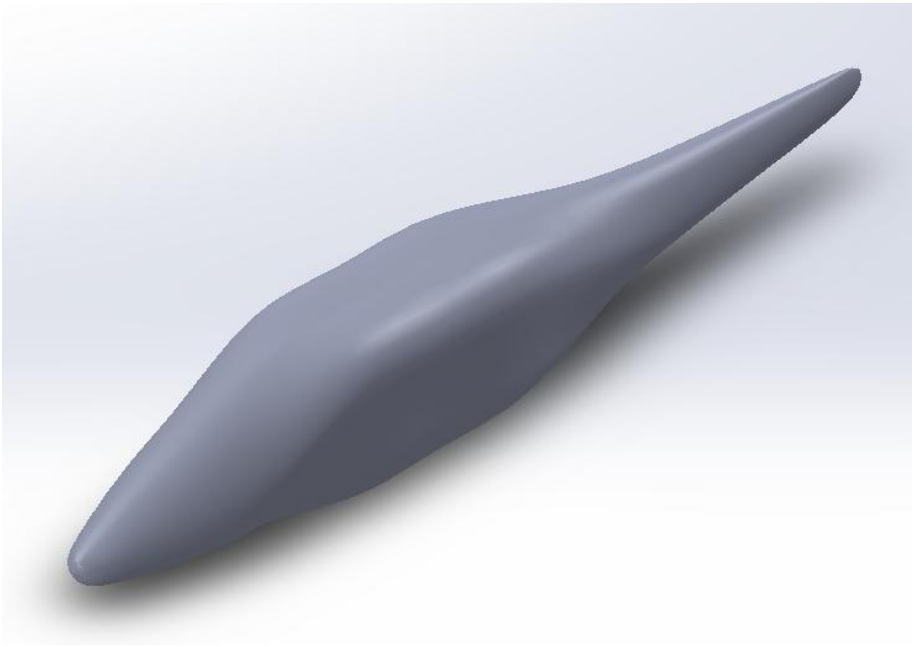

**Figure A1. 3D Representation of Tecnam's Fuselage.**

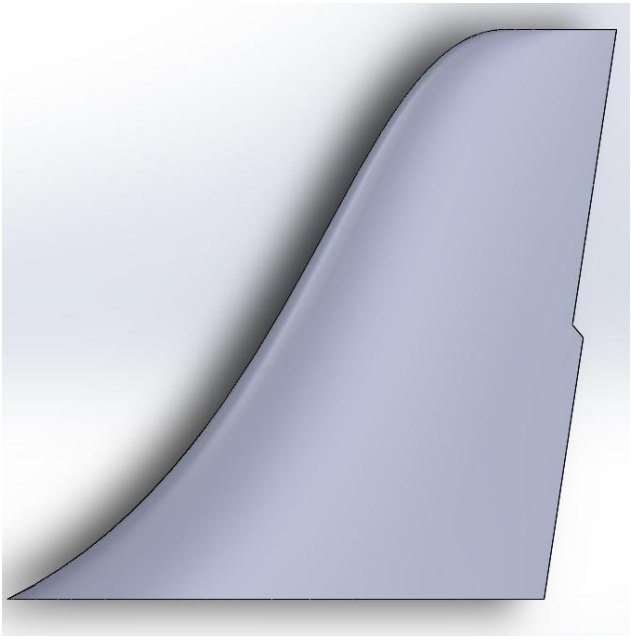

**Figure 2A. Tecnam's 3D Vertical Tail Representation.**

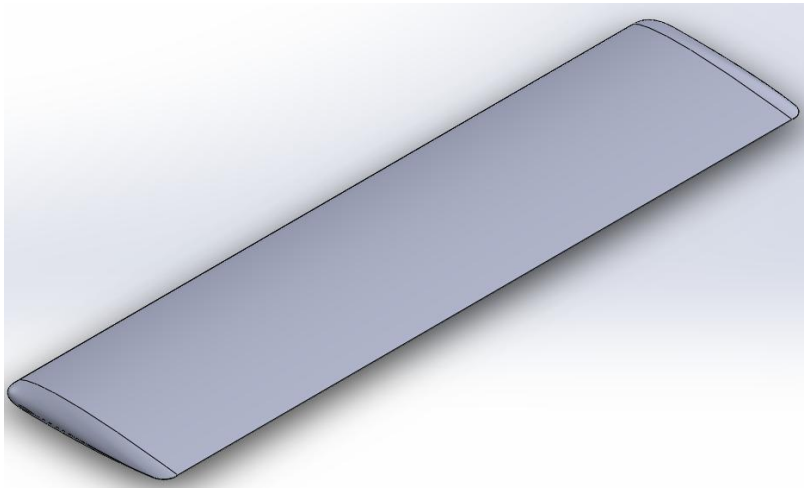

**Figure 3A. Tecnam 3D Horizontal Tail Representation.**

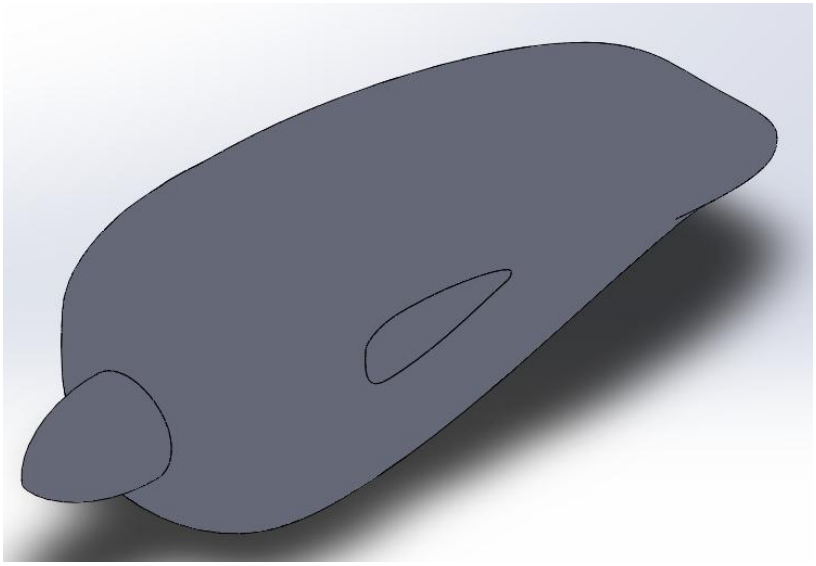

**Figure 4A Tecnam's Nacelles 3D Model.**

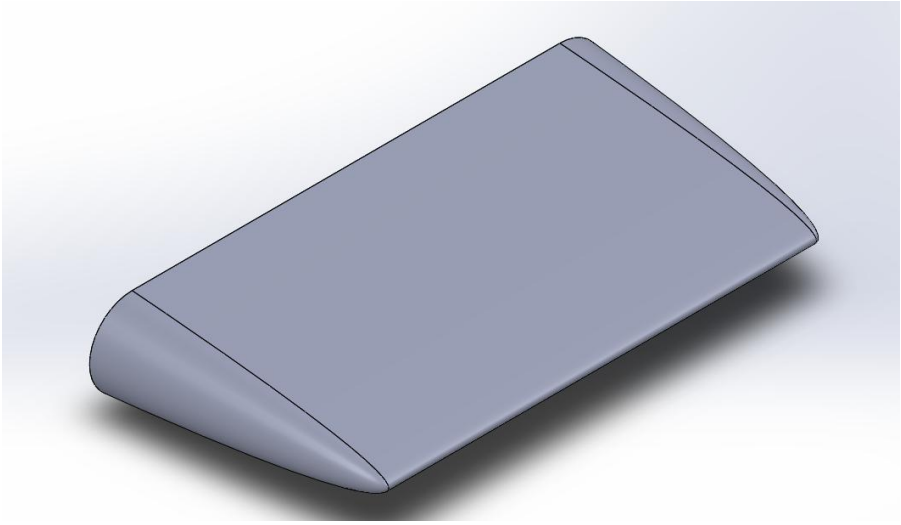

**Figure 5A. Tecnam's Gear Slots 3D Model**

**Table A-1. TecnamP2006T CFD Results at 1 Degree Angle of Attack**

| Iter | Mach | AoA | Beta | CL | CDo | CDi | CDtot | CS | L/D | E | CFx | CFy | CFz | CMx | CMy | CMz | T/QS |
|---|---|---|---|---|---|---|---|---|---|---|---|---|---|---|---|---|---|
| 1 | 0.21 | 1.00000 | 0.00000 | 0.18977 | 0.02542 | 0.00371 | 0.02913 | 0 | 6.51474 | 0.35065 | 0.0004 | 0 | 0.18981 | 0 | 0.3009 | 0 | 0 |
| 2 | 0.21 | 1.00000 | 0.00000 | 0.18974 | 0.02542 | 0.00371 | 0.02913 | 0 | 6.51423 | 0.35079 | 0.0004 | 0 | 0.18978 | 0 | 0.30091 | 0 | 0 |
| 3 | 0.21 | 1.00000 | 0.00000 | 0.18972 | 0.02542 | 0.00371 | 0.02913 | 0 | 6.51378 | 0.35078 | 0.0004 | 0 | 0.18976 | 0 | 0.30095 | 0 | 0 |
| 4 | 0.21 | 1.00000 | 0.00000 | 0.18975 | 0.02542 | 0.00371 | 0.02913 | 0 | 6.51459 | 0.35083 | 0.0004 | 0 | 0.18979 | 0 | 0.30094 | 0 | 0 |
| 5 | 0.21 | 1.00000 | 0.00000 | 0.18975 | 0.02542 | 0.00371 | 0.02913 | 0 | 6.51464 | 0.35089 | 0.0004 | 0 | 0.18978 | 0 | 0.30093 | 0 | 0 |

**Table A-2. TecnamP2006T CFD Results at 5 Degree Angle of Attack**

| Iter | Mach | AoA | Beta | CL | CDo | CDi | CDtot | CS | L/D | E | CFx | CFy | CFz | CMx | CMy | CMz | T/QS |
|---|---|---|---|---|---|---|---|---|---|---|---|---|---|---|---|---|---|
| 1 | 0.21 | 5.00000 | 0.00000 | 0.56050 | 0.02542 | 0.01298 | 0.0384 | 0 | 14.59616 | 0.87489 | -0.03592 | 0 | 0.5595 | 0.00001 | 0.31085 | 0 | 0 |
| 2 | 0.21 | 5.00000 | 0.00000 | 0.56041 | 0.02542 | 0.01296 | 0.03837 | 0 | 14.60419 | 0.87646 | -0.03593 | 0 | 0.5594 | 0.00001 | 0.31079 | 0 | 0 |
| 3 | 0.21 | 5.00000 | 0.00000 | 0.56000 | 0.02542 | 0.01294 | 0.03836 | 0 | 14.5994 | 0.87622 | -0.03591 | 0 | 0.559 | 0.00001 | 0.31198 | 0 | 0 |
| 4 | 0.21 | 5.00000 | 0.00000 | 0.55965 | 0.02542 | 0.01294 | 0.03835 | 0 | 14.59174 | 0.87538 | -0.03589 | 0 | 0.55865 | 0.00001 | 0.31299 | 0 | 0 |
| 5 | 0.21 | 5.00000 | 0.00000 | 0.55937 | 0.02542 | 0.01293 | 0.03835 | 0 | 14.58612 | 0.8748 | -0.03587 | 0 | 0.55837 | 0.00001 | 0.31368 | 0 | 0 |

**Table A-3. TecnamP2006T CFD Results at 6 Degree Angle of Attack**

| Iter | Mach | AoA | Beta | CL | CDo | CDi | CDtot | CS | L/D | E | CFx | CFy | CFz | CMx | CMy | CMz | T/QS |
|---|---|---|---|---|---|---|---|---|---|---|---|---|---|---|---|---|---|
| 1 | 0.21 | 6.00000 | 0.00000 | 0.66904 | 0.02542 | 0.01789 | 0.0433 | 0 | 15.44985 | 0.90484 | -0.05214 | 0 | 0.66724 | 0.00001 | 0.27219 | 0 | 0 |
| 2 | 0.21 | 6.00000 | 0.00000 | 0.65824 | 0.02542 | 0.01732 | 0.04274 | 0.00001 | 15.40146 | 0.90444 | -0.05158 | 0.00001 | 0.65645 | 0.00001 | 0.30633 | 0 | 0 |
| 3 | 0.21 | 6.00000 | 0.00000 | 0.65743 | 0.02542 | 0.01729 | 0.04271 | 0 | 15.39417 | 0.90391 | -0.05152 | 0 | 0.65564 | 0.00001 | 0.30765 | 0 | 0 |
| 4 | 0.21 | 6.00000 | 0.00000 | 0.65532 | 0.02542 | 0.01723 | 0.04264 | 0 | 15.3681 | 0.90149 | -0.05137 | 0 | 0.65353 | 0.00001 | 0.31332 | 0 | 0 |
| 5 | 0.21 | 6.00000 | 0.00000 | 0.65290 | 0.02542 | 0.01716 | 0.04257 | 0 | 15.3357 | 0.89838 | -0.05118 | 0 | 0.65112 | 0.00001 | 0.32006 | 0 | 0 |

**Table A-4. TecnamP2006T CFD Results at 10 Degree Angle of Attack**

| Iter | Mach | AoA | Beta | CL | CDo | CDi | CDtot | CS | L/D | E | CFx | CFy | CFz | CMx | CMy | CMz | T/QS |
|---|---|---|---|---|---|---|---|---|---|---|---|---|---|---|---|---|---|
| 1 | 0.21 | 10.00000 | 0.00000 | 1.04316 | 0.02542 | 0.04274 | 0.06816 | 0 | 15.30502 | 0.92061 | -0.13905 | 0 | 1.03473 | 0.00001 | 0.31533 | 0 | 0 |
| 2 | 0.21 | 10.00000 | 0.00000 | 1.04224 | 0.02542 | 0.04253 | 0.06795 | 0 | 15.33923 | 0.92357 | -0.1391 | 0 | 1.03379 | 0.00001 | 0.31671 | 0 | 0 |
| 3 | 0.21 | 10.00000 | 0.00000 | 1.04054 | 0.02542 | 0.04237 | 0.06778 | 0 | 15.35071 | 0.92407 | -0.13896 | 0 | 1.03209 | 0.00001 | 0.32114 | 0 | 0 |
| 4 | 0.21 | 10.00000 | 0.00000 | 1.03681 | 0.02542 | 0.04213 | 0.06755 | 0 | 15.34979 | 0.92266 | -0.13855 | 0 | 1.02837 | 0.00001 | 0.33153 | 0 | 0 |
| 5 | 0.21 | 10.00000 | 0.00000 | 1.03477 | 0.02542 | 0.04198 | 0.06739 | 0 | 15.35454 | 0.9224 | -0.13835 | 0 | 1.02634 | 0.00001 | 0.33659 | 0 | 0 |

**Table A-4. TecnamP2006T CFD Results at 11 Degree Angle of Attack**

| Iter | Mach | AoA | Beta | CL | CDo | CDi | CDtot | CS | L/D | E | CFx | CFy | CFz | CMx | CMy | CMz | T/QS |
|---|---|---|---|---|---|---|---|---|---|---|---|---|---|---|---|---|---|
| 1 | 0.21 | 11.00000 | 0.00000 | 1.14376 | 0.02542 | 0.05152 | 0.07694 | 0 | 14.86584 | 0.91812 | -0.16766 | 0 | 1.13258 | 0.00001 | 0.30947 | 0 | 0 |
| 2 | 0.21 | 11.00000 | 0.00000 | 1.14264 | 0.02542 | 0.05122 | 0.07664 | 0 | 14.90944 | 0.9217 | -0.16774 | 0 | 1.13142 | 0.00001 | 0.31116 | 0 | 0 |
| 3 | 0.21 | 11.00000 | 0.00000 | 1.14124 | 0.02542 | 0.05105 | 0.07646 | 0 | 14.92542 | 0.9226 | -0.16765 | 0 | 1.13001 | 0.00001 | 0.31427 | 0 | 0 |
| 4 | 0.21 | 11.00000 | 0.00000 | 1.13896 | 0.02542 | 0.05086 | 0.07627 | 0 | 14.93282 | 0.92236 | -0.1674 | 0 | 1.12773 | 0.00001 | 0.31948 | 0 | 0 |
| 5 | 0.21 | 11.00000 | 0.00000 | 1.13679 | 0.02542 | 0.05064 | 0.07606 | 0 | 14.9466 | 0.92277 | -0.1672 | 0 | 1.12557 | 0.00001 | 0.32474 | 0 | 0 |

**Table A-4. TecnamP2006T CFD Results at 15 Degree Angle of Attack**

| Iter | Mach | AoA | Beta | CL | CDo | CDi | CDtot | CS | L/D | E | CFx | CFy | CFz | CMx | CMy | CMz | T/QS |
|---|---|---|---|---|---|---|---|---|---|---|---|---|---|---|---|---|---|
| 1 | 0.21 | 15.00000 | 0.00000 | 1.55700 | 0.02542 | 0.0974 | 0.12281 | 0 | 12.67798 | 0.90006 | -0.3089 | 0 | 1.52916 | 0.00002 | 0.27345 | 0 | 0 |
| 2 | 0.21 | 15.00000 | 0.00000 | 1.55433 | 0.02542 | 0.09636 | 0.12178 | 0 | 12.76394 | 0.90662 | -0.30921 | 0 | 1.52631 | 0.00002 | 0.27677 | 0 | 0 |
| 3 | 0.21 | 15.00000 | 0.00000 | 1.55179 | 0.02542 | 0.09582 | 0.12124 | 0 | 12.79941 | 0.90871 | -0.30908 | 0 | 1.52372 | 0.00002 | 0.28014 | 0 | 0 |
| 4 | 0.21 | 15.00000 | 0.00000 | 1.54906 | 0.02542 | 0.0953 | 0.12071 | 0 | 12.8326 | 0.91052 | -0.30888 | 0 | 1.52094 | 0.00002 | 0.28394 | 0 | 0 |
| 5 | 0.21 | 15.00000 | 0.00000 | 1.54709 | 0.02542 | 0.0949 | 0.12031 | 0 | 12.85906 | 0.91205 | -0.30875 | 0 | 1.51893 | 0.00002 | 0.28693 | 0.00001 | 0 |

**Table A-5. TecnamP2006T's Fuselage CFD Result**

| Iter | Mach | AoA | Be | CDo | CDi | CDtot | CS | L/D | E | CFx | CFy | CFz | CMx | CMy | CMz | T/QS | |
|---|---|---|---|---|---|---|---|---|---|---|---|---|---|---|---|---|---|
| 1 | 0.21 | 15.00000 | | 0.00754 | 0 | 0.00754 | 0 | -0.2928 | 2.3E+10 | 0.00057 | 0 | -0.00213 | 0 | 0.08556 | 0 | 0 | 0 |
| 2 | 0.21 | 15.00000 | | 0.00754 | 0 | 0.00754 | 0 | -0.2928 | -1.8E+10 | 0.00057 | 0 | -0.00213 | 0 | 0.08556 | 0 | 0 | 0 |
| 3 | 0.21 | 15.00000 | | 0.00754 | 0 | 0.00754 | 0 | -0.2928 | -5E+10 | 0.00057 | 0 | -0.00213 | 0 | 0.08556 | 0 | 0 | 0 |
| 4 | 0.21 | 15.00000 | | 0.00754 | 0 | 0.00754 | 0 | -0.2928 | -1.4E+10 | 0.00057 | 0 | -0.00213 | 0 | 0.08556 | 0 | 0 | 0 |
| 5 | 0.21 | 15.00000 | | 0.00754 | 0 | 0.00754 | 0 | -0.2928 | -1.5E+10 | 0.00057 | 0 | -0.00213 | 0 | 0.08556 | 0 | 0 | 0 |

**Table A-6. TecnmaP2006T's Wing CFD Result**

| Iter | Mach | AoA | Beta | CL | CDo | CDi | CDtot | CS | L/D | E | CFx | CFy | CFz | CMx | CMy | CMz | T/QS |
|---|---|---|---|---|---|---|---|---|---|---|---|---|---|---|---|---|---|
| 1 | 0.21 | 0.00000 | 0.00000 | 0.14901 | 0.00947 | 0.00085 | 0.01032 | 0 | 14.43393 | 4.36543 | 0.00085 | 0 | 0.14901 | 0.00008 | -0.00742 | 0 | 0 |
| 2 | 0.21 | 0.00000 | 0.00000 | 0.14902 | 0.00947 | 0.00085 | 0.01032 | 0 | 14.43477 | 4.36665 | 0.00085 | 0 | 0.14902 | 0.00008 | -0.00742 | 0 | 0 |
| 3 | 0.21 | 0.00000 | 0.00000 | 0.14902 | 0.00947 | 0.00085 | 0.01032 | 0 | 14.43519 | 4.36728 | 0.00085 | 0 | 0.14902 | 0.00008 | -0.00742 | 0 | 0 |
| 4 | 0.21 | 0.00000 | 0.00000 | 0.14902 | 0.00947 | 0.00085 | 0.01032 | 0 | 14.43537 | 4.36765 | 0.00085 | 0 | 0.14902 | 0.00008 | -0.00742 | 0 | 0 |
| 5 | 0.21 | 0.00000 | 0.00000 | 0.14903 | 0.00947 | 0.00085 | 0.01032 | 0 | 14.43554 | 4.36788 | 0.00085 | 0 | 0.14903 | 0.00008 | -0.00742 | 0 | 0 |

**Table A-7. TecnmaP2006T's Horizontal Tail CFD Result**

| Iter | Mach | AoA | Beta | CL | CDo | CDi | CDtot | CS | L/D | E | CFx | CFy | CFz | CMx | CMy | CMz | T/QS |
|---|---|---|---|---|---|---|---|---|---|---|---|---|---|---|---|---|---|
| 1 | 0.21 | 0.00000 | 0.00000 | -0.07273 | 0.00184 | 0.00215 | 0.00399 | 0 | -18.2238 | 0.08889 | 0.00215 | 0 | -0.07273 | 0 | -0.00753 | 0 | 0 |
| 2 | 0.21 | 0.00000 | 0.00000 | -0.07272 | 0.00184 | 0.00215 | 0.00399 | 0 | -18.2266 | 0.08891 | 0.00215 | 0 | -0.07272 | 0 | -0.00753 | 0 | 0 |
| 3 | 0.21 | 0.00000 | 0.00000 | -0.07271 | 0.00184 | 0.00215 | 0.00399 | 0 | -18.2297 | 0.08894 | 0.00215 | 0 | -0.07271 | 0 | -0.00754 | 0 | 0 |
| 4 | 0.21 | 0.00000 | 0.00000 | -0.07270 | 0.00184 | 0.00215 | 0.00399 | 0 | -18.2316 | 0.08895 | 0.00215 | 0 | -0.0727 | 0 | -0.00754 | 0 | 0 |
| 5 | 0.21 | 0.00000 | 0.00000 | -0.07270 | 0.00184 | 0.00215 | 0.00399 | 0 | -18.2334 | 0.08897 | 0.00215 | 0 | -0.0727 | 0 | -0.00754 | 0 | 0 |

**Table A-8. TecnmaP2006T's Vertical Tail CFD Result**

| Iter | Mach | AoA | Beta | CL | CDo | CDi | CDtot | CS | L/D | E | CFx | CFy | CFz | CMx | CMy | CMz | T/QS |
|---|---|---|---|---|---|---|---|---|---|---|---|---|---|---|---|---|---|
| 1 | 0.21 | 0.00000 | 0.00000 | -0.00000 | 0.00126 | 0 | 0.00126 | 0 | 0 | 0 | 0 | 0 | 0 | 0 | 0 | 0 | 0 |
| 2 | 0.21 | 0.00000 | 0.00000 | -0.00000 | 0.00126 | 0 | 0.00126 | 0 | 0 | 0 | 0 | 0 | 0 | 0 | 0 | 0 | 0 |
| 3 | 0.21 | 0.00000 | 0.00000 | -0.00000 | 0.00126 | 0 | 0.00126 | 0 | 0 | 0 | 0 | 0 | 0 | 0 | 0 | 0 | 0 |
| 4 | 0.21 | 0.00000 | 0.00000 | -0.00000 | 0.00126 | 0 | 0.00126 | 0 | 0 | 0 | 0 | 0 | 0 | 0 | 0 | 0 | 0 |
| 5 | 0.21 | 0.00000 | 0.00000 | -0.00000 | 0.00126 | 0 | 0.00126 | 0 | 0 | 0 | 0 | 0 | 0 | 0 | 0 | 0 | 0 |

## Appendix Codes

### Engine CG

```
prompt={'Engine Weight:','Propeller Weight:'};
title='Engine Data';
data1=inputdlg(prompt,title);
xe = 1.84055;
ye = 1.88;
ze = 1.29411;
We = str2num(data1{1});
Wp = str2num(data1{2});
xcge = xe/1.7834296;
xcg = ((We*(xcge+1)+Wp*1)/(We+Wp))-1
ycge = ye/1.86364;
ycgp = ye/2;
ycg = (We*ycge+Wp*ycgp)/(We+Wp)
zcge = ze/1.58753;
zcgp = ze/1.04195;
zcg = (We*zcge+Wp*zcgp)/(We+Wp)
```

### Fuel Consumption

```
prompt={'Engine Power percent:'};
title='Engine Data';
data1=inputdlg(prompt,title);
Eng_Pow = str2num(data1{1});
Eng_RPM = .0124*(Eng_Pow^3)-2.3492*(Eng_Pow^2)+186.01*Eng_Pow-1704.7
fuel_consumption_l = (9*10^-8)*(Eng_RPM^2.2588);
fuel_consumption_gal_per_hour = fuel_consumption_l*.26417
fuel_consumption_lb_per_hour = fuel_consumption_gal_per_hour*6
```

### Fuel Tank Size

```
%Boundary Conditions
```

```
prompt={'Distance from leading edge to main beam(in):','Distance from leading
edge to secondary beam(in)','thickness of main beam(in):','thickness of
secondary beam(in):','Tank maximum fuel load(gal):'};
title='Fuel Tank Geometry';
data1=inputdlg(prompt,title);
primary_beam_length = str2num(data1{1});
secondary_beam_length = str2num(data1{2});
primary_beam_thickness = str2num(data1{3});
secondary_beam_thickness = str2num(data1{4});
fuel_tank_volume_gal = str2num(data1{5});

% a reduction factor for later material calculations
reduction_factor = .8;
primary_beam_length = ((1-reduction_factor)+1)*primary_beam_length;
secondary_beam_length = reduction_factor*secondary_beam_length;
primary_beam_thickness = reduction_factor*primary_beam_thickness;
secondary_beam_thickness = reduction_factor*secondary_beam_thickness;

%length Equations
Distance_from_beam_to_beam = secondary_beam_length-primary_beam_length;
y2_minus_y1 = secondary_beam_thickness-primary_beam_thickness;
m1 = (y2_minus_y1/Distance_from_beam_to_beam);
xf = 0:1:Distance_from_beam_to_beam;
Top_fuel_tank_slope = m1*(xf - primary_beam_length)+primary_beam_thickness;

%length and Height Geometry
fuel_tank_2D_geometry_in_square =
secondary_beam_thickness*(Distance_from_beam_to_beam)+.5*(Distance_from_beam_
to_beam)*(-y2_minus_y1);

%fuel tank Boundary Condition
fuel_tank_volume_in_cubed = fuel_tank_volume_gal*231

%Width of Fuel Tank
Geometry_width_inches =
fuel_tank_volume_in_cubed/fuel_tank_2D_geometry_in_square;

%change in airfoil thickness across wing
decreasing_airfoil_thickness = questdlg('Does the airfoil thickness decrease
with length along wing?','thickness change along wing','Yes','No','No');
switch decreasing_airfoil_thickness
    case 'Yes'
        airfoil_change = 1;
    case 'No'
        airfoil_change = 0;
end

%Airfoil thickness change with wing length
if airfoil_change == 1
```

```
    prompt={'thickness of primary beam midway through wing(in)','thickness of
primary beam near wing tip(in)','thickness of secondary beam midway through
wing(in)','thickness of secondary beam near wing tip(in)'};
title='change in thickness across wing';
data2=inputdlg(prompt,title);
primary_beam_thickness_mid = str2num(data2{1});
primary_beam_thickness_wing_tip = str2num(data2{2});
secondary_beam_thickness_mid = str2num(data2{3});
secondary_beam_thickness_wing_tip = str2num(data2{4});
primary_beam_thickness_mid = reduction_factor*primary_beam_thickness_mid;
primary_beam_thickness_wing_tip =
reduction_factor*primary_beam_thickness_wing_tip;
secondary_beam_thickness_mid = reduction_factor*secondary_beam_thickness_mid;
secondary_beam_thickness_wing_tip =
reduction_factor*secondary_beam_thickness_wing_tip;
%Width of Fuel Tank

geometry_thickness_Equations_1 =
.5*primary_beam_thickness+.5*primary_beam_thickness_mid
geometry_thickness_Equations_2 =
.5*secondary_beam_thickness+.5*secondary_beam_thickness_mid
Geometry_width_inches_varying_airfoil_thickness_1 =
fuel_tank_volume_in_cubed/(Distance_from_beam_to_beam*geometry_thickness_Equa
tions_1);
Geometry_width_inches_varying_airfoil_thickness_2 =
fuel_tank_volume_in_cubed/(Distance_from_beam_to_beam*geometry_thickness_Equa
tions_2);

if Geometry_width_inches_varying_airfoil_thickness_2 >
Geometry_width_inches_varying_airfoil_thickness_1;
    Geometry_width_inches_varying_airfoil_thickness =
Geometry_width_inches_varying_airfoil_thickness_2;
else
    Geometry_width_inches_varying_airfoil_thickness =
Geometry_width_inches_varying_airfoil_thickness_1;
end
else
end


%Change in angle across fuel tank calculator
prompt={'Fuel tank angle ( degrees)'};
title='Fuel tank angle for a gravity fuel flow';
data1=inputdlg(prompt,title);
fuel_tank_angle_degrees = str2num(data1{1});
fuel_tank_angle_radians = (3.1415/180)*fuel_tank_angle_degrees;
new_required_height_primary_thickness =
Geometry_width_inches*sin(fuel_tank_angle_radians)+primary_beam_thickness*cos
(fuel_tank_angle_radians);
```

```
new_required_height_secondary_thickness =
Geometry_width_inches*sin(fuel_tank_angle_radians)+secondary_beam_thickness*c
os(fuel_tank_angle_radians);
if new_required_height_primary_thickness >
.15*primary_beam_thickness+primary_beam_thickness;
    disp('Lower angle value required for Primary Beam')
elseif new_required_height_secondary_thickness
>.15*secondary_beam_thickness+secondary_beam_thickness;
    disp('Lower angle value required for Secondary Beam')
else
    disp('Angle is viable for fuel tank')
end


disp('so the geometry can be broken up into 2 parts, one being a rectangle
and one being a triangle and put together from there')

disp('with the rectangle length and height to be (in)')
rectangle_length = Distance_from_beam_to_beam
rectangle_height = secondary_beam_thickness

disp('with the triangle length and height to be (in)')
triangle_length = Distance_from_beam_to_beam
triangle_height = -y2_minus_y1

disp('with the rectangle and triangle 2D geometry being')
fuel_tank_2D_geometry_in_square

disp('And the width being')
if airfoil_change == 1
    Geometry_width_inches_varying_airfoil_thickness
else
Geometry_width_inches
end
```

**Flight Envelope Matlab**

```
h = 0:1000:20000;
w = 2700;
s = 175.5;
b = 35.05;
prompt={'e0:','Cd0L:','thrust per engine:','Max Coefficient of lift'};
title='FLight Envelope';
data1=inputdlg(prompt,title);
e0 = str2num(data1{1});
cd0l = str2num(data1{2});
tsl = 2*str2num(data1{3});
clmax = str2num(data1{4});
w = 2700;
s = 175.5;
```

```
b = 35.05;
rho=[.002377,.002308,.002241,.002175,.002111,.002048,.001987,.001927,.001868,
.001811,.001755,.001701,.001648,.001596,.001545,.001496,.001448,.001401,.0013
55,.00131,.001267];
%Preliminary calculations
AR=b^2/s; k=1/(pi*AR*e0);
%
% calculate the lift coefficients for high and low speed T=D flight from
% the Eqn.: KCL^2 - T/W CL + CD0L = 0
for ii=1:length(h);
t(ii)=tsl*rho(ii)/rho(1);
cl1=(t(ii)/w+sqrt((t(ii)/w)^2-4*k*cd0l))/(2*k);
cl2=(t(ii)/w-sqrt((t(ii)/w)^2-4*k*cd0l))/(2*k);
v1(ii)= sqrt(w/(0.5*rho(ii)*s*cl1));
v2(ii)= sqrt(w/(0.5*rho(ii)*s*cl2));
vstall(ii)=sqrt(w/(0.5*rho(ii)*s*clmax));
end
fid=fopen('F:\1 College\7th year\fall 2016\Senior Design 1\Power plant and
propeller\Propeller Efficiency\flight envelope data.txt','wt');
fprintf(fid,' Altitude Vstall Vmin Vmax \n');
for m= 1:length(h)-1
hr(m) = h(m); v1r(m) = v1(m); v2r(m)=v2(m); vstallr(m)=vstall(m)
fprintf(fid,'%8.0f %8.4f %8.4f %8.4f \n',...
hr(m),vstallr(m),v1r(m),v2r(m));
end
fclose(fid);
Fig.(6); hold;
plot(v1r,hr); plot(v2r,hr); plot(vstallr, hr);
xlabel('Airspeed');
ylabel('Altitude');
axis([0, 200, 5000, 20000]);
hold
```

**Thrust Available MatLab Code**

```
clear all
h = 5000:250:7500;
v=40:10:300;
%
%Enter aircraft properties
w = 2700;
s = 175.5;
b = 35.05;
e0 = .8;
cd0l = .0280;
tsl = 200*2;
clmax = 1.6;
%
%Enter densities of interest
```

```
rho=[.0020482,.002033,.002017,.002002,.001987,.001972,.001957,.001942,.001927
,.001912,.001898];
%
%Preliminary calculations
AR=b^2/s; k=1/(pi*AR*e0);
%
%Calculate thrust and drag - Use indices ii for altitude, and jj for
%airspeed
for ii = 1:length(h);
for jj = 1:length(v);
d0(ii,jj)=cd0l*0.5*rho(ii)*v(jj)^2*s;
di(ii,jj)=k*w^2/(0.5*rho(ii)*v(jj)^2*s);
dtot(ii,jj)=d0(ii,jj)+di(ii,jj);
t(ii,jj)=tsl*rho(ii)/rho(1);
end
vstall(ii)=sqrt(w/(0.5*rho(ii)*s*clmax));
end
for k=1:length(h);
Fig.(k);hold;
plot(v,dtot(k,:));
plot(v,t(k,:));
xlabel('airspeed (ft/sec)');
ylabel('Thrust, Drag (lbs)')
title('Thrust, Drag vs Airspeed');
grid on; hold;
end
fid=fopen('F:\1 College\7th year\fall 2016\Senior Design 1\Power plant and
propeller\Propeller Efficiency\thrust drag curve data.txt','wt');
for m=1:11
fprintf(fid,'\n');
fprintf(fid,'altitude=%8.00f  ft,\n', h(m));
fprintf(fid,' Airspeed Thrust Drag \n');
for n= 1:1:length(v)
fprintf(fid,'%8.0f %8.4f %8.4f\n',v(n),t(m,n),dtot(m,n));
end
end
```

## Acknowledgments

I.A.D. authors thank Dr. Smith for his guidance, exceptional instruction and inspiration to practice lifelong learning and to the Mechanical and Aerospace Engineering Program at the University of Texas at Arlington that has allowed for the acquisition of knowledge necessary to be successful in the industry.

## References

*Books*

[1]Innovative Aerospace Design, (I.A.D) *MAE 4350 Aircraft Design End of the Year Report*, University of Texas at Arlington, Arlington, Texas, 2016

[2]Roskam, Jan., *Airplane Design Part I: Preliminary Sizing of Airplanes*, Roskam Aviation and Engineering Corporation, Ottawa, Kansas, 1985, Chaps. 2, 3.

[3]Roskam, Jan., *Airplane Design Part II: Preliminary Configuration Design and Integration of the Propulsion System.,* Roskam Aviation and Engineering Corporation, Ottawa, Kansas, 1985, Chaps. 1-14.

[4]Nicolai, Leland M., Carichner, Grant E., *Fundamentals of Aircraft and Airship Design Volume I: Aircraft Design.*, American Institute of Aeronautics and Astronautics, Inc., Reston, VA, 2010, Chaps. 20.

[5]Abbot, Ira H., Von Doenhoff, Albert E., *Theory of Wing Sections: Including a Summary of Airfoil Data.*, Dover Publications, Inc., New York, NY, 1959, Pp. 465-466, 479-480.

[6]Courtland, Perkins D., Hage, Robert E., *Airplane Performance Stability and Control.*, John Wiley & Sons., New York, NY, 1959, Chap. 5.

[7]Oates, G. C. (ed.), *Aerothermodynamics of Gas Turbine and Rocket Propulsion*, AIAA Education Series, AIAA, New York, 1984, pp. 19, 136.

[8]Roskam, Jan., *Airplane Design Part VI: Preliminary Calculation of Aerodynamic Thrust and Power Characteristics.,* Roskam Aviation and Engineering Corporation, Ottawa, Kansas, 1985, Chaps. 1-14.

[9]Perkins, C. D., Hage, R. E. *Airplane Performance, Stability and Control.,* John Wiley & Sons., New York, NY, 1949, Ch. 5.

*Electronic Publications*

[9]Atkins, C. P., and Scantelbury, J. D., "The Activity Coefficient of Sodium Chloride in a Simulated Pore Solution Environment," *Journal of Corrosion Science and Engineering* [online journal], Vol. 1, No. 1, Paper 2, URL: http://www.cp/umist.ac.uk/JCSE/vol1/vol1.html [cited 13 April 1998].

[10]Vickers, A., "10-110 mm/hr Hypodermic Gravity Design A," *Rainfall Simulation Database* [online database], URL: http://www.geog.le.ac.uk/bgrg/lab.htm [cited 15 March 1998].

Propulsion

[1] [7]Aero Propulsion Technologies, "Rotax Service," 1 June 2000. [Online]. Available: http://www.rotaxservice.com/rotax_engines/rotax_912ULSs.htm. [Accessed 20 October 2016].

[2] [8]Mt- Propeller, "Propeller Overview," 16 February 2015. [Online]. Available: http://www.mt-propeller.com/en/entw/pro_hydr.htm. [Accessed 20 October 2016].

[3] [9]MIT, "Performance of Propellers," 1 August 2016. [Online]. Available: http://web.mit.edu/16.unified/www/FALL/thermodynamics/notes/node86.html. [Accessed 20 October 2016].

[4] [15]MIT, "Aircraft Performance," 1 January 2016. [Online]. Available: https://ocw.mit.edu/ans7870/16/16.unified/propulsionS04/UnifiedPropulsion4/UnifiedPropulsion4.htm. [Accessed 20 October 2016].

[5] [11]J. Roskam, Airplane Design Part I: Preliminary Sizing of Airplanes, Ottawa: Roskam Aviation, 1985.

[6] [17]Aviation Bull, "Light sport aircraft engine comparison," 1 January 2010. [Online]. Available: http://www.aviationbull.com/light-sport-aircraft-engine-comparison. [Accessed 20 October 2016].

[17] **http://www.amesweb.info/SectionalPropertiesTabs/SectionalPropertiesIbeam.aspx (for Lofting & Refining)**